Urinary metabolomics investigation of *Ndufs4* knockout mice

W Horak

orcid.org 0000-0003-2626-615X

Dissertation accepted in partial fulfilment of the requirements for the degree *Master of Science in Biochemistry* at the North-West University

Supervisor:	Prof R Louw
Co-supervisor:	Prof FH Van der Westhuizen
Assistant Supervisor:	Dr JZ Lindeque

Graduation July 2020

24690562

ACKNOWLEDGEMENTS

Hereby, I want to acknowledge the following people and institutions whose contributions have made the completion of this study possible, and I want to apologise in advance for anyone who I may have forgotten:

- **Prof Roan Louw**, **Prof Francois van der Westhuizen** and **Dr Zander Lindeque**, my supervisors, for not only fulfilling their respective roles, but also for going beyond what is required of them. Their patience, understanding and trust in me are immensely appreciated.
- **Michelle Mereis**, for her assistance in the breeding- and genotyping strategy of the mice used in this study, as well as her assistance in the technical editing of the manuscript.
- The **staff at the Preclinical Drug Development Platform (PCDDP)** of the **North-West University (NWU)**, Potchefstroom Campus, for their assistance in the breeding, husbandry and euthanasia of the mice used in this study.
- The **NWU** and **National Research Foundation (NRF)**, for financial support. The opinions expressed and conclusions arrived at, are those of the author and are not necessarily to be attributed to the NRF.
- **Peet Jansen van Rensburg**, for his assistance on the LC-MS/MS.
- **Elmarie Davoren** and **Jano Jacobs**, at the Potchefstroom Laboratory for Inborn Errors of Metabolism (PLIEM); and **Brenda Klopper**, at the Newborn Screening Laboratory, for generously providing me with chemicals that were used in this study.
- **Elize Altona**, for generously providing me with new glassware used in this study.

I want to thank my family, especially my **parents**, to whom I dedicate this dissertation, for giving me the opportunity to further my studies and for all their endless love and support. Together, we went through many tribulations, but through the grace of our Heavenly Father, we have prevailed and came out stronger on the other side. Thank you for carrying my burden with me. I am eternally grateful to have you as my parents.

Lastly, but most importantly, I want to thank my Heavenly Father יהוה for the salvation He has provided through the redemptive work of His Son **Yeshua** the Messiah, without which my works would be in vain. I also want to thank Him, not only for all the privileges He has bestowed upon me, but for always bringing me back to Him during the times when I was lost. Yours' is the kingdom, the power and the glory, forever and ever.

ABSTRACT

Mitochondrial diseases (MDs) are the most common inborn errors of metabolism, with an estimated prevalence of approximately 1 in 5 000 live births, and are mainly caused by deficiencies of complex I (CI) of the oxidative phosphorylation (OXPHOS) system. Clinical presentations of CI deficiency are highly heterogeneous, with the most commonly reported, being Leigh syndrome (LS) – a devastating progressive, multi-systemic, neurodegenerative disorder. The *Ndufs4* gene, which encodes for an 18 kDa subunit of CI, is a mutational hotspot in LS patients.

To date, the efficacy of the limited available therapeutic interventions remains inconclusive, and can, in large, be attributed to our poor understanding of the pathological mechanisms behind these highly complex diseases. Fortunately, with a whole-body *Ndufs4* knockout (KO) mouse model available, researchers have a great opportunity to gain a better understanding of this commonly reported MD. What remains lacking, however, is the incorporation of multi-platform metabolomics using urine. This biofluid shows promise in revealing global metabolic perturbations in MDs, and thus possesses the potential to elucidate disease mechanisms.

The aim of this study, therefore, was to investigate the metabolic consequences of *Ndufs4* deficiency by analysing the urine of the whole-body *Ndufs4* KO mouse model. This was accomplished by implementing two main objectives: firstly, by validating the mouse model via genetic and phenotypic evaluation and the measurement of CI activity in the liver; and secondly, by comparing the urinary metabolome of *Ndufs4* KO and wild-type mice, acquired via both untargeted and targeted analyses, in order to obtain a comprehensive view of the metabolic consequences.

In this study, the mouse model was successfully validated on the genetic and phenotypic level, with *Ndufs4* KO mice displaying well-reported phenotypic characteristics, including growth retardation, transient alopecia and hunched back posture. Biochemically, the mouse model was further confirmed with *Ndufs4* KO mice exhibiting 15% residual CI activity in the liver. Urinary metabolomic analyses revealed multiple metabolic perturbations in the *Ndufs4* KO mice. Most notably, were the markers classically observed in MDs and commonly believed to be the result of an altered redox status, namely elevated levels of pyruvate, lactate and alanine as well as some tricarboxylic acid cycle intermediates (2-ketoglutarate, fumarate and malate). A downregulation in protein/amino acid catabolism was observed, as indicated by decreased levels of numerous amino acids (e.g. glutamine, glutamate, leucine, isoleucine, valine and phenylalanine), 3-methylhistine (index of skeletal muscle breakdown) and metabolites associated with the urea cycle (arginine, citrulline and *N*-acetylglutamate). Similarly, lipid/fatty acid catabolism also

appeared to be downregulated, as shown by lowered levels of glycerol as well as numerous carnitine- and glycine fatty acid conjugates (octanoyl- and decanoylcarntine; butyryl-, valeryl- and hexanoylglycine). Metabolites present in pathways associated with biosynthetic processes and/or ROS scavenging (including the pentose phosphate pathway, one-carbon metabolism and *de novo* pyrimidine synthesis) were also decreased. Taken together, the implementation of urinary metabolomics proved to be successful in revealing global metabolic perturbations in *Ndufs4* KO mice.

Keywords: Metabolomics • Complex I deficiency • Mitochondrial disease • Leigh syndrome • *Ndufs4* knockout mice • Metabolism • Urine

CONTENTS

LIST OF FIGURES

CHAPTER 2

CHAPTER 3

CHAPTER 4

APPENDIX B

LIST OF TABLES

CHAPTER 3

CHAPTER 4

APPENDIX A

LIST OF EQUATIONS

CHAPTER 3

LIST OF SYMBOLS, UNITS AND ABBREVIATIONS

Symbols

#	number
~	approximately
↑	increase
↓	decrease
♀	female
♂	male
α	alpha
β	beta
Δ	delta/change in
Δp	proton motive force
ΔpH	pH/proton gradient
ΔΨ	membrane potential

Units

%	percentage
°C	degrees Celcius
µg	microgram
µl	microlitre
µm	micrometre
µM	micromolar
µmole	micromole
bp	base pairs
Da	dalton
eV	electronvolt
g	gram
kDa	kilodalton
l	litre
m	metre
M	molar
m/z	mass-to-charge ratio
mAU	milli-absorbance unit
mg	milligram

min	minute
ml	millilitre
mm	millimetre
mM	millimolar
ms	milliseconds
Mw	molecular weight
ng	nanogram
nm	nanometre
nmol	nanomole
pH	potential of hydrogen
ppm	parts per million
psi	pound-force per square inch
V	volt
v/v	volume (of solute) per volume (of solvent)
w/v	weight (of solute) per weight (of solvent)
xg	relative centrifugal force

Abbreviations

%RSD or RSD (%)	relative standard deviation (expressed as percentage)
^{14}C	carbon-14
5’ to 3’	direction of the polynucleotide, i.e. from the 5’-end to the 3’-end
AA	amino acid
ACN	acetonitrile
ADP	adenosine-5’-diphosphate
ANT	adenine nucleotide translocator
ATP	adenosine-5’-triphosphate
BCA	bicinchoninic acid
BCAA	branched chain amino acid
BSA	bovine serum albumin
BSTFA	*N,O*-bis(trimethylsilyl)trifluoroacetamide
CA	California
Ca^{2+}	calcium ion
cAMP	cyclic adenosine monophosphate
CE	collision energy
CI	complex I (NADH:ubiquinone oxidoreductase)
CII	complex II (succinate:ubiquinone oxidoreductase)

CIII	complex III (ubiquinol:cytochrome c oxidoreductase)
CIV	complex IV (cytochrome c oxidase)
CO_2	carbon dioxide
CoA	coenzyme A
CS	citrate synthase
Cu^{+}	cuprous ions
Cu^{2+}	cupric ions
CuSO4.5H2O	copper(II) sulphate pentahydrate
CV	complex V (ATP synthase) or coefficient of variance (depending on the context)
Cyt c	cytochrome c
DCIP	2,6-dichloroindophenol
DHAP	dihydroxyacetone phosphate
DHODH	dihydroorotate dehydrogenase
DMSO	dimethyl sulfoxide
DNA	deoxyribonucleic acid
DTNB	2,2'-dinitro-5,5'-dithiobenzoic acid
DUQ	decylubiquinone
EC	enzyme commission number
EDTA	ethylenediaminetetraacetic acid
EGTA	ethylene glycol tetraacetic acid
EI	electron impact ionisation
EMV	electron multiplier voltage
ESI	electrospray ionisation
ETC	electron transport chain
ETF	electron transfer flavoprotein
ETF:QO	electron transfer flavoprotein:ubiquinone oxidoreductase
FA	formic acid
FAD	flavin adenine dinucleotide
FMN	flavin mononucleotide
FV	fragmentor voltage
G3P	glycerol-3-phosphate
GC-TOF-MS	gas chromatography time-of-flight mass spectrometry
GSH	glutathione
H^{+}	proton
H_2O	water
H_2O_2	hydrogen peroxide

H_2S	hydrogen sulfide
HEPES	2-[4-(2-hydroxyethyl)piperazin-1-yl]ethanesulfonic acid
HET	heterozygote/heterozygous
HIF-1	hypoxia-inducible factor 1
HIF-1α	alpha subunit of hypoxia-inducible factor 1
HIF-1β	beta subunit of hypoxia-inducible factor 1
ID	identification
IMM	inner mitochondrial membrane
IMS	intermembrane space
IS	internal standard
KO	knockout
KPi	potassium phosphate
LC-MS/MS	liquid chromatography-tandem mass spectrometry
loxP	locus of X(cross)-over in P1
LS	Leigh syndrome
MA	Massachusetts
MCU	mitochondrial calcium uniporter
MD	mitochondrial disorder/disease
ME	Maine
MELAS	mitochondrial encephalomyopathy with lactic acidosis and stroke-like episodes
mGPDH	mitochondrial glycerol-3-phosphate dehydrogenase
MM	mitochondrial matrix
MO	Missouri
Mox2-Cre	mesenchyme homeobox 2-cre
MRM	multiple reaction monitoring
mRNA	messenger RNA
MSTUS	mass spectral total useful signal
$MSTUS_{(excl.ssf)}$	mass spectral total useful signal excluding statistically significant features
mtDNA	mitochondrial deoxyribonucleic acid
n	number analysed
N module	NADH binding module
N/A	not applicable
NAD^+	nicotinamide adenine dinucleotide (oxidised)
NADH	nicotinamide adenine dinucleotide (reduced)
$NADP^+$	nicotinamide adenine dinucleotide phosphate (oxidised)

NADPH	nicotinamide adenine dinucleotide phosphate (reduced)
NAG	*N*-acetylglutamate
NaN_3	sodium azide
NaOH	sodium hydroxide
nDNA	nuclear deoxyribonucleic acid
Ndufs4 or *NDUFS4*	NADH:ubiquinone oxidoreductase iron-sulfur protein 4 gene (in mice or humans, respectively)
NDUFS4 or Ndufs4	NADH:ubiquinone oxidoreductase iron-sulfur protein 4 (in mice or humans, respectively)
NIST	National Institute of Standards and Technology
NJ	New Jersey
NNT	nicotinamide nucleotide transhydrogenase
NWU	North-West University
O_2	molecular oxygen
$O_2^{\bullet-}$	superoxide anion radical
OH•	hydroxyl radical
OMM	outer mitochondrial membrane
OXPHOS	oxidative phosphorylation
P	postnatal day
P module	proton binding module
PC	principle component
PCA	principle component analysis
PCDDP	Preclinical Drug Development Platform
PCR	polymerase chain reaction
PDHc	pyruvate dehydrogenase complex
PHD	prolyl hydroxylase
Pi	inorganic phosphate
PiC	mitochondrial phosphate carrier
PMF	proton motive force
PRODH	proline dehydrogenase
Q module	ubiquinone binding module
Q	ubiquinone
QC	quality control
R^2	R-squared value, i.e. how well the data fits the regression line
RC	respiratory chain
Redox	reduction-oxidation
RNA	ribonucleic acid

ROS	reactive oxygen species
SH	thiol
SIL	stable isotopic labelling
SQR	sulfide-ubiquinone oxidoreductase
SUOX	sulfite oxidase
T cell	thymus cell
TCA	tricarboxylic acid
Tim23	translocase of the inner membrane 23
T_m	melting temperature
TMCS	trimethylchlorosilane
TNB	2-nitro-5-thiobenzoic acid
Trx	thioredoxin
UCP1	uncoupling protein 1
UCS	units of citrate synthase
USA	United States of America
UV	ultraviolet light
vs	versus
VT	Vermont
WT	wild-type

CHAPTER 1:

INTRODUCTION

Located in nearly all mammalian cells, are multi-functional, subcellular structures called mitochondria. These organelles are primarily known to meet the majority of the cell's energy demands through a process termed oxidative phosphorylation (OXPHOS) – a series of reactions accomplished by the cooperation of five multi-subunit complexes (CI-CV) (Spinelli & Haigis, 2018). Given the mitochondrion's multifaceted contribution to cellular function, it is of no surprise that mitochondrial diseases (MDs) are the most prevalent among all inborn errors of metabolism and that these disorders can wreak havoc in cells by compromising energy production, causing oxidative stress and leading to metabolic derangements (Esterhuizen *et al.*, 2017).

Unfortunately, MDs are by no means simplistic, but instead, are highly sophisticated diseases that continue to prevail against the scientific community. This is evident from the limited therapeutic interventions available against MDs (Dimond, 2013; Lehmann & McFarland, 2018) and the lack of compelling evidence supporting their efficacy (Pfeffer *et al.*, 2012). Specifically, this hurdle is the result of the poor genotype-phenotype correlation displayed in MDs (Pfeffer *et al.*, 2012; Rahman & Rahman, 2018), as well as the overall poor understanding of the pathological mechanisms of these disorders (Rahman & Rahman, 2018; Vafai & Mootha, 2012).

MDs are mainly caused by deficiencies in complex I (CI) of the OXPHOS system (Loeffen *et al.*, 2000; Scaglia *et al.*, 2004; von Kleist-Retzow *et al.*, 1998), which predominantly manifest as Leigh syndrome (LS), the most frequently reported clinical presentation of MDs (Bugiani *et al.*, 2004; Koene *et al.*, 2012; Lake *et al.*, 2015). In cases of LS, the gene encoding for NADH dehydrogenase:ubiquinone iron-sulfur protein 4 (NDUFS4) is considered a mutational hotspot (Ortigoza-Escobar *et al.*, 2016).

Therefore, NDUFS4-related LS is an apposite disease to research in order to gain a better understanding of MDs in general, which may lead to effective treatment options. Fortunately, a whole-body *Ndufs4* knockout (KO) mouse model is available, and thus provides an excellent opportunity for researchers to investigate MD. To date, research on the metabolism of this mouse model is not only limited, but has also not yet incorporated the use of multi-platform metabolomics in urine – an information-rich biofluid that can reveal global metabolic perturbations. The aim of this study, therefore, was to investigate the metabolic consequences in whole-body *Ndufs4* KO mice using a urinary metabolomics approach.

The structure of this dissertation can be summarised as follows:

- **Chapter 2** provides a comprehensive overview of literature relevant to this study. Additionally, the chapter presents the problem statement, the aim of this study and the objectives followed to address the aim, as illustrated in the study design.
- In **Chapter 3**, detailed descriptions of the experimental- and data handling procedures used to achieve the objectives are provided, followed by the findings that are presented and discussed in **Chapter 4**.
- **Chapter 5** provides a conclusive summary of the results, the strengths and limitations of this study and recommendations for future endeavours.
- **Appendix A** provides a list of all the materials/reagents used in the experimental procedures described in Chapter 3.

Finally, additional data handling procedures and the results thereof – which are not presented in Chapter 3 and 4, respectively – are provided in **Appendix B**.

CHAPTER 2:
LITERATURE REVIEW

2.1 The mitochondrion

Mitochondria (mitochondrion, singular) are maternally inherited organelles (Giles *et al.*, 1980), located in all nucleated mammalian cells, with the exception of cells that lose their nuclei during cell maturation (Rogerson *et al.*, 2018). These organelles are semi-autonomous, requiring nuclear deoxyribonucleic acid (nDNA), as well as their own deoxyribonucleic acid (DNA; of which multiple copies – anywhere from 100 to 10 000 – exist in each mitochondrion), in order to be synthesised (Chinnery & Hudson, 2013). Only ~1% of the ~1 000 to 1 500 proteins that comprise mammalian mitochondria is encoded by mitochondrial DNA (mtDNA) (Calvo & Mootha, 2010).

Mitochondria are responsible for orchestrating a myriad of cellular processes; functioning not only as bioenergetic organelles, for which they are most well-known, but also as biosynthetic, signalling and waste disposal/detoxifying organelles (Spinelli & Haigis, 2018; Vakifahmetoglu-Norberg *et al.*, 2017). Furthermore, mitochondria do not function in isolation, but rather in conjunction with the rest of the cell to fulfil many of these cellular tasks (Xia *et al.*, 2019).

Structurally, mitochondria are composed of two phospholipid bilayer membranes with two distinct compartments, as illustrated in Figure 2.1. These include a highly permeable outer membrane (OMM) that allows uncharged molecules of <5 000 Da to freely diffuse across it, and a highly impermeable inner membrane (IMM) that requires a vast amount of transport proteins to allow the import of even inorganic ions. The intermembrane space (IMS) is positioned in between the two membranes, and the mitochondrial matrix (MM) is enclosed by the IMM. The IMM is characterised by numerous folds that project inwards, known as cristae, which house the machinery required for energy production. These folds greatly enhance the surface area, and as a result, the capacity for energy production.

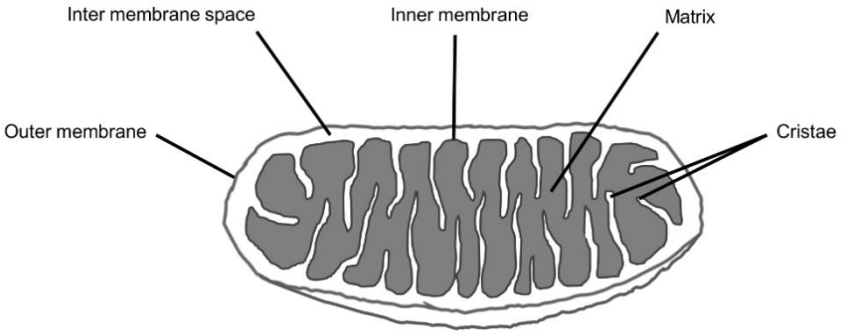

Figure 2.1: Mitochondrial architecture. Schematic representation of the mitochondrial architecture. Mitochondria are double membrane organelles with two distinct compartments, namely the inter membrane space, located between the outer and inner mitochondrial membrane, and the mitochondrial matrix, surrounded by the inner mitochondrial membrane.

2.2 The respiratory chain and oxidative phosphorylation

Mitochondria are most well-known to provide the majority of our cellular energy, under normal conditions, in the form of adenosine-5'-triphosphate (ATP) (Marquez *et al.*, 2016). ATP has been labelled the main “energy currency” in cells because it is utilised in a multitude of cellular processes relevant to healthy functioning, including: (i) muscle contraction (Kuo & Ehrlich, 2015); (ii) the transport of various solutes (e.g. inorganic ions and metabolites) across cell and organelle membranes (Vasiliou *et al.*, 2009); (iii) the transport of cellular components (e.g. proteins and organelles) to specific intracellular destinations along microtubules by kinesin and dynein motor proteins (Abraham *et al.*, 2018); (iv) biosynthetic pathways (Buhaescu & Izzedine, 2007; Marí *et al.*, 2010; Martinez *et al.*, 2014); and (v) the regulation of gene expression and protein activity by chromatin remodelling and post-translational modification, respectively (Mazina & Vorobyeva, 2016; Vlastaridis *et al.*, 2017).

The utilisation of ATP is truly astonishing, with a turnover rate of 50-75 kg per day in the average person (Okuno *et al.*, 2011). To put it in a different perspective, in the human brain alone, 4.7 billion ATP molecules are utilised per second by a single cortical neuron at resting state (Zhu *et al.*, 2012). This impressive feat of maintaining high levels of ATP is accomplished via oxidative phosphorylation (OXPHOS).

The components responsible for orchestrating OXPHOS, collectively known as the OXPHOS system (Figure 2.2), comprise five multi-protein IMM-bound complexes: complex I (CI, NADH:ubiquinone oxidoreductase); complex II (CII, succinate:ubiquinone oxidoreductase); complex III (CIII, ubiquinol:cytochrome c oxidoreductase); complex IV (CIV, cytochrome c

oxidase); and complex V (CV, ATP synthase), of which all, except CII, are encoded by both nDNA and mtDNA (Koopman *et al.*, 2013).

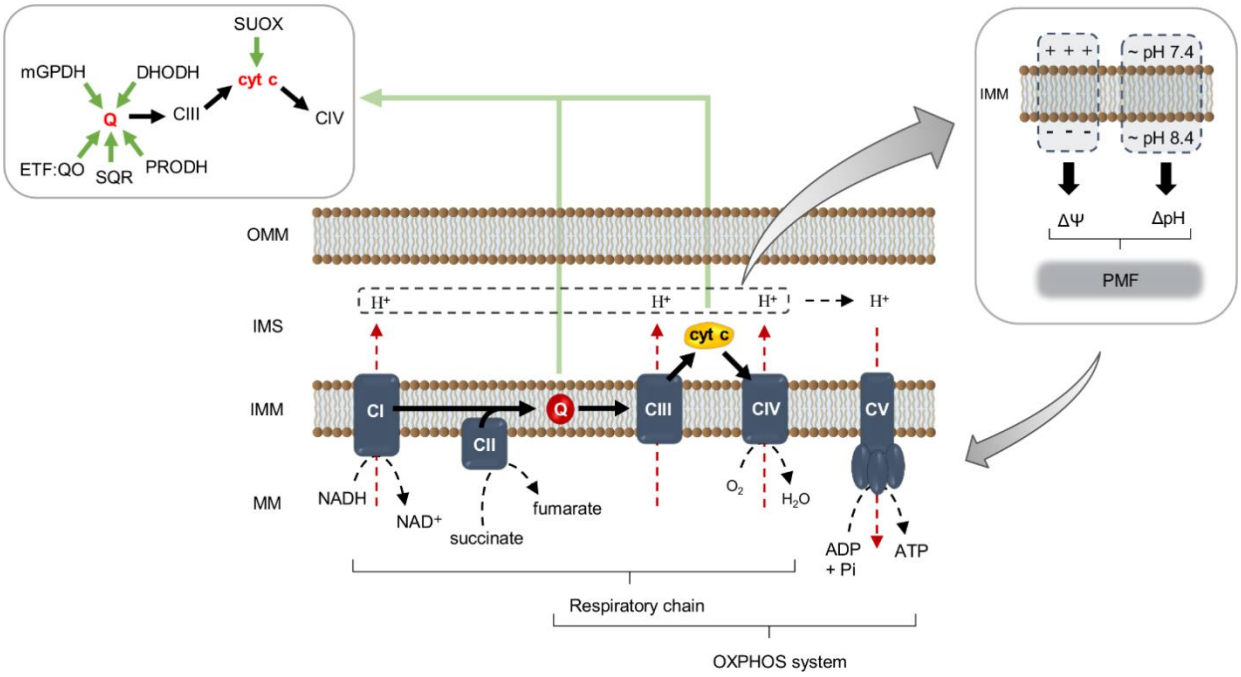

Figure 2.2: The OXPHOS system. Schematic representation of the OXPHOS system comprising the canonical RC (CI-IV, the two mobile electron carriers Q and cyt c, and CV). Electrons derived from the appropriate substrates are sequentially transferred from CI-II, as well as from the auxiliary enzymes (top left), through the RC and ultimately donated to the final electron acceptor, O_2. During this process, protons (H^+) are translocated into the IMS via CI, CII and CIII. This generates the PMF required for the phosphorylation of ADP via CV. Abbreviations: ΔΨ, membrane potential; ΔpH, pH/proton gradient; ADP, adenosine-5'-diphosphate; ATP, adenosine-5'-triphosphate; CI-V, complexes I to V; cyt c, cytochrome c; DHODH, dihydroorotate dehydrogenase; ETF:QO, electron transfer flavoprotein:ubiquinone oxidoreductase; H^+, protons; H_2O, water; IMM, inner mitochondrial membrane; IMS, intermembrane space; mGPDH, mitochondrial glycerol-3-phosphate dehydrogenase; MM, mitochondrial matrix; OMM, outer mitochondrial membrane; NAD^+, nicotinamide adenine dinucleotide (oxidised); NADH, nicotinamide adenine dinucleotide (reduced); pH, potential of hydrogen; Pi, inorganic phosphate; O_2, molecular oxygen; OXPHOS, oxidative phosphorylation; PMF, proton motive force; PRODH, proline dehydrogenase; Q, ubiquinone; RC, respiratory chain; SQR, sulfide-ubiquinone oxidoreductase; SUOX, sulfite oxidase.

The first four complexes (CI-IV) make up the respiratory chain (RC), otherwise known as the electron transport chain (ETC), which further contains two mobile electron carriers: a lipophilic quinone known as ubiquinone (Q) and a small heme protein called cytochrome c (cyt c) that are located in the IMM and IMS, respectively. The RC is designed to sequentially transfer electrons [derived from the oxidation of reduced nicotinamide adenine dinucleotide (NADH) and succinate, and donated to CI and CII, respectively] to the final electron acceptor, molecular oxygen (O_2)

through a series of reduction-oxidation (redox) reactions in the following order: CI-II → Q → CIII → cyt c → CIV → O_2 (Koopman *et al.*, 2013). This represents the classical RC model, but there are, in fact, a number of other enzymes that feed electrons into the RC (Figure 2.2). These enzymes are: sulfite oxidase (SUOX; which reduces cyt c); and mitochondrial glycerol-3-phosphate dehydrogenase (mGPDH) (Mráček *et al.*, 2013); electron transfer flavoprotein:ubiquinone oxidoreductase (ETF:QO) (Watmough & Frerman, 2010); dihydroorotate dehydrogenase (DHODH) (Löffler *et al.*, 1998); sulfide-ubiquinone oxidoreductase (SQR) (Goubern *et al.*, 2007); and proline dehydrogenase (PRODH) (Hancock *et al.*, 2016) [all of which transfer electrons to Q (Garrett *et al.*, 1998)]. These enzymes (including CI-II) and the pathways to which they are linked, are discussed in Sections 2.3 and 2.4.

During the sequential transfer of electrons to O_2, energy is liberated and utilised by the three transmembrane complexes CI, CIII and CIV to translocate protons from the IMM into the IMS. In turn, this generates an electrochemical gradient, also known as the proton motive force (Δp or PMF), comprising an electrical component, the membrane potential (ΔΨ), and a chemical component, the pH/proton gradient (ΔpH). This form of potential energy is subsequently harnessed to phosphorylate adenosine-5'-diphosphate (ADP), thereby creating ATP, when protons diffuse back into the MM through CV (Nicholls & Ferguson, 2002a).

2.3 Other processes linked to the respiratory chain

2.3.1 Electrochemical gradient-dependent processes

The importance of CV being coupled to the RC is exemplified by its bi-genomic origin and its role in, and astonishing rate of, ATP turnover. There are, however, other processes driven by the electrochemical gradient that rely either on one, or both of its components (ΔΨ or ΔpH) (Nicholls & Ferguson, 2002a).

The IMM, being almost completely impermeable, is gated by many transport proteins that are driven by the electrochemical gradient, to translocate solutes in and out of the mitochondrion. Some examples include: (i) the import of inorganic phosphate [Pi; via the mitochondrial phosphate carrier (PiC)] and the exchange of ATP and ADP [via the adenine nucleotide translocator (ANT)], to ensure the delivery of Pi and ADP to the OXPHOS system and the availability of ATP in the cytosol (Kunji *et al.*, 2016; Mayr *et al.*, 2007); (ii) the import of pre-proteins that are required for proper mitochondrial biogenesis and function via translocase of the inner membrane 23 (Tim23) (Wiedemann & Pfanner, 2017); (iii) the aspartate-glutamate carriers that form part of the malate-aspartate shuttle (discussed in Section 2.4) and make cytosolic-derived electrons available to the

RC (Amoedo *et al.*, 2016); and (iv) the mitochondrial calcium (Ca^{2+}) uniporter (MCU) that is involved in Ca^{2+} homeostasis (Mammucari *et al.*, 2018).

Besides solute transport, the electrochemical gradient is also required for the reduction of oxidised nicotinamide adenine dinucleotide phosphate ($NADP^+$), at the expense of NADH via nicotinamide nucleotide transhydrogenase (NNT), which is required for biosynthetic reactions as well as the detoxification of reactive oxygen species (ROS) (discussed in the following section) (Rydström, 2006). Another example is the generation of heat (thermogenesis) in response to cold exposure via uncoupling protein 1 (UCP1) or thermogenin, which are mainly expressed in the brown adipose tissue of infants and small mammals (Sell *et al.*, 2004).

2.3.2 Reactive oxygen species

Mitochondria are the primary consumers of O_2, and accordingly, the main sites of ROS production (Valko *et al.*, 2007). A variety of mitochondrial enzymes contribute to the production of ROS, with the greatest portion being those involved in the RC, including CI-III, ETF:QO, mGPDH, DHODH, PRODH and SQR. Of all these, CI and CIII are conventionally regarded as the prime contributors to ROS production (Mailloux, 2015).

ROS can be defined as highly reactive oxygen derivatives, capable of oxidising cellular components such as DNA, lipids and proteins. Examples include free radicals, such as the superoxide anion radical ($O_2^{\bullet-}$) and the hydroxyl radical ($OH^{\bullet}$), as well as non-radicals (e.g. hydrogen peroxide, H_2O_2) (Valko *et al.*, 2007). Under normal physiological conditions, it is estimated that ROS is derived from 0.1-2% of mitochondrial consumed O_2 (Orrenius *et al.*, 2007; Tahara *et al.*, 2009). ROS is formed as a result of the RC becoming highly reduced and causing electrons to "leak", thereby leading to the partial reduction of O_2 to $O_2^{\bullet-}$ (Barja, 2007), which is subsequently transformed into other forms of ROS.

Originally viewed as exclusively destructive by-products that cause cellular damage and result in eventual cell death, ROS has since been shown to form part of normal metabolism – playing important roles in a variety of processes, such as the adaptation to hypoxic conditions and the regulation of autophagy, immunity, stem cell differentiation and aging (Sena & Chandel, 2012). Therefore, ROS homeostasis is of the utmost importance to keep ROS levels within physiological ranges and is achieved through a number of ROS scavenging pathways.

The first line of defence involves the conversion of $O_2^{\bullet-}$ to H_2O_2, which can occur either spontaneously, or via the enzyme superoxide dismutase [at a conversion rate that is 10 million times faster (Weydert & Cullen, 2010)]. $O_2^{\bullet-}$ is also scavenged by cyt c, which oxidises it back to O_2 and transfers the gained electron to CIV (Pereverzev *et al.*, 2003). Following this, H_2O_2 is subsequently detoxified by the enzyme catalase to form water (H_2O) and O_2, and also by the two

main H_2O_2 scavenging systems, namely the glutathione (GSH) and thioredoxin (Trx) systems, via glutathione peroxidase and thioredoxin peroxidase, respectively (Munro *et al.*, 2016). During the reduction of ROS by these two scavenging systems, two molecules of GSH are oxidised in the GSH system to form glutathione disulfide, whereas Trx is concurrently oxidised in the Trx system to convert H_2O_2 to H_2O. Both systems contain reduced nicotinamide adenine dinucleotide phosphate (NADPH)-dependant reductases that reduce glutathione and oxidised Trx, thereby ensuring the continuation of these ROS scavenging pathways.

2.4 Electron-feeding pathways involved in energy metabolism

The RC derives most of its electrons from a number of metabolic pathways involved in the catabolism of sugars, fats and amino acids (AAs). Located within the MM is the tricarboxylic acid (TCA) cycle, which is the central and final catabolic pathway responsible for the complete oxidation of substrates to carbon dioxide (CO_2). The pathway comprises eight enzymatic reactions, with three generating the intermediate electron carrier NADH, which is oxidised by CI. In addition, the TCA cycle and the RC are directly linked via CII, which catalyses the sixth step of the TCA cycle, transferring electrons to Q via the oxidation of succinate to fumarate (Rutter *et al.*, 2010).

There are numerous pathways that feed partially oxidised substrates into the TCA cycle. Glycolysis, which occurs in the cytosol, is responsible for the oxidation of glucose to pyruvate. Pyruvate is then imported into the MM and oxidised to acetyl-coenzyme A (CoA), forming NADH in the process. The IMM, however, is impermeable to cytosolic NADH; thus, its re-oxidation is critical for the continuation of the glycolytic pathway. There are two pathways that ensure the re-oxidation of NADH: the malate-aspartate shuttle (Nicholls & Ferguson, 2002b) and the glycerol-3-phosphate shuttle (Gvozdjáková, 2008). In the malate-aspartate shuttle, NADH is re-oxidised during the reduction of oxaloacetate to malate. Malate is then transported through an antiporter protein, during which 2-ketoglutarate is exported into the cytoplasm. In the MM, malate is then oxidised back to oxaloacetate, thereby reducing oxidised nicotinamide adenine dinucleotide (NAD^+) to NADH. The glycerol-3-phosphate shuttle consists of two glycerol-3-phosphate dehydrogenases, one of which is NADH-dependant and located in the cytosol, and a second, namely mGPDH, which is one of the auxiliary enzymes of the RC. During this shuttle, dihydroxyacetone phosphate (DHAP), produced from the glycolytic pathway, is reduced to glycerol-3-phosphate (G3P), which then enters the MM where it is oxidised back to DHAP, thereby transferring electrons from mGPDH to Q (Gvozdjáková, 2008). mGPDH is also involved in the synthesis of glucose via gluconeogenesis, which primarily occurs in the liver. Here, glycerol, derived from lipolysis, is phosphorylated and subsequently oxidised by mGPDH to

DHAP, which enters the gluconeogenic pathway. Hence, mGPDH is at a “crossroad” – linking glucose and lipid metabolism (Madiraju *et al.*, 2014).

The β-oxidation pathway is responsible for the oxidation of fatty acids, which serve as an important energy source during fasting, starvation or prolonged exercise when glucose reserves become limited. Cardiomyocytes are an exception, since these cells primarily depend on fatty acids for energy (60-70% ATP), even in a fed state (Kudo *et al.*, 1995). Fatty acids, after being imported into the MM, are broken down to acetyl-CoA, which subsequently enters the TCA cycle. During β-oxidation, electrons are provided to CI and ETF:QO via NADH and the electron transfer flavoprotein (ETF), respectively (Houten & Wanders, 2010).

When acetyl-CoA levels exceed the TCA cycle’s capacity, the substrate is diverted towards the production of ketone bodies [acetoacetate, 3-hydroxybutyrate and acetone], which occurs primarily in the liver. These ketone bodies are exported and utilised by extra-hepatic tissues for energy. Within these tissues, acetoacetate and 3-hydroxybutyrate are oxidised back to acetyl-CoA, which can enter the TCA cycle, with the latter ketone body providing NADH to CI. Ketone bodies are an important energy source for the brain, since fatty acids are unable to cross the blood-brain barrier (Houten & Wanders, 2010). Acetone is commonly viewed as a dead-end metabolite that is not metabolised, but rather excreted via exhalation and urination. In addition to this view, it is also widely accepted that fatty acids do not contribute to gluconeogenesis. However, through the use of ^{14}C tracing analysis on mammals (including humans), several studies have provided evidence that acetone is indeed metabolised and contributes to gluconeogenesis, as proven by the detection of acetone-derived ^{14}C in glucose (Kalapos, 2003).

Even though glucose and fatty acids are the body’s preferred energy sources, as is evident from the body’s ability to respectively store these substrates in the form of glycogen and triglycerides, AAs also serve as an energy source (Salway, 2017). Owing to the structural diversity of AAs, the catabolic pathways thereof – which occur in both the cytosol and the mitochondria – are also diverse and thus beyond the scope of this literature review. AAs can be classified based on the partially oxidised metabolites they produce. Gluconeogenic AAs are broken down to pyruvate and various intermediates of the TCA cycle and subsequently enter the gluconeogenic pathway for the synthesis of glucose. Only thereafter, when glucose is oxidised to acetyl-CoA, are the carbon skeletons of these AAs completely oxidised to CO_2 via the TCA cycle. Ketogenic AAs on the other hand, are degraded to acetoacetyl-CoA and acetyl-CoA, which not only enter the TCA cycle, but serve as substrates for the synthesis of ketone bodies (Salway, 2017).

During the partial oxidation of AAs to the above-mentioned substrates, many AAs also reduce NAD^+ (similar to glucose and fatty acid catabolism), examples of which include the branched chain amino acids (BCAAs: leucine, isoleucine and valine), lysine, tryptophan and proline

(Salway, 2017). Furthermore, these AAs in particular also provide electrons that enter the RC via auxiliary enzymes. BCAAs, lysine and tryptophan, like the oxidation of fatty acids, reduce ETF during their oxidation, thus providing electrons to ETF:QO (Olpin, 2013). By contrast, the oxidation of proline to Δ^1-pyrroline-5-carboxylate is mediated by PRODH, which is embedded in the interior side of the IMM and results in electron transfer to Q (Hancock *et al.*, 2016).

2.5 Non-bioenergetic pathways linked to the respiratory chain

The pathways discussed in the previous sections are known to be the main contributors in energy metabolism – providing electrons to not only CI-II, but also to the auxiliary enzymes, ETF:QO and mGPDH. There are, however, non-bioenergetic pathways that provide electrons to the RC.

2.5.1 Hydrogen sulfide metabolism

Mitochondria play an important role in the metabolism of hydrogen sulfide (H_2S), a gaseous molecule derived from a number of enzymes involved in the catabolism of sulfur-containing AAs (methionine, cysteine and homocysteine), as well as anaerobic bacteria located in the intestinal lumen (Fu *et al.*, 2012). Once considered exclusively to be a toxic gas, H_2S has been revealed to be a gasotransmitter involved in many physiological processes, including regulation of the heart rate, upregulation of the anti-oxidant systems and increased production of cyclic adenosine monophosphate (cAMP), to name but a few. However, similar to ROS, it is toxic to cells should the concentration thereof rise above normal levels. H_2S homeostasis is maintained by the enzyme SQR, which is located on the MM side of the IMM and converts H_2S to thiosulfate, transferring electrons to Q in the process (Libiad *et al.*, 2014). Thereafter, thiosulfate undergoes several reactions to form sulphite, which is oxidised to sulfate by the IMS enzyme SUOX, thereby transferring electrons to cyt c of the RC. SQR and SUOX are therefore unique, being the only mammalian auxiliary enzymes of the RC to date, that contribute to the electrochemical gradient via the oxidation of inorganic substrates.

2.5.2 *De novo* pyrimidine synthesis

Pyrimidines are vital aromatic, heterocyclic, organic molecules, required for many cellular processes, including the synthesis of DNA, ribonucleic acid (RNA), membrane lipids, glycoproteins and glycogen (Evans & Guy, 2004). The synthesis of pyrimidines can occur via either salvage pathways, where nucleotides are recycled, or via the *de novo* pathway (Robinson *et al.*, 2020). The latter pathway comprises six enzymatic reactions, of which five occur in the cytosol and one in the mitochondrion. Embedded in the IMM adjacent to the IMS, is the enzyme DHODH, which is responsible for catalysing the fourth step of *de novo* pyrimidine synthesis.

During this step, dihydroxyorotate, derived from glutamine, is oxidised by DHODH to orotate, with the concomitant reduction of Q. This pathway has an important contribution in proliferating cells [e.g. during development and the activation of thymus cells (T cells)], where an increased rate of DNA replication, transcription and synthesis of cellular components exists.

2.5.3 One-carbon metabolism

One-carbon metabolism is an interlinked network of metabolic pathways, comprising two cycles – the methionine and folate cycle – that revolve around the transfer of one-carbon units (as methyl groups carried by folate molecules), which are required for a variety of cellular processes, including the synthesis of nucleotides, the methylation of histones and DNA, as well as the synthesis of GSH (Ducker & Rabinowitz, 2017). One-carbon units are derived from a variety of dietary sources, including glucose, serine, glycine and choline, to name but a few. Interestingly, a feature not commonly mentioned is the link between the RC and one-carbon metabolism. Two metabolites, dimethylglycine and sarcosine, are donors of one-carbon units to the folate carrier known as tetrahydrofolate. During this process, electrons are transferred to ETF and finally introduced to Q via ETF:QO. It is worth mentioning that one enzyme in particular, known as choline dehydrogenase – which catalyses the conversion of choline to trimethylglycine – is believed among many researchers to use Q as an electron acceptor (Barrett & Dawson, 1975; Wang & Hekimi, 2016). However, further studies are required to confirm this, since the electron acceptor is not known with certainty.

2.6 Mitochondrial disease

2.6.1 Introduction

Given the plethora of cellular processes orchestrated by mitochondria, it should come as no surprise that these organelles have been implicated in many diseases. The term “mitochondrial disorder/disease (MD)” is a very broad term that can refer to any disease occurring as a result of the impairment of mitochondrial function (Chinnery & Hudson, 2013). In the scientific community, however, there remains a lack of consensus with regards to the term and it is often restricted to specifically refer to the impairment of the OXPHOS system (Niyazov *et al.*, 2016). This definition of MD will be used in further discussion.

MDs may be categorised as either primary or secondary MDs. Primary MDs arise via genetic defects that are directly involved in the biogenesis, assembly and function of the OXPHOS system, whereas secondary MDs arise via unrelated genetic defects or non-genetic factors. Unrelated genetic defects include upstream metabolic pathways that partake in energy

metabolism, such as the TCA cycle, β-oxidation, oxidation of pyruvate and AAs or defects in ROS scavenging pathways. Non-genetic factors can also have a profound effect on mitochondrial function, including chronic stress and inflammation, as well as the use of certain pharmacological drugs that are known to be mitotoxic (Picard & McEwen, 2018; Suski *et al.*, 2011).

2.6.2 Genetics of primary mitochondrial disorders

The OXPHOS system, being of bi-genomic origin, can be impaired as a result of mutations in either nDNA, which are inherited in an autosomal recessive, autosomal dominant or X-linked manner; or mtDNA, which are inherited either maternally or sporadically (Davison *et al.*, 2019). These mutations can cause deficiencies in either a single site (isolated) or multiple sites (combined) of the OXPHOS system. Examples of isolated deficiencies are mutations in structural subunits or assembly factors. In turn, combined defects typically arise due to defects that impair mtDNA replication or translation (required for the biogenesis of CI, CIII, CIV and CV of the OXPHOS system), or impair the synthesis of cofactors like Q that would affect all complexes that transfer electrons to Q (Mayr *et al.*, 2015).

Interestingly, the mutation rate of mtDNA is ten- to 17-fold higher than nDNA (Tuppen *et al.*, 2010). This can be ascribed to a number of possible reasons, including (i) the close proximity of mtDNA to the ROS generated by the RC and (ii) the continual replication of mtDNA (even in post-mitotic cells) that not only occurs at a much higher rate, but also displays a higher error rate (Li *et al.*, 2019). As a result, it has been estimated that approximately 1 in 200 of the population are asymptomatic carriers of pathogenic mtDNA mutations (Elliott *et al.*, 2008). To understand why these carriers are asymptomatic, one needs to take into account that there are multiple copies of mtDNA in each cell. This alone has a profound effect on the onset of disease, which is governed by the ratio of mtDNA copies carrying (mutant mtDNA) or lacking [wild-type (WT) mtDNA] the mutation in a cell – a state referred to as heteroplasmy. This is in contrast to homoplasmy, where 100% of all mtDNA copies are identical. As illustrated by Figure 2.3, the proportion of mutant mtDNA needs to exceed a certain threshold for the onset of disease to occur (known as the threshold effect) (DiMauro & Paradas, 2015), with greater mutation loads above the threshold generally displaying increased disease severity (Burr *et al.*, 2018; Craven *et al.*, 2017). This threshold is high and may vary between 60-90%, depending on the location and type of mutation (Amato *et al.*, 2014).

The degree of heteroplasmy, however, is not static, but can fluctuate and thus have an effect on whether the phenotypic threshold will be breached or not. This fluctuation can occur (i) during mitotic segregation, where WT and mutant mtDNA are randomly distributed (DiMauro & Paradas, 2015); and (ii) during the bottleneck effect, which refers to the transmission of a very small

percentage of the mtDNA population during germline development, which could result in offspring having variable levels of mutant mtDNA (Craven *et al.*, 2017; Wallace, 2018).

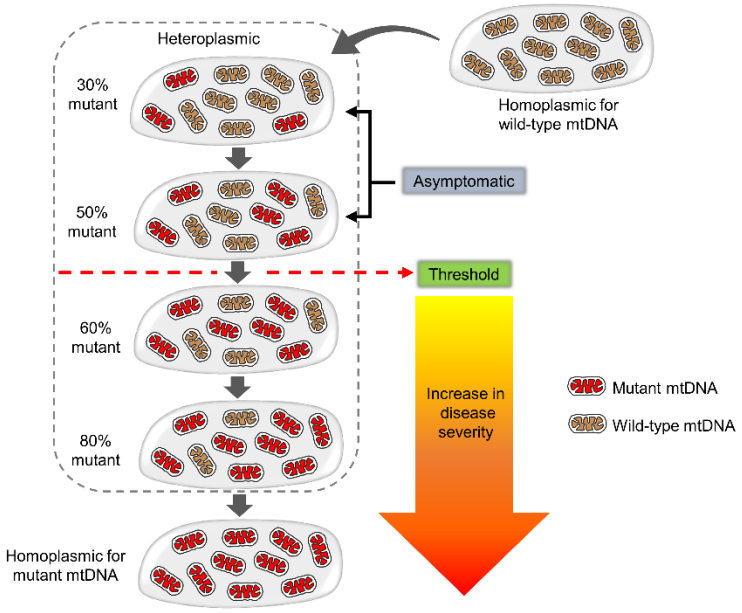

Figure 2.3: Heteroplasmy and the threshold effect. Schematic representation illustrating the concept of how the onset of mtDNA-related MD is governed. Cells containing a percentage of mutant mtDNA below the threshold effect (indicated by the dashed, red line) do not cause impairment of the OXPHOS system (carriers are thus asymptomatic). However, when the percentage of mutant mtDNA breaches the threshold (cells located below the threshold), the onset of disease occurs. Disease tends to be more severe, with higher mutation loads above the threshold (indicated by the progressive colour change of the arrow, where: yellow = least severe; red = most severe). Abbreviations: MD, mitochondrial disorder/disease; mtDNA, mitochondrial DNA; OXPHOS, oxidative phosphorylation.

2.6.3 Heterogeneity of primary mitochondrial disorders

MDs display a high level of heterogeneity in terms of clinical presentation. The onset of MDs can occur at any age and affect any tissue; however, it mainly affects tissues with high energy demands such as the skeletal muscle, brain and heart (Liang *et al.*, 2014). Furthermore, these disorders can affect either a single organ (e.g. the eyes in Leber's hereditary optic neuropathy), or, as seen most often, be multi-systemic. In a few cases, depending on the combination of symptoms, multi-systemic MDs will fall into a well-defined syndrome [e.g. mitochondrial encephalomyopathy, with lactic acidosis and stroke-like episodes (MELAS)] (Davison *et al.*, 2019).

Unfortunately, to date, diagnosing MDs remains a challenge, since these disorders display very little genotype-phenotype correlation. In other words, there is an overlap, where identical or

different DNA mutations, respectively, result in variable or similar clinical presentations (Liang *et al.*, 2014). This suggests that other factors, which determine the final outcome of genetic defects, are at play, and could include: (i) the random distribution of mutant mtDNA during embryonic development, which leads to different mutation loads in various somatic tissues (Kirches *et al.*, 2001; Lee *et al.*, 2006); (ii) the differences in genetic background, where the expression of genes known as modifier genes can influence the expression or function (and thus the cellular effect) of other genes (Bénit *et al.*, 2010; Brown, 1997); and (iii) environmental factors such as macronutrient composition (Aw *et al.*, 2016), medication, gut microbiome-host interactions and viral infections (Vafai & Mootha, 2012).

2.6.4 Metabolic consequences of mitochondrial disorders

As reviewed in the previous sections, the RC is not only linked to the phosphorylation of ADP, but many other biochemical processes as well. It can thus be expected that any disturbance of the RC will consequently affect those processes as well. The consequences of MDs, however, are vast and beyond the scope of this literature review. This section will therefore not provide an exhaustive review of every cellular consequence.

One of the most well-known observations in MD is an alteration in the redox status of the cell. NADH is generated in many metabolic pathways and the re-oxidation thereof is imperative for the efficient continuation of those pathways (Handy & Loscalzo, 2012). A defect in the OXPHOS system leads to a lowered NAD^+/NADH ratio, thereby impairing NAD^+-dependant enzymes; this subsequently results in the accumulation of upstream metabolites and the “spillover” of some metabolites into other metabolic pathways. The mechanism by which the redox status is altered will depend on where the defect lies in the OXPHOS system. For example, in CI defects, NADH levels will increase, either due to impairment in the catalytic site of CI, or the transfer of electrons through CI to Q (Smeitink *et al.*, 2004). However, in the case of defects in other upstream complexes such as CIII and CIV, in which an altered redox status is also observed, NADH accumulation is the result of an over-reduced RC downstream instead, which ultimately hinders oxidation of NADH due to the over-reduced state of the electron acceptor, flavin mononucleotide (FMN) in CI.

MD frequently causes increased levels of lactate, pyruvate and alanine, due to the impairment of pyruvate dehydrogenase, which forms part of the pyruvate dehydrogenase complex (PDHc) (Esterhuizen *et al.*, 2017). Accumulated pyruvate is then destined to either be converted to lactate via lactate dehydrogenase (which re-oxidises NADH and permits the continuation of glycolysis), or to alanine via alanine aminotransferase. Increased glycolytic activity, indicated by increased glycolytic intermediates, is another factor that contributes to the accumulation of pyruvate in order

to compensate for decreased ATP levels via substrate-level phosphorylation (Maldonado & Lemasters, 2014).

The accumulation of the TCA cycle intermediates also occurs due to the altered redox status, as it contains three NAD^+-dependant dehydrogenases (Esterhuizen *et al.*, 2017). One of the accumulated intermediates, namely 2-ketoglutarate, also results in accumulated 2-hydroxyglutarate, due to the conversion thereof via malate dehydrogenase. The congested TCA cycle also impairs the entrance of acetyl-CoA, which leads to increased levels of ketone bodies (acetoacetate and 3-hydroxybutyrate) as accumulated acetyl-CoA is diverted towards ketogenesis, re-oxidising NADH in the process.

Perturbations in fatty acid and AA catabolism are also observed as a result of an altered redox status (Esterhuizen, 2018). In β-oxidation, the incomplete oxidation of fatty acids is often observed due to the impairment of the third NAD^+-dependent reaction, which leads to the accumulation of upstream metabolites, such as 3-hydroxy-acyl-carnitines and acyl-carnitines. In AA catabolism, the lower NAD^+ levels may also explain the accumulated metabolites, indicating perturbations in some AA catabolic pathways. This includes the inhibition of branched chain 2-ketoacid dehydrogenase complex activity, resulting in elevated levels of 2-ketoisocaproate, 2-keto-3-methylvalerate and 2-ketoisovalerate in leucine, isoleucine and valine catabolism, respectively. Elevated 2-ketobutyrate and 2-hydroxybutyrate are also seen in MD. Methionine and threonine catabolism result in 2-ketobutyrate, which is oxidised to propionate and thereafter to succinyl-CoA, through a series of enzyme reactions. However, an altered redox status will inhibit 2-ketobutyrate dehydrogenase, leading not only to accumulated 2-ketobutyrate, but also to 2-hydroxybutyrate, due to the conversion of 2-ketobutyrate via lactate dehydrogenase. The redox status is not limited to these well-documented metabolites and pathways. More recently, one-carbon metabolism has also been identified as an affected pathway in mitochondrial OXPHOS dysfunction (Bao *et al.*, 2016; Nikkanen *et al.*, 2016). This methylation cycle and transsulfuration pathway forms an intricate web of pathways that are also regulated by the redox status.

Apart from the redox status, it has been reported that fatty acid and AA catabolism are also perturbed by increased levels of reduced flavin adenine dinucleotide (FAD)-flavoproteins, which are indicative of elevated metabolites (Chokchaiwong *et al.*, 2019). ETF:QO accepts electrons from ETF, which in turn accepts electrons from a variety of acyl-CoA dehydrogenases located in the fatty acid and AA catabolism. In the case of a defective ETF:QO enzyme or an impaired ETC, especially upstream from Q, electron transfer from ETF:QO to Q will be inhibited. This will consequently result in an over-reduced state of the upstream flavoproteins. In fatty acid catabolism, this will inhibit the first step, leading to accumulated levels of acylcarnitines.

A second direct consequence of OXPHOS defects is a decrease in ATP synthesis (Rodenburg, 2016). A decrease in ATP synthesis will lower GSH levels, since the synthesis thereof requires two ATP-dependant reactions (Hargreaves *et al.*, 2005; Lindeque *et al.*, 2010). A decrease in GSH, being the most abundant antioxidant, can significantly decrease ROS scavenging capabilities, thus increasing $OH^{\bullet}$ as a result of increased combinations of super oxide and H_2O_2, thereby causing oxidative stress. In turn, oxidative stress can lead to damaged mitochondrial content, subsequently causing secondary mitochondrial dysfunction and ultimately, cell death. Oxidative stress can also occur independently of decreased ATP synthesis, due to an impairment in the OXPHOS system, leading to increased electron leakage.

2.6.5 Complex I deficiency and Leigh syndrome

Isolated CI deficiencies are the most common biochemical basis in patients with MDs/OXPHOS deficiencies (Loeffen *et al.*, 2000; Scaglia *et al.*, 2004; von Kleist-Retzow *et al.*, 1998). CI, otherwise known as NADH:ubiquinone oxidoreductase (EC 1.6.5.3.), is the largest complex (Mw ~ 980 kDa) of the OXPHOS system and is the largest contributor to the generation of the electrochemical gradient (approximately 40%) (Hunte *et al.*, 2010). As illustrated in Figure 2.4, it has a characteristic boot or L-shape structure, consisting of a hydrophobic arm residing in the IMM, and a hydrophilic peripheral arm protruding into the MM.

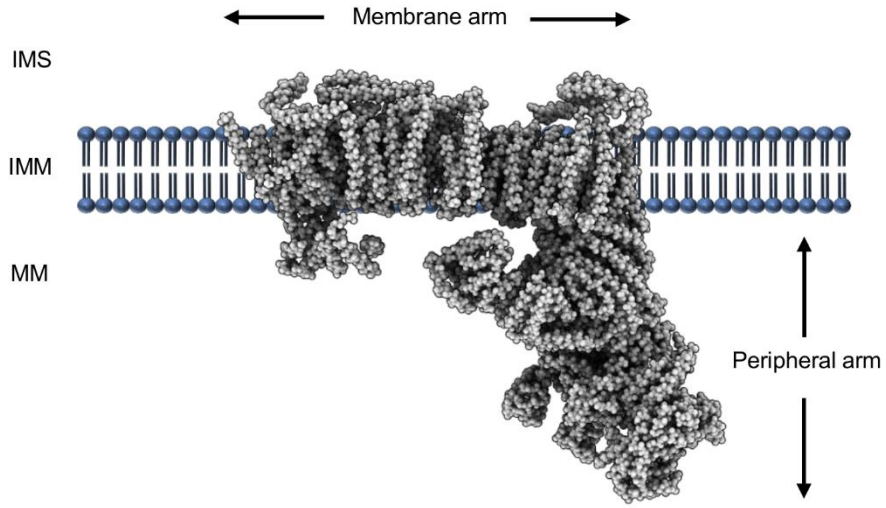

Figure 2.4: Structure of CI. Schematic representation of CI, depicting its characteristic boot or L-shaped structure. The structure consists of two arms: one embedded in the IMM and the other protruding into the MM. The representation of CI is based on the bovine heart cryo-electron microscopy structure (PDB 4UQ8 generated in QuteMol version 0.4.1) (Vinothkumar *et al.*, 2014). Abbreviations: CI, complex I; IMM, inner mitochondrial membrane; IMS, intermembrane space; MM, mitochondrial matrix.

In total, CI consists of 44 subunits, which are encoded by both nDNA and mtDNA (Rodenburg, 2016), and requires at least 14 assembly factors for the assembly thereof (Guerrero-Castillo *et al.*, 2017). Fourteen of the 44 subunits form the "catalytic core" of the enzyme, which is responsible for catalysing the energy transducing reactions, namely NADH oxidation, Q reduction and proton translocation. Of these 14 core subunits, the hydrophilic arm contains seven nuclear-encoded subunits and harbours an FMN required to oxidise NADH, as well as a series of iron-sulfur clusters required for the transfer of electrons from FMN to Q. The final seven mitochondrial-encoded subunits are located in the hydrophobic arm, which contains the proton translocation domains. Based on these energy-transducing steps, CI can be divided into three functional modules: (i) the N (NADH-binding) module, where electrons are extracted from NADH; (ii) the Q (ubiquinone-binding) module, where Q is reduced; and (iii) the P (proton-binding) module, where protons are transported into the IMS (Brandt, 2006). The remaining 30 subunits, which surround the core subunits, are referred to as accessory or supernumerary subunits. While the function of these subunits is not yet completely understood, some seem to be involved in the assembly, structural stability and regulation of CI function (Kmita & Zickermann, 2013).

Given the large number of subunits that comprises CI, it should come as no surprise that deficiencies therein are also the most prevalent in MDs. To date, pathogenic mutations have been identified in all of the catalytic subunits, 12 accessory subunits and nine assembly factors (Rodenburg, 2016; Simon *et al.*, 2019). These mutations manifest in a variety of commonly observed clinical phenotypes, including fatal infantile lactic acidosis, leukoencephalopathy, MELAS and cardiomyopathy (Fassone & Rahman, 2012).

The most prevalent clinical presentation seen in patients with CI deficiency, however, is Leigh syndrome (LS) (Bugiani *et al.*, 2004; Koene *et al.*, 2012) – a disorder named after the British psychiatrist Denis Leigh, who first reported the condition in 1951 (Leigh, 1951). LS (also known as subacute, necrotising encephalopathy) is a devastating, progressive, neurodegenerative disorder affecting approximately 1 in 40 000 new-borns (Chen *et al.*, 2018; Rahman *et al.*, 1996). It is characterised by bilateral symmetrical focal lesions in various parts of the central nervous system, such as the basal ganglia, brainstem, cerebellum and spinal cord (Lake *et al.*, 2015). Ever since the discovery of the first mutation for LS in 1991 (Chen *et al.*, 2018; Hammans *et al.*, 1991), mutations have been identified in more than 75 genes, which may cause deficiencies in CI-V, multiple OXPHOS complexes, the PDHc, Q and biotinidase (Lake *et al.*, 2016). LS, however, is primarily caused by defects in CI (Ma *et al.*, 2013; Rahman *et al.*, 1996; Sofou *et al.*, 2014).

2.7 *Ndufs4* knockout mouse model

Even though MDs are the most common inborn errors of metabolism, the group remains rare as a whole. Consequently, this prevents researchers from conducting intensive and continuous research, in an attempt to gain a better understanding of the pathological mechanisms involved (Koene *et al.*, 2011). The only option remaining to accelerate research into MDs, is to utilise disease models. Of particular value are mouse models, which offer numerous advantages, including: (i) a homogenous genetic background; (ii) a physiology similar to humans; (iii) the benefit of controlled environmental conditions; (iv) greater group sizes due to shorter gestation periods and large numbers of offspring; and (v) a shorter life expectancy, which is beneficial for studying the progression of diseases.

The *Ndufs4* whole-body knockout (KO) mouse model, which was developed by the Palmiter group, represents the first genetic mouse model of CI deficiency (Kruse *et al.*, 2008). The *Ndufs4* gene, which encodes for an 18 kDa accessory subunit of CI, known as NDUFS4 (nuclear-encoded NADH:ubiquinone oxidoreductase iron-sulfur protein 4), is commonly affected in patients with LS (Ortigoza-Escobar *et al.*, 2016). The subunit, which forms part of the N module of CI, is incorporated during the late stage of CI assembly and appears to be essential for the assembly, stability and activity of CI (Guerrero-Castillo *et al.*, 2017). In this model, the *Ndufs4* gene was inactivated in the germline by crossing mice of which the second exon of *Ndufs4* had been flanked by *loxP* sites [locus of X(cross)-over in P1 sites] with Mox2-Cre mice (mesenchyme homeobox 2-cre mice), thereby resulting in the deletion of exon 2 from the five-exon gene (Kruse *et al.*, 2008).

2.7.1 Phenotype

At postnatal day 21 (P21), the majority of *Ndufs4* KO mice appear physically smaller than the *Ndufs4* WT and heterozygous (HET) mice, and will have begun to display transient alopecia (hair loss), with hair growing back during the next hair-growth cycle. HET mice, however, do not display symptoms and are indistinguishable from WT mice. Prior to P30, the KO mice display normal locomotor activity, show behaviour similar to control mice and reach a maximum weight at approximately P30. At around P35, the onset of disease becomes apparent, with the *Ndufs4* KO mice displaying symptoms similar to LS patients, including encephalopathy, blindness, hypotonia and ataxia, which result in early fatality at a median age of P50 (Kruse *et al.*, 2008).

2.7.2 Altered bioenergetics and metabolism

Whole brain metabolomics in *Ndufs4* KO mice (Johnson *et al.*, 2013) further reveals an altered metabolism similar to that seen in LS patients. This includes an increase in lactate and pyruvate

levels, indicating an altered redox status. There is also a shift towards a glycolytic state due to an increase in glycolytic intermediates and lowered AAs/fatty acids.

Elevated levels of fumarate have also been reported in this model. In a study conducted by Piroli *et al.* (2016), fumarate is believed to be a potential biomarker, contributing to the neuropathology of this disease. Here, increased fumarate levels led to an increase in irreversible protein succination in the brainstem, which has been shown to decrease the functionality of certain proteins susceptible to succination. However, no increased protein succination was seen in the skeletal muscle. This finding seems to support other studies, in which the skeletal muscle displays normal maximum pyruvate oxidation and ATP synthesis, as well as normal polygonal morphology, with peripheral nuclei in both glycolytic and oxidative skeletal muscle (Alam *et al.*, 2015). These findings seem to suggest that this disease is neurodegenerative.

2.8 Metabolomics

Metabolomics is an emerging field that can simply be defined as the study of the metabolome, i.e. the downstream products of the genome, consisting of the complete set of metabolites within a biological fluid, cell, organ, or an organism. Since, per definition, this methodology aims to identify and quantify all metabolites within a defined biological system, it is an unbiased approach that is conducted to provide a "global snapshot" of the biological system's metabolic status. However, this definition has since been abandoned; today it also refers to the investigation of pre-determined sets of metabolites. This has led to metabolomics being categorised as either untargeted (unbiased) or targeted (a pre-determined set of metabolites). With this taken into consideration, one can thus state that metabolomics is much older, and in truth, a re-emerging field (with the introduction of untargeted analyses), as technologies used in metabolomic studies today have long been used in the study of inborn errors of metabolism (Esterhuizen *et al.*, 2017).

Since the metabolome is the endpoint of cellular processes, its study can overcome many limitations observed in other methods of studying MDs. In many cases, such analyses lack the capability to discriminate between different MDs, even though metabolite analyses have been performed for decades, since some of these diseases show the same metabolite profile. Therefore, additional analytical techniques are required in order to obtain the correct diagnosis. For example, a study conducted by Reinecke *et al.* (2012) reported no metabolite profile differences between CI, CIII and combined deficiencies (combinations of CI, CII, CIII and CIV deficiency) in urine samples. This could be due to the targeted approach utilised (organic acid extraction), which excluded a significant number of metabolites that could possibly have provided differentiation between the above-mentioned deficiencies. Another popular technique used in diagnostic work, is enzyme analyses. This technique is very effective in the diagnosis of patients,

however, it also lacks discriminative power. For example, recent research has shown that CIII deficiency can also be the result of a defect in the auxiliary enzyme, DHODH (Fang *et al.*, 2013). Since diagnostic laboratories typically measure only the activities of complexes that form part of the classic RC model (CI-IV), it could also very well explain why the origin of many complex deficiencies remains unknown. Metabolomics (especially an untargeted approach) has the potential of eliminating the need for additional analytical techniques or, at the least, being highly complementary. Since the metabolome is the end point of cellular activity, and thus the closest to a patient's phenotype, it has the potential of providing novel biomarkers and ultimately a biosignature, which comprises a number of biomarkers unique to a specific disease. This biosignature would not only be beneficial in diagnostics, but also in research, as it may provide insight into the pathologic mechanisms, and further researchers' understanding of diseases, with the potential of developing novel therapeutic interventions.

Deciding on which metabolomics approach to use will depend on whether the research question is hypothesis-generating, or whether a hypothesis must be tested. Untargeted metabolomics is the ideal route in generating a hypothesis, since it is an unbiased approach and aims at potentially revealing perturbed metabolic pathways and novel metabolites. Therefore, it is also known as discovery metabolomics. A targeted approach, although not ideal, can also be used should a specific group of metabolites be in question (Esterhuizen *et al.*, 2017). Once a hypothesis has been generated through untargeted studies, targeted approaches that can validate the suspected metabolites typically follow, since they provide much higher sensitivity and selectivity.

Metabolomic studies can be further categorised based on the type of quantification applied, which can be either quantitative, or semi-quantitative (Liu & Locasale, 2017). Quantitative metabolomics aims to accurately quantify metabolites by providing absolute concentrations using calibration curves and stable isotopes. Semi-quantitative metabolomics on the other hand, aims to provide relative concentrations and is seen in both untargeted and targeted studies, since obtaining stable isotopic labelling (SIL) for hundreds/thousands of metabolites is unfeasible in terms of price and availability.

It is important to mention that even though untargeted metabolomics is unbiased, since no prior knowledge of any metabolite is brought into consideration (i.e. the assay is thus non-selective), bias is unavoidable and can be inherently introduced at various stages of a metabolomic assay, including via the type of sample preparation applied and analytical instrument used, to name but a few (Liu & Locasale, 2017). The metabolome, being so diverse in chemical properties (including polarity, volatility, chemical reactivity/stability) and concentrations, makes it impossible to capture the entire metabolome, since the sample preparation applied and the analytical instrument used are biased towards certain chemical properties.

Therefore, designing a metabolomics study (i.e. selecting the sample preparation and analytical instrument) is extremely important in order to capture as much of the metabolome within a sample as possible. Even when these considerations are taken into account, the outcome of an untargeted approach will only be improved to a certain degree. To further overcome this, many researchers incorporate multiple analytical platforms that significantly improve overall metabolic coverage. This approach is more laborious, but if gaining a better understanding of the metabolism is the primary goal, it should be the deciding factor when considering to follow such an approach, if of course, sufficient funding and multiple instruments are available (Esterhuizen *et al.*, 2017).

2.9 Problem statement, aim, objectives and experimental strategy

2.9.1 Problem statement

To date, the available treatment options for MDs are not only limited (Dimond, 2013; Lehmann & McFarland, 2018), but, as concluded by Pfeffer *et al.* (2012), lack compelling evidence to support their use. This can most likely be attributed to the poor genotype-phenotype correlation (i.e. the high degree of heterogeneity) observed in patients (Pfeffer *et al.*, 2012; Rahman & Rahman, 2018), which consequently makes gaining a greater insight into the pathological mechanisms of these highly complex and elusive diseases, extremely difficult (Rahman & Rahman, 2018; Vafai & Mootha, 2012). Thus, the use of mouse models is extremely valuable in order to limit the phenotypic variability, particularly due to the homogenous genetic background they provide, as well as the controlled environmental conditions that can be applied, thereby aiding researchers to obtain sounder conclusions. Although limited mouse models of MDs exist (Ruzzenente *et al.*, 2016), a successful whole-body KO mouse model has been generated by Kruse *et al.* (2008), which mimics the most common clinical presentation observed in MD, namely LS.

From a methodological perspective, the poor understanding of the pathological mechanisms involved can also be attributed to the limited incorporation of metabolomics in MD research (Esterhuizen *et al.*, 2017). With the metabolome being the end-point of all cellular processes, and therefore a representation of the phenotype, the use of metabolomic technologies can shed new light on the pathological mechanisms of these disorders. To date, no metabolomic research on Ndufs4 KO mouse urine exists. Urine has been shown to be an important contributor to our understanding of both physiological and pathophysiological processes. In fact, the value of urine has been demonstrated throughout history by its ability to provide information on a person's health status by merely inspecting the physical properties thereof, such as the colour and odour (Bouatra *et al.*, 2013). This simple evaluation of urine has continued to be valuable in modern times in the

screening of specific metabolic diseases (Bijarnia-Mahay & Kapoor, 2019), and since the birth of metabolomics, its application on urine successfully expanded our knowledge on MDs (Esterhuizen, 2018; Reinecke *et al.*, 2012; Smuts *et al.*, 2013).

Although urine is mainly composed of H_2O, the small percentage of waste products therein – which include a vast number of metabolite classes that collectively comprise more than 2 600 confirmed metabolite species – provide a wealth of information. These metabolite species can vary greatly depending on many factors and, as such, provide a comprehensive picture of a person's overall physiological status (Bouatra *et al.*, 2013). From a practical standpoint, urine is an ideal biological specimen due to it being sterile, non-invasive in collection and lower in protein content, which makes sample preparation less tedious. Thus, when taking the above into consideration, it is only fitting that urinalysis be incorporated in the quest to understand the pathological mechanisms of *Ndufs4* deficiency.

2.9.2 Aim and study design

The **aim of this study** was, therefore, to investigate the metabolic consequences in whole-body *Ndufs4* KO mice using a urinary metabolomics approach, and was addressed via **two main objectives:** (1) the validation of the whole-body *Ndufs4* KO mouse model and (2) the urinary metabolomics analyses of the *Ndufs4* KO and WT mice.

A general overview of the study design used to address the aim is depicted in Figure 2.5. The first objective, namely to validate the *Ndufs4* KO mouse model, entailed three levels of confirmation, including: (1) genotyping of the mouse model, to confirm the deletion of exon 2 of the *Ndufs4* gene from the nuclear genome; (2) phenotypic investigation of the *Ndufs4* KO and WT mice via bodyweight monitoring and visual inspection (♂: WT = 3, KO = 2; ♀: WT = 4, KO = 3); and (3) biochemical investigation by measurement of the activity of CI of the mitochondrial RC in the liver (WT: n = 5; KO: n = 5). As indicated by the two black, dashed arrows in Figure 2.5, genotyping was conducted using tail-snips, to differentiate between *Ndufs4* KO, WT and HET mice during animal selection (for the biochemical evaluation and urinary metabolomics investigation) and genotype confirmation (for the phenotypic and biochemical evaluation, as well as the urinary metabolomics investigation). Genotyping, therefore, not only served to validate the findings obtained from the second objective, but was also used to validate the results obtained from the phenotypic and biochemical evaluations, by ensuring that incorrect mice were not included in the study, and thus, that accurate comparisons were made between the *Ndufs4* KO and WT mice.

The group of mice used for the phenotypic evaluation were separate from the group used to validate the mouse model via the biochemical evaluation and metabolomics analyses (indicated by the red, dashed line in Figure 2.5). This was done because the mice used for the phenotypic

evaluation had *ad libitum* access to food during the whole course of the evaluation (commenced at P22/23) and as already mentioned, included female mice. By contrast, the biological specimens (liver and urine samples) destined for biochemical evaluation and metabolomic analyses, were collected solely from male mice (at P45-50) and were stored for further use after the mice were housed in metabolic cages for 12 hours with *ad libitum* access to only water.

For the second objective of this study, a pre-acquisition normalisation approach was followed, where the amount of each urine sample used was based on a fix amount of creatinine. The urine samples were prepared and analysed according to each analytical platform (untargeted GC-TOF-MS and targeted LC-MS/MS). The acquired data from both platforms were then extracted and subjected to several data processing steps and evaluation procedures to minimise irrelevant data (e.g. noise, highly variable peaks, sample outliers, etc.) and ensure data reliability. Thereafter, univariate statistical analysis was performed to identify variables/metabolites of which the quantity differed between the *Ndufs4* KO and WT mice (WT: n = 30; KO: n = 23), and which could be interpreted to derive insights into the metabolic consequences of *Ndufs4* deficiency in this mouse model.

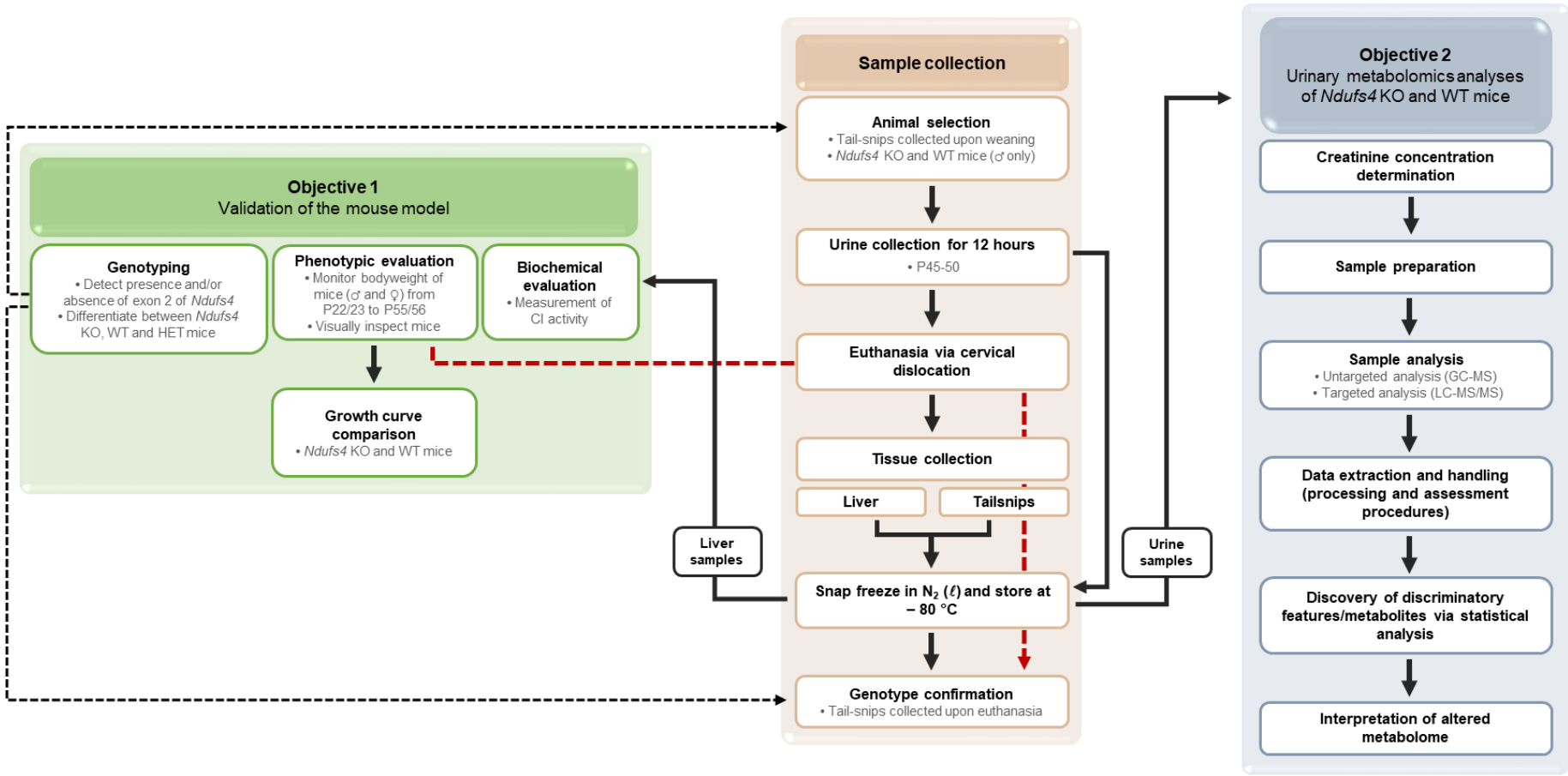

Figure 2.5: Schematic representation of the study design. The aim of the study was addressed via two objectives. The first objective (left, green panel) was conducted to validate the mouse model and consisted of: (1) genotyping (using tail-snips) to confirm the knockout of exon 2 of the *Ndufs4* gene, selection of the appropriate mice and genotype confirmation of the mice used in all investigations; (2) phenotypic investigation by bodyweight monitoring and visual inspection; and (3) biochemical investigation by measuring liver CI activity. The second objective (right, blue panel) entailed the urinary metabolomics investigation where both an untargeted and targeted metabolomics approach was incorporated. Symbols: ♀, female; ♂, male. Abbreviations: CI, complex I; GC-TOF-MS, gas chromatography time-of-flight mass spectrometry; HET, heterozygous; KO, knockout; LC-MS/MS, liquid chromatography-tandem mass spectrometry; P, postnatal day; WT, wild-type.

CHAPTER 3:
MATERIALS AND METHODS

3.1 Ethical approval

This study was approved in 2015 by the AnimCare Ethics Committee of the North-West University (NWU), with the reference number: NWU-00001-15-S1.

3.2 Materials and chemicals

Refer to Appendix A for information regarding the materials/chemicals used in the methods that follow.

3.3 Experimental animals, housing and identification

Ndufs4 HET mice acquired from the Jackson Laboratory (ME, USA) were used to breed the *Ndufs4* KO mice (B6.129S4-*Ndufs4*$^{tm1.1Rpa}$/J) and controls (wild-type, WT). The mice were housed at the Vivarium of the Preclinical Drug Development Platform (PCDDP, NWU) under the following conditions: a day/night cycle of 12 hours; temperature of 22°C ± 2°C; and relative humidity of 55% ± 10%. During this time, the mice had *ad libitum* access to standard laboratory chow and H_2O. For this study, male mice were used to eliminate any variation due to physiological differences between genders.

The mice were identified by assigning a unique number to each. This was accomplished by punching a hole, or multiple holes, into one or both ears in different locations, as illustrated in Figure 3.1. Each location represented a specific number, and different combinations thereof enabled the identification of mice by numbers 1-99. Furthermore, mice were additionally identified by assigning each with a litter number (e.g. 2a-2z, 3a-3z, etc.) in order to discriminate between samples with the same identification number.

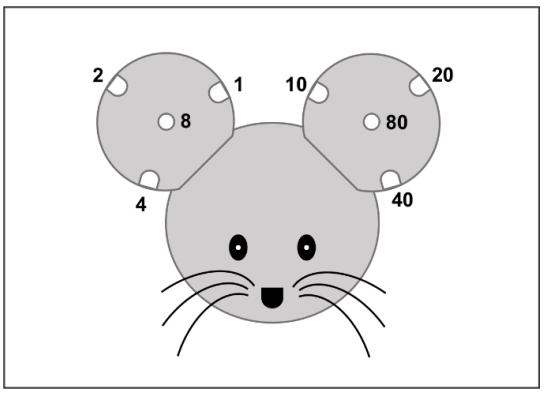

Figure 3.1: An illustration of the ear punching method used to identify mice. Each hole represents a different number that can be used as a standalone, or in combination with other holes, to assign each mouse with an identification number ranging from 1-99. For example, punching the centre of both ears will assign a mouse with the number 88.

3.4 Phenotypic evaluation of the *Ndufs4* knockout mice

For the phenotypic evaluation, mice derived from two litters were evaluated to monitor disease progression. Here, mice were evaluated by means of bodyweight monitoring and visual inspection every second day. KO mice were euthanised after losing 10% of their bodyweight. Thereafter, the genotypes of all mice were determined that left a total of 3 WT and 2 KO male mice, and 4 WT and 3 KO female mice for phenotypic comparison.

3.5 Sample collection

The male mice that were used for the biochemical (Section 3.7) and metabolomic analyses (Section 3.8), were housed individually in metabolic cages for 12 hours, during the night cycle, with *ad libitum* access to only H_2O. The urine collection tubes of the WT and KO mice contained 100 µl and 50 µl sodium azide (NaN_3; 0.1% w/v), respectively. A smaller volume of NaN_3 was added to the urine collection tubes of the KO mice in order to prevent over-dilution, since these mice yielded less urine. In order to collect as much KO mouse urine as possible, the cages' separating cone and collection funnel were treated with NaN_3 solution using a paper towel. This was done to prevent bacterial growth in the urine droplets that did not reach the urine collection tube, thereby ensuring the urine remained viable for experimental use. For consistency, the same was done for the cages housing the WT mice. After 12 hours, the urine samples were collected from each cage and transferred to microcentrifuge tubes. For each cage, additional NaN_3 solution (approximately 200-250 µl) was used to collect the urine that had failed to reach the urine collection tube. Using a pipette, the additional NaN_3 was gently pipetted up and down the slightly

dried urine to ensure proper reconstitution, and transferred to the microcentrifuge tube. Following urine collection, the mice were euthanised (P45-50) via cervical dislocation. A tail-snip and the liver of each were collected for genotype confirmation (Section 3.6) and biochemical analysis, respectively. The urine, tail-snip and liver samples were immediately snap-frozen in liquid nitrogen upon collection and stored at -80°C until further use. Samples were collected from a total of 35 WT and 31 KO mice, of which 5 WT and 5 KO liver samples were randomly selected for biochemical analysis.

3.6 Genotyping

Genotyping was performed twice using DNA derived from the tail-snips collected (i) upon weaning (P21-23) of the mice, as a means of initial identification, and (ii) from euthanised mice, to confirm the genotype of the animals used in the experiments.

3.6.1 DNA extraction and quantification

DNA isolation was performed using the Quick-DNA™ Miniprep Plus Kit. The tail-snips (~ 3 mm) were firstly digested by adding 95 µl nuclease-free H_2O, 95 µl 2x Digestion Buffer and 10 µl Proteinase K to each sterile microcentrifuge tube containing a tail-snip. Samples were then vortexed for 15 seconds and incubated at 55°C for approximately 2.5 hours. After incubation, 400 µl Genomic Binding Buffer was added to each sample to allow the DNA to bind to the silica column and the samples were vortexed for 15 seconds. Samples were then centrifuged at 12 000 *xg* for 1 min to remove the insoluble debris. Next, the supernatant was transferred to a Zymo-Spin™ IIC-XL Column inserted in a collection tube and centrifuged at 12 000 *xg* for 1 min. The DNA in the Zymo-Spin™ IIC-XL Column then underwent three purification steps, each of which consisted of adding a buffer, followed by centrifugation at 12 000 *xg* for 1 min and disposal of the filtrate. For the first step, 400 µl DNA Pre-Wash Buffer was used, followed by 700 µl and 200 µl of g-DNA Wash Buffer during the second and third wash steps, respectively. Next, the Zymo-Spin™ IIC-XL Column was transferred to a clean 1.5 ml microcentrifuge tube and the DNA was eluted by adding 25 µl pre-warmed (to 65°C) DNA Elution Buffer, followed by incubation at room temperature for 5 min. Thereafter, the reaction was centrifuged at 16 000 *xg* for 1 min. The elution step was performed twice to increase the DNA yield.

The isolated DNA was then quantified using the NanoDrop® 1000 Spectrophotometer (NanoDrop Technologies, Thermo Fisher Scientific™, MA, USA) by measuring the ultraviolet absorbance thereof at a wavelength of 260 nm. The sample DNA concentrations were subsequently adjusted to 25 ng/µl, using nuclease-free H_2O.

3.6.2 DNA amplification by polymerase chain reaction

DNA amplification was performed via the polymerase chain reaction (PCR). The primers used (purchased from Inqaba Biotec, Pretoria) were originally designed by Valsecchi *et al.* (2012) and corresponded to the introns flanking exon 2 (Table 3.1):

Table 3.1: Sequences of the PCR primers

Primer	Primer sequence (5' to 3')	T_m (°C)	Size (bp)
NDUFS4 1060 (Forward)	AGC CTG TTC TCA TAC CTC GG	62.45	20
NDUFS4 (Reverse)	TTG TGC TTA CAG GTT CAA AGT GA	59.2	23

Abbreviations: 5' to 3', direction of the polynucleotide, i.e. from the 5'-end to the 3'-end; T_m, melting temperature.

Each reaction consisted of 1 µl sample (containing 25 ng DNA), mixed with 5 µl 2X Phire™ Tissue Direct PCR Mastermix, 0.5 µl of both the forward and reverse primers and 3 µl nuclease-free H_2O. The samples were subjected to PCR using a T100™ Thermal cycler (Bio-Rad, Pretoria), according to the following conditions: Firstly, the DNA was denatured by incubating the samples at 98°C for 5 min. This was followed by 35 cycles of DNA denaturation, primer annealing and DNA elongation at 98°C for 5 seconds, 57.3°C for 5 seconds and 72°C for 20 seconds, respectively. Finally, the samples were incubated at 72°C for 1 min to ensure the complete amplification of all amplicons. The samples were then kept at 4°C until further use.

3.6.3 DNA characterisation by agarose gel electrophoresis

After completion of the PCR, the amplicons were separated by electrophoresis on a 1% agarose gel containing 5 µg/ml ethidium bromide in 1x Bionic™ Buffer. To achieve this, 10 µl of each diluted [30% (v/v)] sample (including the WT, KO and HET controls) was loaded per well (the samples already contained loading dye, present in the Phire™ Tissue Direct PCR Mastermix). In addition, 10 µl of diluted [30% (v/v)] GeneRuler™ 100 bp DNA Ladder (containing a 2:1:3 ratio of DNA ladder:6x DNA loading dye:nuclease-free H_2O) was loaded on the left side of the gel as a DNA size reference. Gel electrophoresis was initiated by applying a voltage of 40 V to the gel container, which was submerged in 1x Bionic™ Buffer. The voltage was then adjusted to 75 V once the DNA bands had migrated from the wells, after which electrophoresis continued for approximately 1 hour. Finally, following electrophoresis, the gel was photographed under ultraviolet light (UV) illumination using the ChemiDoc™ MP Imaging System with Image Lab software (version 5.2.1; Bio-Rad).

The genotypes were identified based on the expected amplicon sizes of the WT, KO and HET DNA bands. As illustrated in Figure 3.2, the first lane in the gel contained a DNA ladder of 100-1 000 bp fragments, while lanes 3, 4 and 5 contained the amplicons of the KO, WT and HET control DNA, respectively. Depending on the presence of the *Ndufs4* mutation, PCR amplification yielded the following amplicons:

- WT amplicon: ~ 1 229 bp, signifying the intact *Ndufs4* gene on both alleles.
- KO amplicon: ~ 429 bp, signifying the disrupted *Ndufs4* gene – shortened by 800 bp (which includes exon 2) – on both alleles.
- HET amplicon: ~ 1 229 bp and ~ 429 bp, signifying the intact and disrupted *Ndufs4* gene on the first and second allele, respectively.

In addition, faint bands were observed across all samples assessed in this study. These bands were considered to be PCR artefacts produced due to non-specific amplification. This did, however, not affect the validity of the genotyping assay, since the results were in agreement with that reported by Valsecchi *et al.* (2012) and, therefore, displayed adequate specificity to allow the differentiation between the WT, KO and HET genotypes.

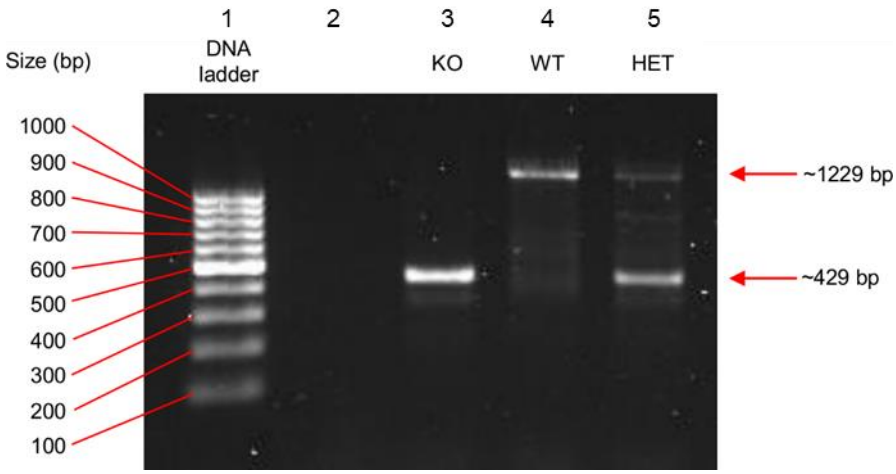

Figure 3.2: Photographic example of the genotyping results obtained following agarose gel electrophoresis. A representative agarose gel depicting a 100-1 000 bp DNA ladder in lane 1 (band sizes indicated to the far left in bp) and the following PCR products (band sizes indicated to the far right in bp) used for genotype identification: KO (lane 3; ~ 429 bp), WT (lane 4; ~ 1229 bp) and HET (lane 5; ~ 1229 bp and ~ 429 bp). Abbreviations: DNA, deoxyribonucleic acid; HET, heterozygous; KO, knockout; WT, wild-type.

3.7 Biochemical assays

This section describes the kinetic spectrophotometric analysis of CI and citrate synthase (CS) according to standardised methodology applied in routine diagnostics at the Mitochondrial Research Laboratory (NWU), based on previously published methods (Janssen *et al.*, 2007; Shepherd & Garland, 1969). These standard operating procedures, originally standardised on human muscle, were modified (results not shown) for the analysis of 600 *xg* supernatants derived from liver samples (WT: n = 5; KO: n = 5) by establishing the required sample volume. The assays were performed on a Synergy™ HT Multi-detection microplate reader (BioTek® Instruments, VT, USA).

3.7.1 Preparation of liver samples

A 10% (w/v) liver homogenate was prepared by suspending small (dissected) pieces of liver in an isotonic buffer (e.g. 100 mg sample per 1 000 µl buffer), consisting of 210 mM mannitol; 70 mM sucrose; 5 mM 2-[4-(2-hydroxyethyl)piperazin-1-yl]ethanesulfonic acid (HEPES); and 0.1 mM ethylene glycol tetraacetic acid (EGTA); pH 7.2. Thereafter, the suspension was homogenised on ice (15 strokes) using a motor-driven glass/Teflon® Potter Elvehjem homogeniser. The homogenate was then centrifuged at 600 *xg* at 4°C for 10 min to remove unbroken cells, nuclei and other cellular debris. Next, the supernatant containing the mitochondrial fraction was transferred to a new microcentrifuge tube and stored at -80°C until further use. Prior to its use in the assays that followed, each sample was thawed and subjected to an additional two freeze-thaw cycles (at -80°C) in order to disrupt the mitochondrial membranes.

3.7.2 Determination of protein content

The protein content of each sample was determined using the bicinchoninic acid (BCA) method, as originally described by Smith *et al.* (1985). The principle of the assay is based on the reduction of cupric ions (Cu^{2+}) to cuprous ions (Cu^{+}) in an alkaline solution by AA residues (cysteine, tyrosine and tryptophan) and peptide bonds in proteins. Following the reduction of Cu^{2+}, a BCA-Cu^{+} complex is formed, which results in an intense purple colour that can be measured spectrophotometrically at a wavelength of 562 nm.

In this assay, 20 µl of diluted [10% (v/v)] 600 *xg* supernatant was mixed with 200 µl working solution [50:1 (v/v) BCA:$CuSO_4.5H_2O$], in triplicate, in a 96-well plate. The plate was then incubated at 37°C for 30 min (in the Synergy™ HT Multi-detection microplate reader), and the absorbance of each reaction was measured at 562 nm. From these values, absolute quantities of protein (in µg/µl) were calculated against a standard curve, set up using 0-20 µg of bovine serum albumin (BSA) as a reference protein.

3.7.3 Citrate synthase enzyme activity

CS, a well-known mitochondrial marker, was used to normalise CI activity in order to compensate for the variation in the mitochondrial content of each sample. The enzyme assay performed is based on the reaction between CoA-SH (CoA with a thiol group), which is released during the condensation of oxaloacetate, and acetyl-CoA via CS, and 2,2'-dinitro-5,5'-dithiobenzoic acid (DTNB), which yields 2-nitro-5-thiobenzoic acid (TNB) – a yellow-coloured product that exhibits a maximum absorbance at 412 nm.

The analysis was performed by mixing, in triplicate, 10 µl of diluted [10% (v/v)] 600 *xg* supernatant with 140 µl of pre-heated (30°C) reaction mixture [0.1 mM DTNB; 0.04% (v/v) Triton™X-100; and 60 µM acetyl-CoA] in a 96-well plate. This was followed by an incubation period of 10 min at 30°C, after which the reaction was initiated by the addition of 50 µl of pre-heated (33°C) oxaloacetate (5 mM). The linear increase at 412 nm was then measured spectrophotometrically for 5 min, in 1 min intervals.

Following enzyme analysis, the initial velocity (V1 in mAU/min) was determined via the linear increase ($R^2 > 0.99$) over 2 min, using the Gen5™ Data Analysis software (version 1.11.5). V1 was then converted to micromoles of TNB using a molar extinction coefficient of 7 465 mM^{-1} per 200 µl (previously determined by a standard series of CoA and chromogen), and normalised against the protein content to obtain the specific activity of CS (Equation 3.1).

Finally, univariate statistical analysis was conducted using the student's t-test, where a p-value < 0.05 indicated a statistically significant difference between the WT and KO CS activities.

Equation 3.1

$$\mu\text{mol/min/mg (CS)} = \left(\frac{V_1}{7465} \times 0.2 \text{ ml}\right) \Big/ \left(\frac{\mu\text{l protein} \times \frac{\mu\text{g}}{\mu\text{l}}}{1000}\right)$$

$$\text{nmol/min/mg} = \text{CS} \times 1000$$

3.7.4 Complex I activity

CI activity was assessed based on a series of redox reactions, initiated by the respective oxidation and reduction of NADH and the Q analogue, decylubiquinone (DUQ), by CI. This was followed by the electron transfer from DUQ to 2,6-dichloroindophenol (DCIP), the reduction of which was measured by an increase in absorbance at 600 nm.

The assay was performed by mixing 5 µl of diluted [20% (v/v)] 600 *xg* supernatant with 125 µl of a pre-heated (30°C) reaction mixture [50 mM potassium phosphate (KPi) buffer (pH 7.4); 0.35% (w/v) BSA; 70 µM DUQ in dimethyl sulfoxide (DMSO); 1 µM antimycin A; and 60 µM DCIP]. The

reaction was initiated by the addition of 20 µl of pre-heated (33°C) NADH (2 mM) and the linear increase was measured spectrophotometrically at 600 nm for 5 min, in 1 min intervals. Samples were analysed in triplicate (i), in the presence of the CI inhibitor rotenone (2.5 µM), to account for the non-CI oxidation of NADH, and (ii) in the presence of a corresponding volume of DMSO.

Following enzyme analysis, the initial velocity (in mAU/min) was determined via the linear increase (R^2 > 0.99) over 3 min, using the Gen5™ Data Analysis software (version 1.11.5). The initial velocity of CI was calculated by subtracting the initial velocity obtained in the presence of rotenone (V2) from that obtained in the absence of rotenone (V1). This value was then converted to micromoles of reduced DCIP, using a molar extinction coefficient of 12 712 mM^{-1} per 200 µl (previously determined by a standard series of DCIP) and normalised against the protein content to obtain the specific activity of CI, expressed per unit of CS (Equation 3.2). Thereafter, univariate statistical analysis was conducted using the student's t-test, where a p-value < 0.05 indicated a statistically significant difference between the WT and KO CI activities.

Equation 3.2

$$\mu\text{mol/min/mg} = \left(\frac{V_1 - V_2}{12712} \times 0.2\ \text{ml}\right) \Big/ \left(\frac{\mu\text{l protein} \times \frac{\mu\text{g}}{\mu\text{l}}}{1000}\right)$$

$$\text{nmol/min/CS} = \mu\text{mol/min/mg} \times 1000/\text{CS}$$

3.8 Metabolomic assays

3.8.1 Determination of urinary creatinine concentration

Urinary creatinine was quantified spectrophotometrically via the Jaffe reaction method, adapted from the manufacturing protocol of the QuantiChrom™ Creatinine Assay Kit (DICT-500, BioAssay Systems, CA, USA). In this assay, creatinine reacts with picric acid in an alkaline solution to form a yellow-orange adduct, of which the increase in absorbance is measured at a wavelength of 510 nm.

Briefly, 10 µl of urine was mixed with 200 µl working solution [0.1 M sodium hydroxide (NaOH); 0.3 mM ethylenediaminetetraacetic acid (EDTA); 0.1% (v/v) DMSO; 0.0004% (v/v) Tween®20; and 3 mM picric acid], in triplicate, in a 96-well plate. Samples were then analysed on a Synergy™ HT Multi-detection microplate reader by measuring the linear increase in absorbance at 510 nm for 5 min, in 1 min intervals. Absolute quantities were calculated against a standard curve, ranging from 0-50 mg%.

All urine samples used in the metabolomic assays were analysed for creatinine on a total of four 96-well plates. To ensure repeatable creatinine quantification (and thus reliable normalisation),

the intra- and inter-plate precision was assessed by calculating the relative standard deviation (expressed as percentage; %RSD), using the test samples and two control samples derived from HET mice, respectively.

3.8.2 Sample preparation

For both untargeted [gas chromatography time-of-flight mass spectrometry (GC-TOF-MS)] and targeted [liquid chromatography-tandem mass spectrometry (LC-MS/MS)] analyses, a pre-determined volume (ranging between 20 µl and 250 µl) of urine containing 0.0625 µmole creatinine was added to microcentrifuge tubes, followed by the addition of internal standards (ISs). For untargeted analysis, 100 µl IS mixture, which contained 3-phenylbutyrate (100 ppm), norleucine (100 ppm) and tropic acid (50 ppm), was added per sample. For targeted analysis, 25 µl IS mixture was added. This mixture consisted of *N,N*-dimethylphenylalanine, $^{2}H_{4}$-arginine, $^{2}H_{4}$-citrulline, $^{2}H_{4}$-lysine, ring-$^{2}H_{5}$-phenylalanine, $^{2}H_{10}$-isoleucine, $^{2}H_{8}$-valine, $^{13}C_{4}{}^{15}N_{2}$-asparagine, $^{13}C_{5}{}^{15}N_{2}$-glutamine, $^{2}H_{3}$-acetylcarnitine, $^{2}H_{3}$-octanoylcarnitine and $^{2}H_{3}$-octadecanoylcarnitine, each with a final concentration of 2.5 ppm.

Following the addition of the IS mixture, the urine samples were deproteinised by adding three volumes of ice-cold methanol, and vortexed for 15 seconds. The samples were then incubated for 20 min at -20°C, followed by centrifugation at 15 000 *xg* for 10 min. Thereafter, the supernatant was transferred to vials and dried under a gentle stream of nitrogen gas at 37°C until dry. To ensure that the samples were completely dry prior to the derivatisation methods of both the untargeted and targeted assays, 80 µl methanol was added and the samples were dried for a second time under nitrogen gas.

3.8.3 Methoximation and trimethylsilylation

For the samples destined for GC-TOF-MS, a two-step derivatisation method was employed. Firstly, methoximation was performed by adding 50 µl methoxyamine hydrochloride (20 mg/ml in pyridine) to the dried samples; thereafter, the samples were vortexed vigorously for 30 seconds to ensure proper reconstitution, and incubated at 60°C for 60 min. During this derivatisation step, methoxyamine groups are added to the aldehyde and ketone functional groups to inhibit ring formation of the reducing sugars, which can otherwise yield a high number of peaks for one sugar. In addition, methoximation also inhibits the decarboxylation of ketoacids (Pasikanti *et al.*, 2008).

After methoximation, the samples were allowed to cool to room temperature. For the final derivatisation step, trimethylsilylation, was carried out by adding 50 µl *N,O*-bis(trimethylsilyl)-trifluoroacetamide(BSTFA):trimethylchlorosilane(TMCS) [99:1 (v/v)] to the samples, which were then mixed briefly by vortexing and incubated at 60°C for 60 min. During this reaction, trimethylsilyl groups replace active hydrogens – located on functional groups such as amino-,

carboxyl-, hydroxyl- and thiol groups. This greatly increases the volatility and thermal stability of most metabolites, which not only makes them compatible for gas chromatography, but also prevents them from thermally degrading during chromatographic separation. Finally, the samples were allowed to cool to room temperature and transferred to flat bottom inserts prior to analysis.

3.8.4 Butyl esterification

For LC-MS/MS analyses, AAs, carnitine and acylcarnitines were subjected to butyl esterification, during which the active hydrogen on the carboxyl functional group is replaced by a butyl group. To this end, 300 µl 1-butanol:acetyl-chloride [80:20 (v/v)] was added to each sample, after which the samples were vortexed for 30 seconds and incubated at 65°C for 15 min. Next, the samples were dried under a gentle stream of nitrogen at 37°C. Finally, the dried samples were reconstituted in 100 µl acetonitrile(ACN):H_2O [50:50 (v/v)] + 0.1% formic acid (FA), vortexed for 15 seconds and transferred to tapered inserts.

3.8.5 GC-TOF-MS analyses

Untargeted GC-TOF-MS analyses were carried out using a 7890A gas chromatograph (Agilent Technologies, CA, USA) coupled to a Pegasus HT time-of-flight mass spectrometer (Leco, Johannesburg). To this end, 1 µl of sample was injected with a split ratio of 1:10. The inlet temperature during sample injection was 250°C. The compounds were chromatographically separated using an Rxi-5Sil MS column (30 m x 250 µm x 0.25 µm) (Restek, PA, USA), and helium was used as a carrier gas at a constant flow rate of 1.5 ml/min. The oven temperature programme used, was as follows: The initial temperature was kept at 70°C for 1 min, after which it was elevated to 120°C (at a rate of 7°C/min). The oven temperature was then increased to 230°C (at a rate of 10°C/min), and finally to 300°C (at a rate of 13°C/min). The temperature was maintained at 300°C for 1 min before being returned to the initial temperature. Following chromatography, the eluent was introduced into the mass spectrometer, with the temperature of the transfer line set at 225°C.

For mass spectrometry, the separated compounds were subjected to electron impact ionisation (EI) (70 eV), with the ion source temperature set at 200°C. After a solvent delay of 230 seconds, mass spectra were acquired (50-950 m/z) at a scan rate of 20 spectra/second.

3.8.6 LC-MS/MS analyses

Targeted LC-MS/MS analyses of the AA-, carnitine- and acylcarnitine butyl esters were conducted on a 1200 series liquid chromatograph coupled to a 6410 triple quadrupole-mass spectrometer (Agilent Technologies). Chromatographic separation was performed by injecting samples (4 µl) on a C18 Zorbax SB-Aq (150 mm x 2.1 mm x 3.5 µm) reverse phase column (Agilent

Technologies), which was kept at 35°C, at a flow rate of 0.25 ml/min throughout the entire run. In addition, the column was equipped with a guard column to protect it against particulate matter. The mobile phases that were used included H_2O (solvent A) and ACN (solvent B), both acidified with 0.1% FA to facilitate metabolite protonation (Cech & Enke, 2001). The chromatographic gradient was started at 5% mobile phase B and maintained for 1 min, followed by an increase in mobile phase B to 18% over a period of 7 min. Next, mobile phase B was linearly increased to 100% at 16 min and maintained for 5 min. Finally, the gradient was returned to 5% mobile phase B over 3 min and maintained for 10 min (post-run) to ensure column equilibrium prior to the next analysis.

The liquid chromatography effluent was introduced to the mass spectrometer, which operated in positive electrospray ionisation (ESI) mode under the following source parameters: capillary voltage of 3 500 V; drying gas (nitrogen) at a flow rate of 7.5 l/min at 300°C; and nebuliser pressure of 30 psi. Spectra were acquired using the multiple reaction monitoring (MRM) mode at an electron multiplier voltage (EMV) of 300 V and a dwell time of 45 ms for all compounds. The compound-specific parameters pertaining to the MRM are provided in Table 3.2. During the analysis, three time windows were used. The first window diverted eluent [prior to the detection of the first analyte (< 1.4 min)] away from the column and towards the waste to limit the exposure of the mass spectrometer to salts in the sample. The MRMs of all the butyl esters were distributed among the final two time windows, thereby ensuring sufficient data points per compound peak.

Table 3.2: Compound specific mass spectrometry parameters

Compound	Precursor ion (m/z)	Product ion (m/z)	FV (V)	CE (eV)
$^{2}H_4$-Citrulline	236.2	219.1	108	5
$^{2}H_4$-Arginine	235.2	74.2	108	32
Citrulline	232.2	215.1	89	5
Arginine	231.2	70.1	103	40
1-Methylhistidine	226.4	124.2	120	15
3-Methylhistidine	226.4	96.2	130	25
5-Hydroxylysine	219.4	82.2	100	20
Carnitine	218.2	103	132	16
Histidine	212.1	110.1	89	16
$^{13}C_5{}^{15}N_2$-Glutamine	210.2	89.1	89	20
$^{2}H_4$-Lysine	207.2	88.2	118	16
Lysine/Glutamine	203.1	84.1	89	20
$^{13}C_4{}^{15}N_2$-Asparagine	195.2	148.1	89	8
Ornithine	189.2	70.2	74	20
Asparagine	189.1	74.1	89	20
Creatine	188.1	90.1	104	16
Hydroxyproline	188.1	68.1	120	35
Threonine	176.1	158.1	94	5
Isothreonine	176.1	74.1	94	12

N,N,N-trimethylglycine	174.2	58.2	130	45
Proline	172.1	70.2	94	20
Serine	162.1	60.1	94	12
N,N-dimethylglycine	160.3	58.2	90	20
4-Aminobutyrate	160.1	87.1	79	8
3-Aminoisobutyrate	160.1	30.1	100	15
3-Alanine	146.2	72.1	90	10
Sarcosine/Alanine	146.1	44.2	80	15
Glycine	132.1	76.1	65	4
$^{2}H_{3}$-Octadecanoylcarnitine	487.5	85.1	160	36
Octadecanoylcarnitine	484	85.1	155	36
Hexadecanoylcarnitine	456.4	85.1	160	36
Tetradecanoylcarnitine	428.4	85.1	150	28
Dodecanoylcarnitine	400.3	85.1	117	32
Decanoylcarnitine	372.3	85.1	125	28
Cystine	353	130	118	16
$^{2}H_{3}$-Octanoylcarnitine	347.3	85.1	136	24
Octanoylcarnitine	344.3	85.1	115	28
Cystathionine	335.2	190.1	97	13
Hexanoylcarnitine	316	85.1	113	20
Isovalerylcarnitine	302.2	85.1	128	20
Butyrylcarnitine	288.2	173.1	110	15
3-Hydroxykynurenine	281.2	152.1	108	12
2-Aminoadipate	274.2	98.1	113	24
Propionylcarnitine	274.2	85.1	127	20
Kynurenine	265.4	136	120	10
$^{2}H_{3}$-Acetylcarnitine	263.2	85.1	127	20
Tryptophan	261.2	244.1	94	8
Acetylcarnitine	260.2	85.1	108	20
Glutamate	260.2	84.1	89	24
N,N-dimethylphenylalanine	250.1	148.1	103	20
Aspartate	246.2	144.1	98	12
Tyrosine	238.2	136.1	94	12
Ring-$^{2}H_{5}$-phenylalanine	227.2	125.1	108	16
Phenylalanine	222.2	120.1	108	16
Methionine	206.1	104.1	94	8
$^{2}H_{10}$-Isoleucine	198.2	96.2	108	12
Isoleucine/Leucine	188.2	86.2	89	8
Pyroglutamate	186.1	84.1	108	16
$^{2}H_{8}$-Valine	182.2	80.2	103	12
Valine	174.2	72.2	89	12

The precursor and product ions refer to the masses (expressed as m/z values) of the protonated butyl esters and their selected fragments, respectively. Abbreviations: m/z, mass-to-charge ratio; FV, fragmentor voltage; CE, collision energy.

3.8.7 Batch composition and quality control

For both GC-TOF-MS and LC-MS/MS analyses, the samples were distributed into three batches, with one batch being analysed per day. To avoid any sample bias, which could have arisen due to possible signal intensity drift, all samples (including KO and WT) were randomised prior to batch allocation (Dunn *et al.*, 2012).

In order to obtain an accurate metabolic snapshot, reliable data is crucial. Quality control (QC) samples, which are derived from pooling an equal amount of each sample to be analysed, not only enable the monitoring of sample preparation and instrument stability, but are also indispensable during data pre-processing (discussed in Section 3.8.9). Therefore, a QC sample was prepared by pooling a small volume (43.2 µl) of all the samples. Unfortunately, due to the small volumes of some of the KO urine samples available in this study, such samples had to be excluded from the QC pool. The pooled QC sample was subsequently aliquoted into smaller volumes (each containing 0.0625 µmole creatinine) and stored at -80°C until the day of analysis. The QC samples were then treated and derivatised exactly like the urine samples, as described in Sections 3.8.2, 3.8.3 and 3.8.4.

The batch composition for the GC-TOF-MS and LC-MS/MS analyses is illustrated in Figure 3.3. Each batch started and ended with a QC sample, with additional QC samples included intermittently between the test samples (WT and KO). For LC-MS/MS analyses, the first QC sample was re-injected five times, of which the first four re-injections were solely used to condition the column and were thus excluded from downstream data processing and analysis in the sections that follow. Furthermore, after each batch, an in-house standard mixture, consisting of all the metabolites analysed (final concentration of each metabolite: 2.5 ppm) as well as a spiked QC sample (with the same standard mixture), was analysed. These 2 samples served to aid in compound identification, if required.

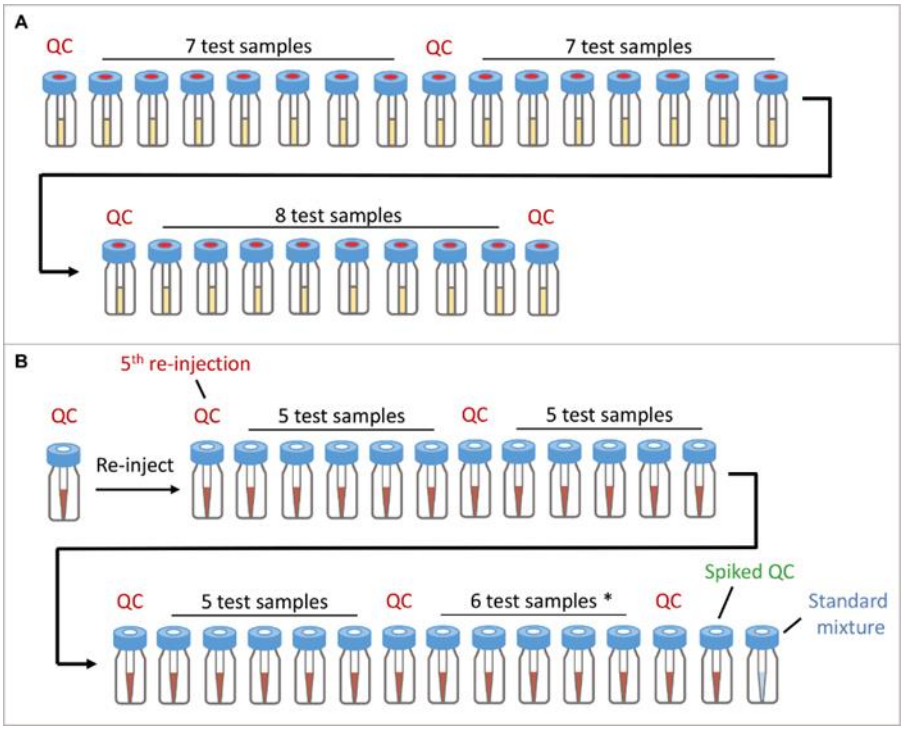

Figure 3.3: Batch composition of metabolomic analyses. Schematic representation of the batch composition for (A) GC-TOF-MS and (B) LC-MS/MS. QC samples were interspersed between the test samples (WT and KO) in every batch to monitor analytical performance. (B) Each batch in the LC-MS/MS analysis commenced with a QC sample, which was re-injected five times in order to condition the column. In addition, a spiked QC sample and a standard mixture consisting of all the targeted metabolites were analysed at the end of each batch for identification purposes. The asterisk indicates that only five test samples were injected between the fourth and fifth QC in the final batch. Abbreviations: GC-TOF-MS, gas chromatography time-of-flight mass spectrometry; KO, knockout; LC-MS/MS, liquid chromatography-tandem mass spectrometry; QC, quality control; WT, wild-type.

3.8.8 Data extraction

The GC-TOF-MS data was processed with ChromaTOF® (Leco). Here, mass spectral deconvolution was performed at a signal-to-noise ratio of 20, with a minimum of five apexing masses. The peaks across all samples were then aligned based on retention time and mass spectra. The peaks were given a tentative identity if their characteristic mass fragmentation patterns displayed at least 80% similarity to that of the National Institute of Standards and Technology (NIST) 2011 mass spectral library and an in-house formulated library.

The data obtained from the LC-MS/MS analyses was extracted using MassHunter Qualitative software (version B.06; Agilent Technologies). Here, analytes in each batch were aligned and peak integration was performed. Afterwards, peak integration was manually inspected to ensure

the correct peak selection as well as the proper integration of the peak areas. Lastly, a compound-aligned data matrix with integrated peak areas was generated.

3.8.9 Data pre-processing

Prior to data pre-processing, three samples were excluded from the data sets of both platforms. These included the data of two KO mice that fell outside of the age range, as well as one HET, which were all originally erroneously included. The latter was confirmed following genotype analysis of the collected samples. Furthermore, four KO mice were removed from the untargeted data set, since these mice had provided insufficient urine for targeted analysis (which was performed after untargeted analysis). The latter four samples were removed due to downstream multivariate statistical analysis, where the data sets of both platforms were combined. This left a total of 34 WT and 25 KO mice for both analytical platforms.

Following the removal of the abovementioned samples, the data was subjected to supervised zero filtering, which removes features with excessive missing values (exceeding a certain percentage). Here, the 80% rule was applied to each group, in which a feature was only kept in the data matrix if more than 80% of the samples in a group (WT and/or KO) contained data. In other words, a feature was removed if more than 20% of the samples in a group had missing values. Next, the peak areas were normalised (relatively quantified) using ISs (by dividing the peak area of the feature/metabolite by that of an IS) to compensate for potential technical variance that might have been introduced during sample preparation and analysis. To this end, the QC samples were first inspected to select the most suitable IS for each feature/metabolite. For the untargeted analysis, features were normalised against the IS that yielded the lowest %RSD. By contrast, features detected by the targeted analysis were normalised against the IS which yielded the highest spearman's coefficient – with the exception that features were normalised against their stable isotope, if available.

Following data normalisation, the %RSD of all features in the QC samples across all three batches was calculated for the targeted analysis (as was done for the untargeted analysis during IS selection). Since the QC samples are identical in composition, they allow for the detection of technical variance that may arise during sample preparation (e.g. metabolite extraction and derivatisation) and instrument analysis. Features that displayed an RSD value greater than 50% (missing values were excluded from the %RSD calculation) were removed from the data set, as these features were considered unreliable to quantify. After applying the %RSD filter, all remaining missing values were imputed with half of the data matrix's minimum peak intensity, since these missing values may have been the result of borderline features (i.e. features with concentration levels close to the instrument's detection limit). Lastly, the data were logarithm transformed (base 2), a technique that not only eliminates heteroscedasticity, but also has a

pseudo-scaling effect as it reduces the differences between large and small values. This is important, since highly abundant metabolites will mask the influence of low abundant metabolites in multivariate analyses.

3.8.10 Data inspection prior to biomarker/feature selection

Before data analyses were conducted to identify discriminatory features/metabolites, the data was inspected in several ways to ensure that any biological findings were reliable.

- Firstly, the viability of creatinine as normalisation factor was investigated (Appendix B), since the constant excretion thereof could be compromised in energy-related disease models as a result of kidney impairment and muscle wasting.
- Secondly, the following data quality assessment procedures were performed to ensure that the data was of a high quality and deemed fit for the discovery of discriminatory metabolites: (i) Prior to applying the %RSD filter during data pre-processing, the precision of all the features in the QC samples were evaluated by constructing %RSD distribution plots to provide an overall view of the technical variance. (ii) For the second procedure, the QC samples were analysed along with the test samples (WT and KO) via principle component analysis (PCA). Since this method aims to reduce the dimensionality of the data and project the greatest variation present, it provides a good visual representation of the overall variance in the data sets. (iii) For the final assessment, the data was inspected for potential batch effects (intra- and inter- batch signal drifts). Here, two approaches were used: In the first approach, the total signal of each sample (y-axis) was plotted as a function of its run order (x-axis) in each batch. This visually aids in inspecting for the presence of potential trends in signal drift. The total signal was calculated by adding together all of the relatively quantified peaks (via IS normalisation) in a given sample. In addition to this, the total signal intensity of each sample was also plotted by first applying logarithm transformation (base 2) to each relatively quantified peak.
- Lastly, following data quality assessment, the data was inspected for potential WT and KO sample outliers by conducting PCA on each individual group at a confidence level of 95%.

3.8.11 Statistical analysis

The data was subjected to both uni- and multivariate statistical analyses. Firstly, the data (KO vs WT) was inspected visually using PCA to observe the clustering of the two groups, as well as whether natural separation existed between the two groups. Thereafter, univariate analyses were performed to identify metabolites/features that differed significantly between the two groups. Features/metabolites were considered significant if their false discovery rate-corrected p-value

(i.e. q-value) and effect size d-value was < 0.05 and > 0.8, respectively. Finally, PCA was performed again using only the combined significant features from both the untargeted- and targeted platforms, to visually inspect the discriminatory power of these features between the two groups.

3.8.12 Confidence of metabolite identities

As described in Section 3.8.8, a feature (from the untargeted platform) was initially given a tentative identity if a spectral match of at least 80% was present between the feature and the libraries. Features that were found to differ significantly between the WT and KO groups, were ranked from level 1-5, based on the confidence of their identities (with level 1 indicating the highest confidence), as defined by Schymanski *et al.* (2014). Only those features with confidence levels ranging from 1 to 3 were interpreted and discussed. Level 3 was assigned to a metabolite that had been identified based solely on a spectrum match (tentative candidate). Level 2 was similar to level 3, except that the probable structure (compound class) could be allocated with more certainty. Lastly, a level 1 (confirmed structure) identity was given to metabolites that matched both the spectral and retention time/index of the reference standards. All the metabolites analysed on LC-MS/MS were assigned a confidence level of 1, since reference standards were available for all these metabolites, and also due to the targeted nature of the analysis. These reference standards were used to: (i) construct MRM transitions; (ii) obtain retention times; and (iii) spike urine samples to confirm the peak of interest, when multiple peaks were present (i.e. untargeted metabolites that could be detected with that particular MRM transition).

CHAPTER 4:
RESULTS AND DISCUSSION

4.1 Introduction

The previous chapter provides a thorough description of all the experimental procedures used to achieve the objectives, as outlined in Section 2.9.2. In this chapter, the results pertaining to the objectives are presented and discussed. Data from other relevant procedures mentioned in Chapter 3, but not presented here, can be found in Appendix B. Conclusions drawn from the results, the strengths and limitations of this study, as well as future recommendations are provided in Chapter 5.

4.2 Phenotypic evaluation of the *Ndufs4* knockout mice

To evaluate the effect of *Ndufs4* deficiency on the postnatal growth of the mice, the bodyweight measurements of WT and KO males and females (♂: WT = 3, KO = 2; ♀: WT = 4, KO = 3), from two litters, were taken every other day from P22/23 (litter one: P22; litter two: P23). For statistical reasons, growth curves were only plotted up until P56/57, when one of the male KO mice was euthanised after having lost > 10% of its maximum bodyweight, thereby leaving only one KO male.

As shown in Figure 4.1, the WT and KO mice initially displayed very small differences in bodyweight, which increased as the mice aged. Similarly, this trend was observed between male and female WT mice, which displayed similar growth curves that did not reach a plateau. Notably, however, while the male and female KO mice also displayed similar growth curves, no significant differences in bodyweight were observed and a plateau in growth was reached at around P38/39 and 40/41 for male and female mice, respectively – in contrast to the male and female WT mice. At around P46, the KO male and female mice, respectively, weighed approximately 44% and 31% less than their WT counterparts. Due to the large difference in bodyweight, it was thus possible to visually distinguish between the WT and KO mice at this age.

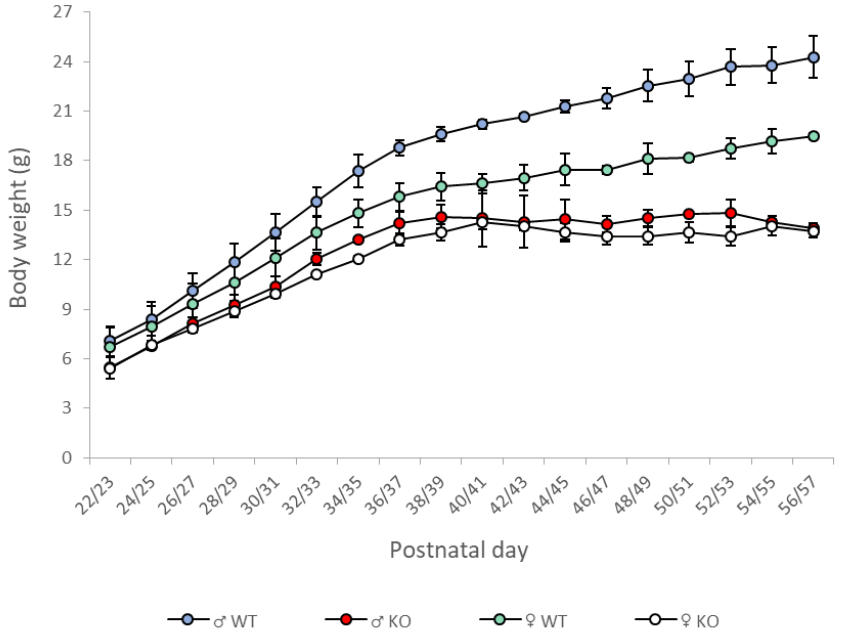

Figure 4.1: Growth curves of *Ndufs4* WT and KO mice. Mice were weighed every other day from the ages of P22/23 to P56/57. The groups consisted of four WT females, three WT males, three KO females and two KO males. Data points and error bars represent the mean bodyweight values (in g) and ± standard deviation, respectively. Symbols: ♀, female; ♂, male. Abbreviations: g, gram; KO, knockout; P, postnatal day; WT, wild-type.

In addition, some of the KO mice presented with alopecia, as depicted in Figure 4.2. Alopecia has been described previously in the *Ndufs4* KO mice (Kruse *et al.*, 2008) and is associated with the infiltration of inflammatory macrophages into the skin of the KO animals (Jin *et al.*, 2014). As can be seen from the figure, the two KO mice (Mouse #2 and #3) developed alopecia around P22, while the WT mouse (Mouse #1) did not show any signs of hair loss. The observed alopecia, however, was only transient, since the hair coats of the KO mice returned to normal around P40. Lastly, the KO mice displayed a typical hunched posture, as can be seen in Figure 4.3.

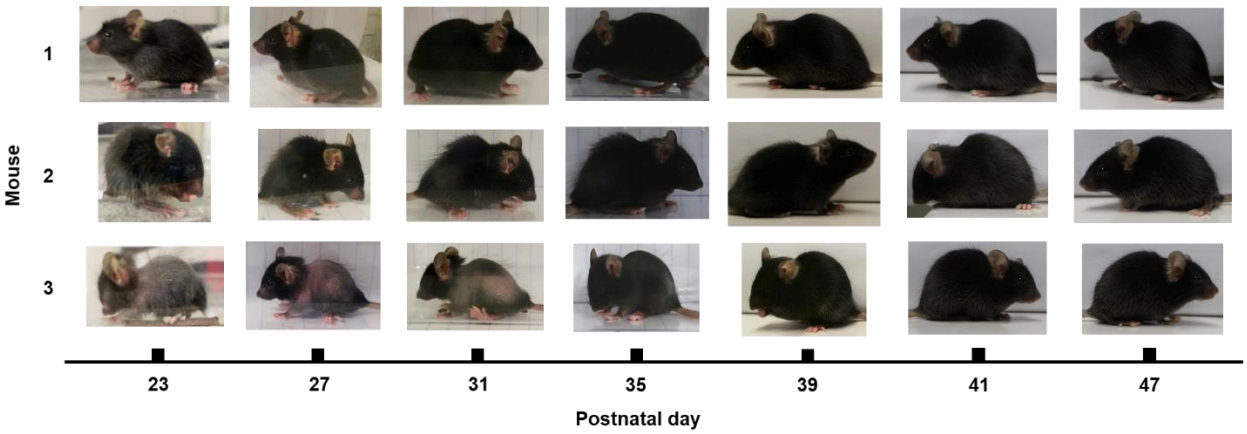

Figure 4.2: Alopecia observed in (some) *Ndufs4* KO mice. Alopecia is a common phenomenon in *Ndufs4* KO mice, which appears at around P20-22. In this study, the mice were examined for signs of alopecia over time (P20-35). Mouse #1 (WT), Mouse #2 (KO) and Mouse #3 (KO) are depicted in this figure, with clear differences visible between the animals. Symbols: #, number. Abbreviations: KO, knockout; P, postnatal day; WT, wild-type.

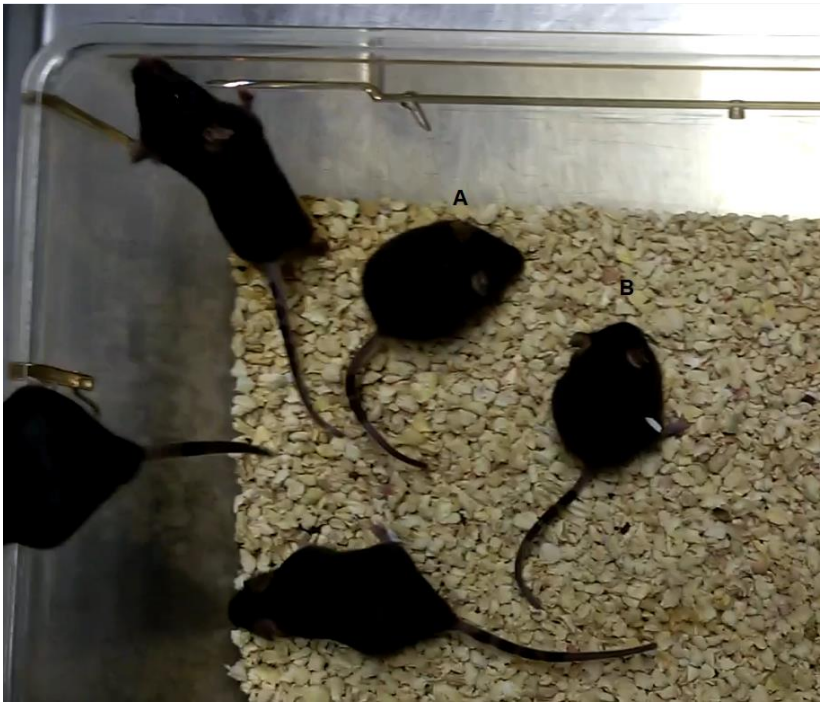

Figure 4.3: Photograph of *Ndufs4* WT and KO mice at P46 days. The two *Ndufs4* KO mice (marked A and B) are clearly smaller in size than the other three animals (WT). Furthermore, the hunched posture of the two KO animals is typical of *Ndufs4* KO mice. Abbreviations: KO, knockout; P, postnatal day; WT, wild-type.

4.3 Biochemical evaluation of *Ndufs4* knockout mice

In order to confirm the lowered activity of CI in the *Ndufs4* KO mice (caused by the knockout of the *Ndufs4* gene), the activity of this enzyme complex was measured in the liver of five WT and five KO male mice (P45-50), as described in Section 3.7.

CI activity is typically normalised to that of CS to compensate for differences in mitochondrial content. This normalisation approach, however, can only be a valid if CS activity remains unaltered in the *Ndufs4* KO mice. For this reason, it was necessary to evaluate CS activity in both the WT and KO groups. As shown in Figure 4.4 A, comparable CS activities were observed in the WT and KO mice ($p = 0.750$), indicating that CS activity remained unaltered in the *Ndufs4* KO mice. Based on these findings, CS activity was proven to be a valid normalisation method and used to normalise CI activity in this study.

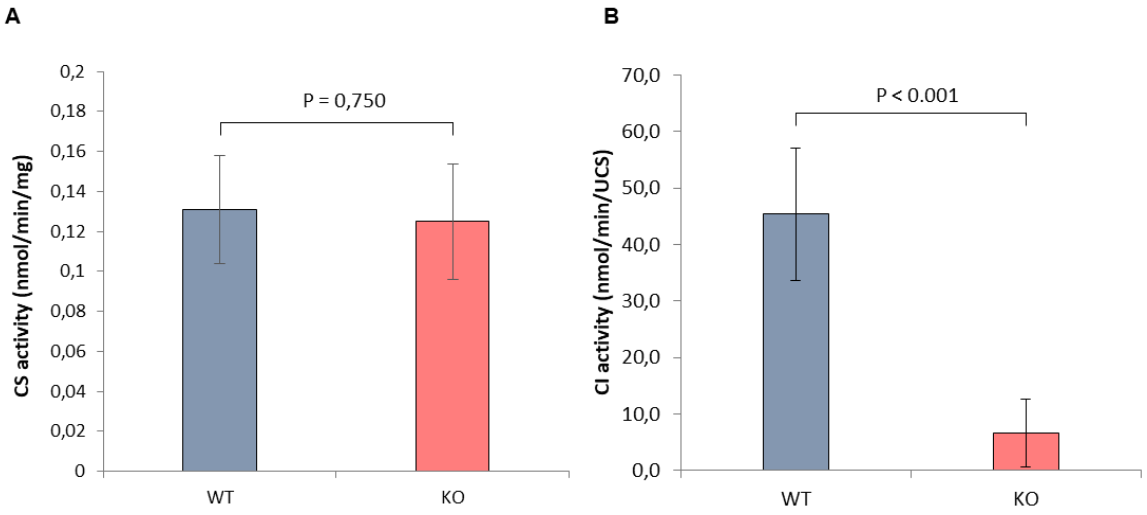

Figure 4.4: CS and CI activity of *Ndufs4* WT vs KO mice. (A) CS and (B) CI activity of WT and KO mice (P45-50; n = 5 per group) were measured in 600 *xg* supernatant derived from liver homogenates. Statistically, the difference between the CS activity of the WT and KO mice was insignificant ($p = 0.750$), whereas the CI activity differed significantly ($p < 0.001$). Each bar represents the mean CI specific activity (expressed per unit of CS, UCS) ± standard deviation (error bars). Abbreviations: CI, complex I; CS, citrate synthase; KO, knockout; n, number analysed; WT, wild-type.

A significant difference ($p < 0.001$) in CI activity (Figure 4.4 B) was observed between the WT (45.5 nmol/min/UCS) and KO mice (6.6 nmol/min/UCS), which equated to a residual CI activity of 15% in the KO mice. These results corresponded relatively closely to the findings of Calvaruso *et al.* (2012), Jin *et al.* (2014) and Leong *et al.* (2012), who reported residual activities of 20%, 16% and 10%, respectively. By contrast, the work of Kruse *et al.* (2008), in which the mice used in this study were first described, reported no residual CI activity in the liver. The authors attributed this

finding to the harsh sample preparation techniques used to generate sub-mitochondrial particles, and postulated that it could have resulted in the complete loss of activity in partially stable CI as a result of the *Ndufs4* deficiency. This theory is further supported by the fact that the mice did not present with any severe phenotypic characteristics of the disease until approximately five weeks (Kruse *et al.*, 2008), whereas a complete absence of CI activity would have most likely led to embryonic death (Calvaruso *et al.*, 2012).

In summary, these results not only indicate kinetically defective CI in the *Ndufs4* KO mice, but further support the findings of Calvaruso *et al.* (2012), Leong *et al.* (2012) and Jin *et al.* (2014), confirming that a significant reduction of CI activity occurs in the liver of *Ndufs4* KO mice.

4.4 Metabolomics evaluation of *Ndufs4* knockout mice

The primary objective of this study was to investigate the metabolic consequences of *Ndufs4* deficiency. To this end, a multi-platform metabolomics approach was used to compare the urinary metabolome of WT (n = 30) and KO (n = 23) mice, incorporating both untargeted (GC-TOF-MS) and targeted (LC-MS/MS) analyses in order to obtain a comprehensive view of the metabolic consequences.

4.4.1 Intra- and inter-plate precision of the creatinine assay

Before any urine samples could be used for metabolomic analyses, the urinary creatinine concentrations were determined to account for differences in urine dilution. Therefore, a pre-acquisition normalisation approach was used.

It is, however, important to obtain repeatable quantification of the creatinine concentrations to ensure reliable normalisation. To this end, both intra- and inter-plate precision were inspected across four 96-well plates. Since all the urine samples (test and QC samples) were analysed in triplicate, the test samples were sufficient to inspect for intra-plate precision, whereas the QC samples were used to evaluate inter-plate precision (as a precautionary measure, two QC samples were used to validate the repeatability of one another).

The precision achieved was satisfactory, with all the test and QC samples exhibiting low intra- and inter-plate variability (RSD < 10%). These results therefore demonstrated that the quantification of creatinine was reliable and thus suitable for the normalisation of the metabolomics data obtained in this study.

4.4.2 Data quality assessment of untargeted and targeted analysis

Using the untargeted GC-TOF-MS platform, a total of 359 features were obtained, along with 47 metabolites (AAs, carnitine and acylcarnitines) using the targeted LC-MS/MS platform. However, before data analysis could be performed to identify discriminatory metabolites, it was crucial to first assess the quality of the data derived from both the untargeted and targeted analyses, in order to ensure that the discovery of discriminatory features was reliable. As a result, the data quality in this study was assessed using approaches (procedures) that are commonly used in metabolomic studies.

4.4.2.1 Analytical precision

Typically, a 30% RSD filter is used in untargeted metabolomic studies (Martin-Blazquez *et al.*, 2019; Pirttila *et al.*, 2019), where the data is considered of high quality if at least 70% of all the features have an RSD of less than 30% (Gika *et al.*, 2014; Le Pogam *et al.*, 2019). Even though a more relaxed filter (50% cut-off) was used in this study, the 30% RSD limit serves as a useful benchmark in assessing the quality of the data. As shown in Figure 4.5 A, the majority of features are distributed below an RSD of 30%, which accounts for 93.3% of all the measured features.

For targeted analysis, many studies use the criteria as specified by the U.S. Food and Drug Administration, which states: “the precision determined at each concentration level should not exceed 15% of the CV [RSD] except for the lower limit of quantification, where it should not exceed 20% of the CV” (Broadhurst *et al.*, 2018; FDA, 2001). One should, however, keep in mind that these criteria were not set out with metabolomics in mind (where precision is the primary concern), but rather for highly targeted analyses, where accuracy is an important factor. A number of other studies have, instead, set the limit of acceptable precision to 25%, which makes more sense in the case of the targeted analysis used in this study, since highly targeted sample preparation (e.g. extracting analytes of interest) and absolute quantification were not performed. As expected, the targeted analyses provided much better precision (Figure 4.5 B), with the variability of almost all of the metabolites below an RSD of 10%, accounting for 95.7% of all targeted metabolites.

The higher degree of technical variation observed in the untargeted data set, compared to that of the targeted data, can be ascribed, in particular, to the trimethylsilylation step used in the untargeted method. Taking into consideration that (i) the samples of each batch were derivatised simultaneously; (ii) the silylation reagent was not removed (derivatisation is therefore not quenched); (iii) time had elapsed between samples injected in the beginning, middle and end of each batch; and (iv) unstable derivatives could have degraded leading to certain metabolites that may not have derivatised completely during the short derivatisation steps (Kanani *et al.*, 2008), one can thus expect varying concentrations of these derivatives within each batch. In addition, the higher variation can also be attributed to low abundant peaks with low signal-to-noise ratios

for certain features/metabolites, which hinder the software from distinguishing the features from noise, and therefore, lead to improper detection and integration (Harada *et al.*, 2018).

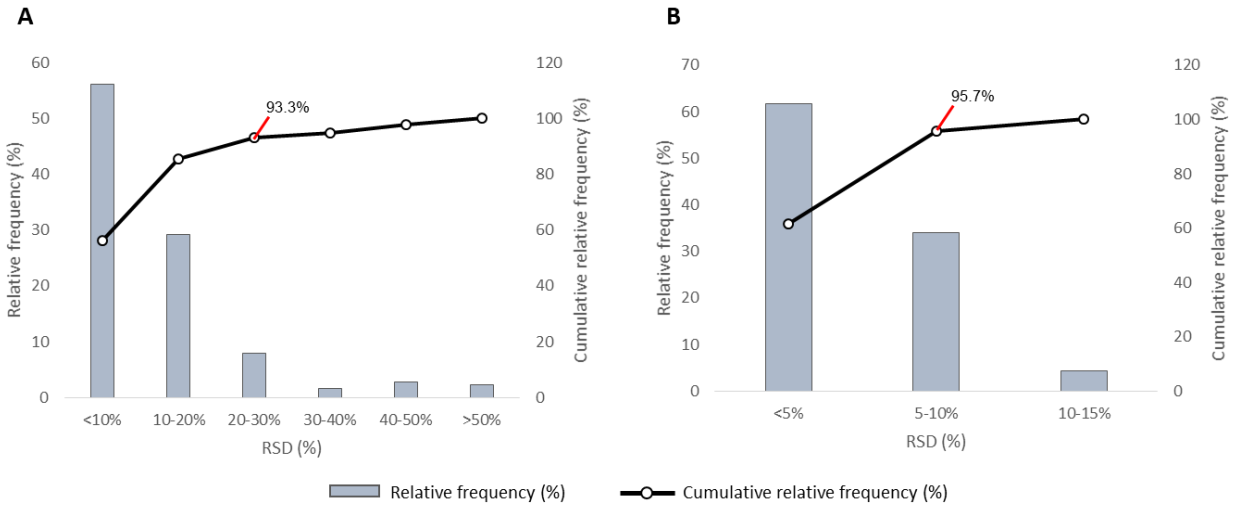

Figure 4.5: The RSD (expressed as a percentage) distribution of all features/metabolites in the QC samples. The precision of (A) GC-TOF-MS and (B) LC-MS/MS was assessed by calculating the RSD (expressed as a percentage) of all features/metabolites in the QC samples across all three batches. Each grey column represents a percentage of the total number of features/metabolites within the specified RSD range, while the black line represents the cumulative sum of the relative frequencies within the specified RSD range. Abbreviations: GC-TOF-MS, gas chromatography time-of-flight mass spectrometry; LC-MS/MS, liquid chromatography-tandem mass spectrometry; RSD (%), relative standard deviation (expressed as a percentage).

4.4.2.2 Evaluation of the technical and biological variation

As illustrated in the PCA score plots (Figure 4.6 A and B), the QC samples clustered together closely in comparison to the test samples (WT and KO), which displayed a much greater variance in both the GC-TOF-MS and LC-MS/MS analyses. This not only indicated excellent analytical performance of both the platforms utilised (i.e. the presence of little technical variance), but also showed that the majority of the variation observed in the test samples was due to biological variation. This variation was observed in the WT and KO groups themselves, but also, more importantly, between the groups – as is evident from the distinct separation tendency shown between the WT and KO groups in Figure 4.6 A and B.

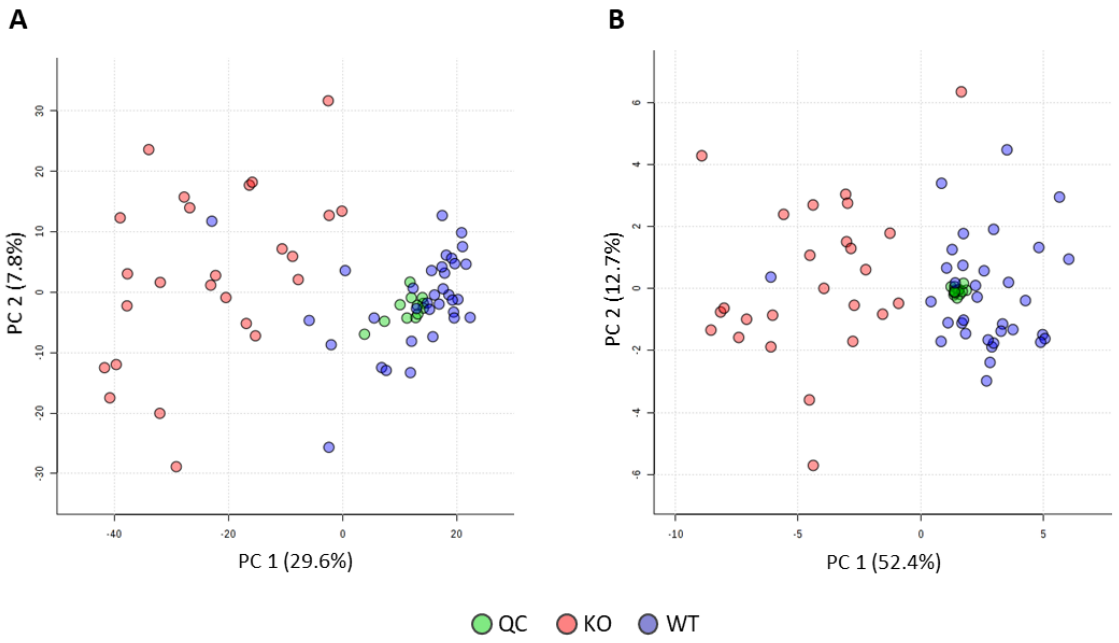

Figure 4.6: Two-dimensional PCA score plots of the QC, WT and KO samples. PCA was performed to visualise variation of the QC (green) samples in relation to that of the WT (blue) and KO (red) samples subjected to (A) GC-TOF-MS untargeted analysis and (B) LC-MS/MS targeted analysis. Abbreviations: GC-TOF-MS, gas chromatography time-of-flight mass spectrometry; KO, knockout; LC-MS/MS, liquid chromatography-tandem mass spectrometry; PC, principle component; PCA, principle component analysis; QC, quality control; WT, wild-type.

4.4.2.3 Batch effect inspection

Figure 4.7 A to D displays the sequential total intensity scatter plots of the collected data. In the figure, the QC samples are distributed in a relatively straight line across all three batches, indicating overall analytical stability across the entire course of data acquisition. Greater fluctuations were observed for the QC samples used in the untargeted analysis (Figure 4.7 A and C). This was to be expected, due to the %RSD acceptance criteria used as well as the occurrence of missing values and the fact that an untargeted approach inherently displays greater variation (as mentioned in Section 4.4.2.1). By contrast, these fluctuations were hardly present in the targeted analysis (Figure 4.7 B and D). With regards to the test samples (WT and KO), however, no noticeable trends were observed.

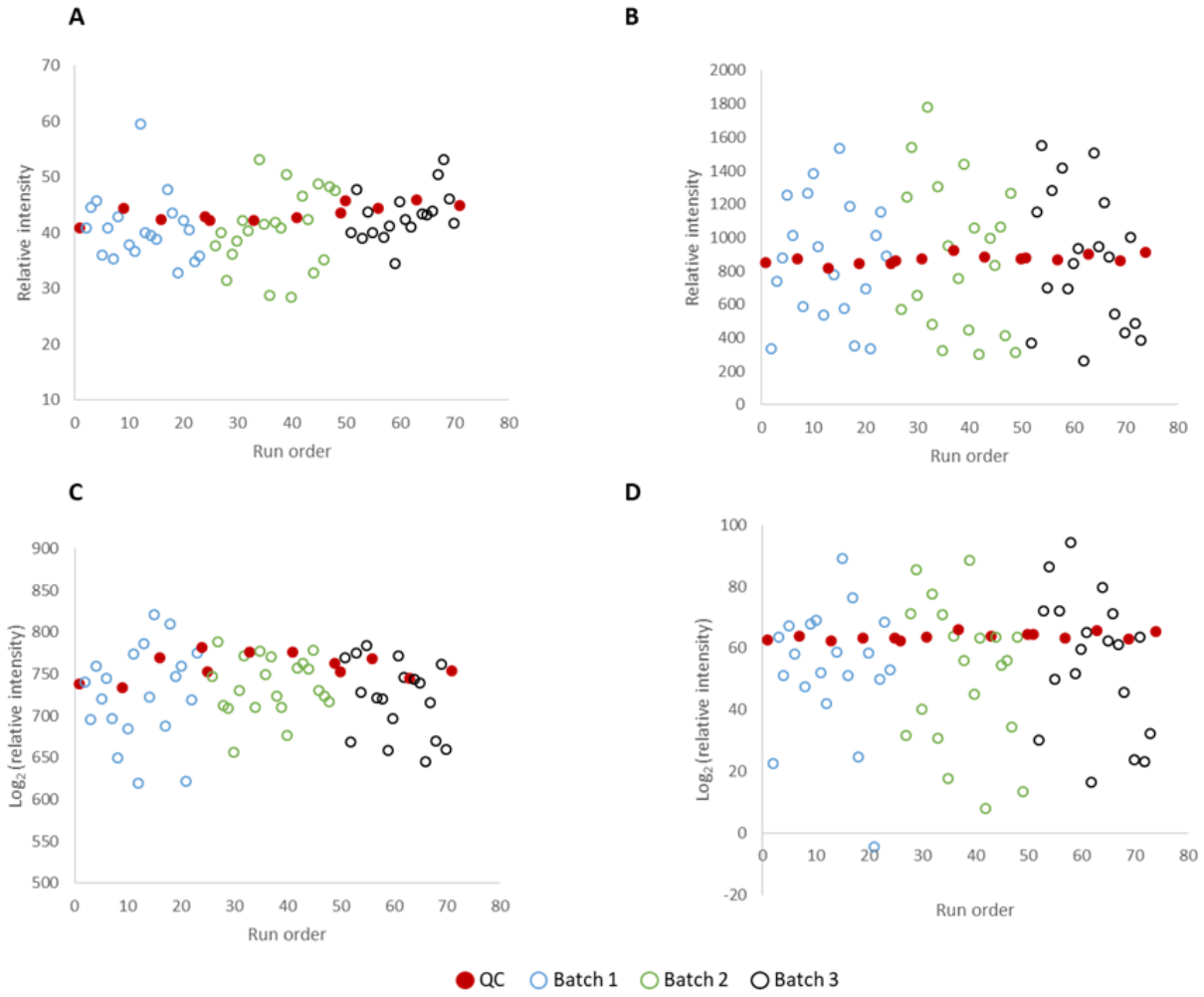

Figure 4.7: Sequential total intensity scatter plots. Scatter plots depicting the total intensity of each sample in the order they were analysed for all batches (blue, green and black represent the first, second and third batch, respectively). Each batch was comprised of QC (red), WT and KO samples. The sum of relative intensity of the GC-TOF-MS untargeted and LC-MS/MS targeted analyses are depicted in (A) and (B), respectively, while the sum of logarithm transformed relative peaks of the GC-TOF-MS untargeted and LC-MS/MS targeted analyses are shown in (C) and (D), respectively. Abbreviations: GC-TOF-MS, gas chromatography time-of-flight mass spectrometry; KO, knockout; LC-MS/MS, liquid chromatography-tandem mass spectrometry; QC, quality control; WT, wild-type.

In the second approach, PCA was used to plot the WT and KO samples in their respective batches. As depicted in Figure 4.8 A and B, all three batches of each platform overlapped with each other, indicating that no batch effects were present in the data.

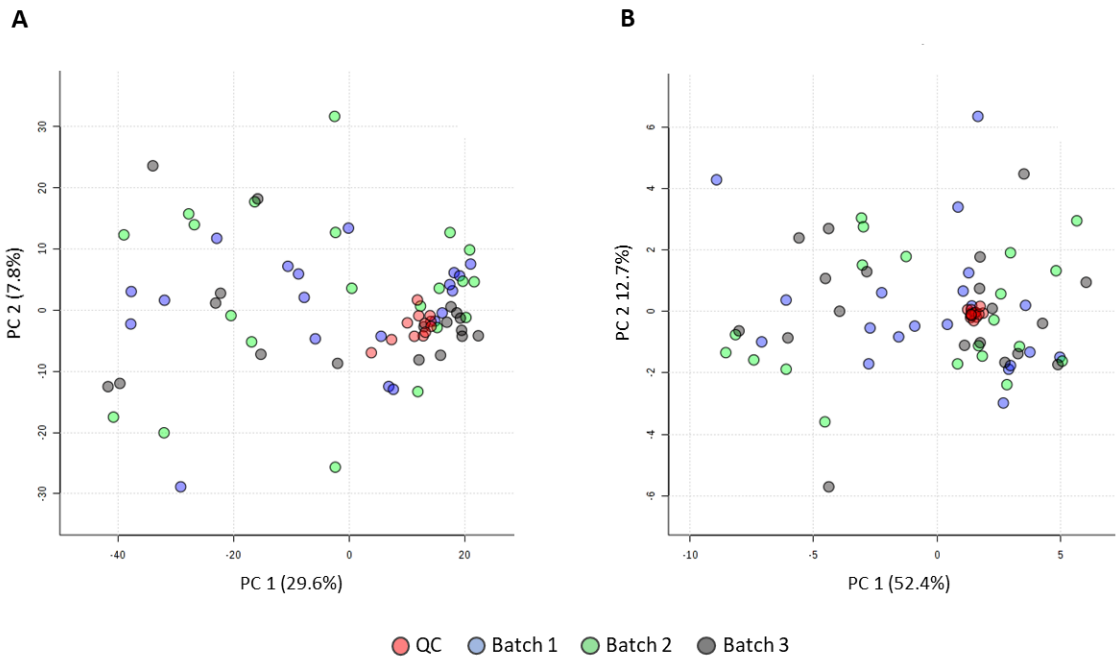

Figure 4.8: Two-dimensional PCA score plot representing the sample batches analysed. PCA was performed to visually observe the presence or absence of a batch effect in (A) GC-TOF-MS untargeted analysis and (B) LC-MS/MS targeted analysis. All three batches [comprised of QC (red) WT and KO samples] from both platforms display integrated distribution, indicating the absence of batch effects (blue, green and black represent the first, second and third batch, respectively). Abbreviations: GC-TOF-MS, gas chromatography time-of-flight mass spectrometry; KO, knockout; LC-MS/MS, liquid chromatography-tandem mass spectrometry; PC, principle component; PCA, principle component analysis; QC, quality control; WT, wild-type.

In metabolomics, technical variance is unavoidable, even when carefully planned steps are taken to minimise it as much as possible. With this in mind, it is critical to assess the quality of the acquired data, in order to ensure that any statistically meaningful results are reliable. Overall, both the untargeted and targeted analyses were able to successfully provide good precision, a high degree of biologically relevant information and signal stability across the entire run of all three batches. The data from both analytical platforms was thus of high quality and deemed fit for identifying potential discriminatory metabolites.

4.4.3 Data reduction

As mentioned in Section 4.4.2, a total of 359 features were obtained using the untargeted GC-TOF-MS platform, along with 47 metabolites (AAs, carnitine and acylcarnitines) using the targeted LC-MS/MS platform. Prior to performing statistical analyses to identify discriminatory features/metabolites, the data was inspected for potential sample outliers via PCA (results not shown), which detected 3 WT outlier samples in the untargeted data set, of which 1 one was

common in both platforms, and 2 KO and 2 WT outlier samples in the targeted data set. These samples were subsequently removed from the data sets of both platforms that left a total of 30 WT and 23 KO mice for the final metabolic comparison. Next, the data was processed to remove contaminant peaks and non-biological compounds. The “80% rule” was first applied to the data, which states that a feature is kept in the data matrix if it has a non-zero value in at least 80% of the samples of any of the experimental groups (Yang *et al.*, 2015). Thus, potential differentiating metabolites that were only detected in one experimental group and not in the other (likely due to concentrations that fell below the detection limit of the instrument), were not removed from the data set. After applying the 80% rule, the number of features from the GC-TOF-MS was reduced from 359 to 185. Hereafter, a 50% RSD rule was applied, where any feature was removed from the data set if the %RSD for that feature exceeded 50% in the QC samples across all three batches. After applying this filter, another four features were removed, resulting in a total of 181 features for the untargeted GC-TOF-MS platform. The data of the targeted LC-MS-MS platform, however, was of such quality that all features (n = 47) were retained after applying the 80% rule and the 50% RSD filter to the data. Altogether, both platforms thus provided a total of 228 features/metabolites that were subjected to statistical analysis to screen for discriminatory features/metabolites. Both data sets, after being log transformed, were combined and subjected to PCA in order to obtain an overview of the data. As depicted in Figure 4.9, significant separation was observed with minimal overlap occurring between the two groups, indicating metabolic differences between the WT and KO mice.

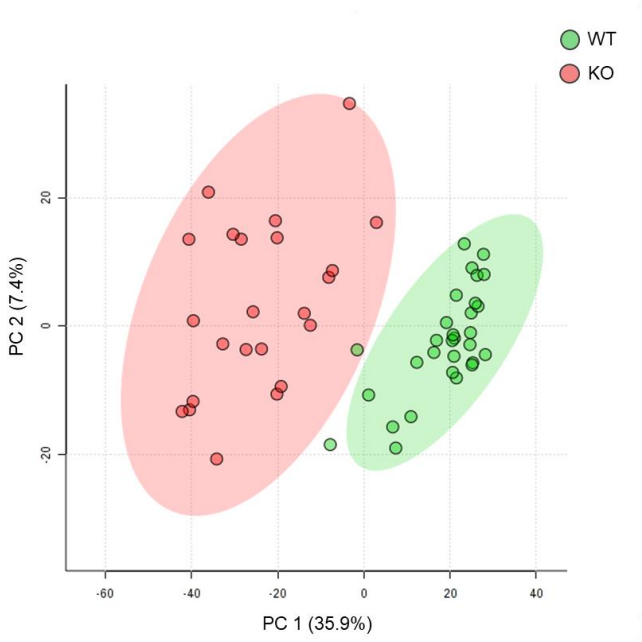

Figure 4.9: Two-dimensional PCA score plots obtained after data reduction. PCA was performed on the combined data sets (GC-TOF-MS and LC-MS/MS) following data reduction (n = 228 metabolites) to visualise the overall clustering of WT (green) and KO (red) mice in relation to each other. Abbreviations:

GC-TOF-MS, gas chromatography time-of-flight mass spectrometry; KO, knockout; LC-MS/MS, liquid chromatography-tandem mass spectrometry; PC, principle component; PCA, principle component analysis; WT, wild-type.

4.4.4 Selection of discriminatory features/metabolites

Next, univariate statistical analyses were applied to identify the discriminatory features/metabolites. In order to be included in the list of important features, these had to display a p-value < 0.05 (t-test) and d-value > 0.8 (effect size). A total of 93 features/metabolites were found to differ significantly between the WT and KO groups, 62 of which were derived from the untargeted GC-TOF-MS platform and the remaining 31 from the targeted LC-MS/MS platform. Metabolite annotation of the discriminatory features, that displayed different intensities of statistical and practical significance between the WT and KO samples, was performed by comparison to known compounds. For this purpose, several in-house, commercial and public libraries/databases were utilised and an identification confidence level was ascribed to each feature, as previously described by Schymanski *et al.* (2014). In short, a Level 3 identity was allocated if a tentative structure was obtained, based on either matching intact molecular mass or fragmentation spectra. A Level 2 identity was allocated if Level 3 conditions held, together with additional evidence on a more probable structure identity. If both the spectral and retention time/index could be matched to that of an authentic reference standard, the metabolite was labelled as Level 1. All unidentified features (> Level 3) were excluded from the data matrix. This resulted in a final list (Table 4.1) containing a total of 73 discriminatory/significant metabolites.

Table 4.1: List of discriminatory metabolites identified between the *Ndufs4* KO and WT groups.

Metabolite	Δ direction	Platform	p-value	d-value	ID Level
1-Methylhistidine	↓	LC-MS/MS	< 0.001	1.03	1
2,6-Dihydroxybenzoate	↑	GC-TOF-MS	< 0.001	1.07	3
2-Aminoadipate	↓	LC-MS/MS	< 0.001	0.88	1
2-Hydroxyadipate	↓	GC-TOF-MS	< 0.001	2.95	3
2-Hydroxyglutarate	↓	GC-TOF-MS	< 0.001	1.09	1
2-Keto-3-methylvalerate	↓	GC-TOF-MS	< 0.001	1.69	3
2-Ketoglutarate	↑	GC-TOF-MS	0.003	0.87	1
3-Alanine	↓	LC-MS/MS	< 0.001	1.38	1
3-Amino-isobutyrate	↓	Both	< 0.001	1.37 (0.97)	1 (3)
3-Methylhistidine	↓	LC-MS/MS	< 0.001	1.13	1
3-Ureidopropionate	↓	GC-TOF-MS	< 0.001	0.97	3
4-Aminobutyrate (GABA)	↓	LC-MS/MS	< 0.001	2.06	1
4-Hydroxymandelate	↓	GC-TOF-MS	< 0.001	2.05	3
4-Hydroxyphenylacetate	↓	GC-TOF-MS	< 0.001	0.99	1
4-Hydroxyphenylpyruvate	↓	GC-TOF-MS	0.003	0.87	3

5-Hydroxy-indole	↓	GC-TOF-MS	< 0.001	1.55	3
5-Hydroxylysine	↓	LC-MS/MS	< 0.001	1.43	1
Alanine	↑	Both	< 0.001	1.06 (1.44)	1 (2)
Alanyl-threonine	↓	GC-TOF-MS	< 0.001	0.81	3
Arginine	↓	LC-MS/MS	< 0.001	1.34	1
Butyrylglycine	↓	GC-TOF-MS	< 0.001	1.58	3
Carbamate	↓	GC-TOF-MS	< 0.001	1.08	3
Carnitine	↑	LC-MS/MS	0.005	0.84	1
Citramalate	↑	GC-TOF-MS	< 0.001	1.80	3
Citrulline	↓	LC-MS/MS	< 0.001	0.98	1
Cystathionine	↓	LC-MS/MS	< 0.001	1.45	1
Cystine	↓	LC-MS/MS	0.002	0.86	1
Decanoylcarnitine	↓	LC-MS/MS	< 0.001	1.29	1
Erythrose	↓	GC-TOF-MS	< 0.001	2.64	2
Fumarate	↑	GC-TOF-MS	< 0.001	1.71	1
Glucarate	↓	GC-TOF-MS	< 0.001	0.87	3
Gluconate	↓	GC-TOF-MS	0.002	0.95	3
Glutamate	↓	LC-MS/MS	< 0.001	1.30	1
Glutamine	↓	LC-MS/MS	< 0.001	2.32	1
Glutarate	↓	GC-TOF-MS	< 0.001	1.21	3
Glycerate	↓	GC-TOF-MS	< 0.001	0.99	1
Glycerol	↓	GC-TOF-MS	< 0.001	1.46	3
Glycine	↓	LC-MS/MS	< 0.001	1.08	1
Gulonate	↓	GC-TOF-MS	< 0.001	1.61	3
Hexanoylglycine	↓	GC-TOF-MS	< 0.001	1.40	3
Histidine	↓	LC-MS/MS	< 0.001	1.05	1
Hydroxy-proline	↓	LC-MS/MS	< 0.001	3.03	1
Isoleucine/Leucine	↓	LC-MS/MS	< 0.001	2.13	1
Isovalerylglycine	↓	GC-TOF-MS	< 0.001	1.31	3
Lactate	↑	GC-TOF-MS	< 0.001	1.31	1
Malate	↑	GC-TOF-MS	< 0.001	1.40	1
Methionine	↓	LC-MS/MS	< 0.001	1.69	1
N,*N*,*N*-trimethylglycine	↓	LC-MS/MS	< 0.001	2.63	1
N,*N*-dimethylglycine	↓	LC-MS/MS	< 0.001	2.78	1
N-acetylglutamate (NAG)	↓	GC-TOF-MS	< 0.001	2.88	3
Octanoylcarnitine	↓	LC-MS/MS	< 0.001	1.32	1
Orotate	↓	GC-TOF-MS	< 0.001	1.55	3
Oxalate	↓	GC-TOF-MS	< 0.001	1.73	1
Phenylalanine	↓	LC-MS/MS	< 0.001	1.24	1
Phosphate	↓	GC-TOF-MS	< 0.001	1.37	1
Phosphoglycerol	↓	GC-TOF-MS	< 0.001	1.06	3
Proline	↓	LC-MS/MS	< 0.001	1.85	1
Propionylcarnitine	↑	LC-MS/MS	< 0.001	1.32	1
Pyroglutamate	↓	GC-TOF-MS	< 0.001	1.11	1
Pyruvate	↑	GC-TOF-MS	< 0.001	1.29	1
Ribitol	↓	GC-TOF-MS	0.002	0.84	3

Ribonate	↓	GC-TOF-MS	< 0.001	2.95	3
Ribose	↓	GC-TOF-MS	< 0.001	0.98	2
Sarcosine	↓	LC-MS/MS	< 0.001	3.24	1
Serine	↓	Both	< 0.001	1.46 (1.27)	1
Sorbose	↓	GC-TOF-MS	< 0.001	1.28	2
Tartronate	↓	GC-TOF-MS	< 0.001	1.49	3
Threonate	↓	GC-TOF-MS	< 0.001	3.45	3
Threonine	↓	LC-MS/MS	0.001	0.92	1
Uracil	↓	GC-TOF-MS	< 0.001	1.89	1
Uric acid	↓	GC-TOF-MS	0.002	0.84	1
Valerylglycine	↓	GC-TOF-MS	< 0.001	1.93	3
Valine	↓	Both	< 0.001	1.50 (1.46)	1

The direction of the arrow indicates the change observed in the metabolite in the KO mice relative to the WT mice (i.e. ↑, increase/ ↓, decrease). If a metabolite was detected using both platforms, information derived from the LC-MS/MS analysis (p-/d-value and ID level) is listed first, followed by that derived from GC-TOF-MS analysis in brackets to specify differences (if present). Abbreviations: GABA, 4-aminobutyrate; GC-TOF-MS, gas chromatography time-of-flight mass spectrometry; ID, identification; KO, knockout; LC-MS/MS, liquid chromatography-tandem mass spectrometry; NAG, *N*-acetylglutamate; WT, wild-type.

The significant metabolites identified from both platforms were combined into a single data matrix and subjected to PCA (Figure 4.10) to visually inspect the discriminatory effect of the selected metabolites. From this figure it can be seen that the significant metabolites resulted in significant differentiation between the two groups, with only a slight overlap. The latter (the slight overlap), along with the higher intra-group variation displayed by the KO mice (i.e. the lesser degree of clustering) were to be expected, since the KO mice had exhibited different levels of disease severity. Therefore, a larger variation in their metabolome was likely.

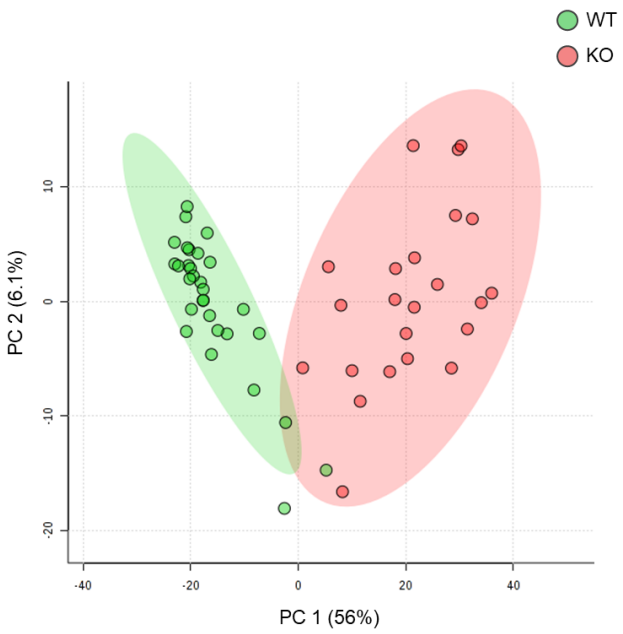

Figure 4.10: Two-dimensional PCA score plot following feature selection. PCA was performed using the statistically significant metabolites derived from both analytical platforms (GC-TOF-MS and LC-MS/MS), to illustrate the discriminatory effect between the urinary metabolome of the WT and KO mice. Abbreviations: GC-TOF-MS, gas chromatography time-of-flight mass spectrometry; KO, knockout; LC-MS/MS, liquid chromatography-tandem mass spectrometry; PC, principle component; PCA, principle component analysis; WT, wild-type.

4.4.5 Urinary metabolic perturbations caused by knocking out *Ndufs4*

4.4.5.1 Glycolysis and the TCA cycle

As anticipated, the examination of the urinary metabolome of the *Ndufs4* KO mice revealed classic perturbations generally observed in MDs, including elevated levels of lactate, pyruvate and alanine. In support hereof, increased levels of lactate have also been described in the brain (Johnson *et al.*, 2013; Lee *et al.*, 2019), cardiac muscle, skeletal muscle (Lee *et al.*, 2019) and serum of *Ndufs4* KO mice (Jin *et al.*, 2014; Kruse *et al.*, 2008; Lee *et al.*, 2019), while increased levels of pyruvate have been reported in the brain (Johnson *et al.*, 2013). These perturbations are believed to reflect a decreased NAD^+/NADH ratio, and thus an altered redox status. Under normal conditions, pyruvate, the end-product of glycolysis, is mainly transported into the mitochondrion, where it is oxidatively decarboxylated to acetyl-CoA by the NAD^+-dependant PDHc. Acetyl-CoA then enters the TCA cycle to be catabolised. However, in the case of a defective CI, brought about by the deficiency of the NDUFS4 protein, the efficiency of NADH oxidation is reduced. Since the activity of the PDHc is inhibited by NADH, a decreased NAD^+/NADH ratio in the KO mice will actively inhibit the activity of the PDHc, and therefore, result in the accumulation of pyruvate. The

accumulated pyruvate can then subsequently be converted to either lactate via lactate dehydrogenase – an enzyme which favours a low NAD^+/NADH ratio, and therefore, provides a way to lower high levels of NADH – or be transaminated to alanine via alanine aminotransferase. This observation is supported by the research of Lee *et al.* (2019), who identified an altered redox status in the brain, liver, heart and skeletal muscle of *Ndufs4* KO mice. In further agreement with this view, the lactate/pyruvate ratio, which serves as an indicator of the cytosolic redox status, was revealed to be significantly higher ($p < 0.001$) in the urine of *Ndufs4* KO mice (median ratio of 36.9) when compared to that of WT mice (median ratio of 3.9) (Munnich *et al.*, 1996).

A decreased NAD^+/NADH ratio can also explain the occurrence of a congested TCA cycle. In the KO mice, increased levels of 2-ketoglutarate, malate and fumarate were detected, of which the former two are NAD^+-dependant. Elevated levels of fumarate are further known to cause protein succination: a non-enzymatic post-translational modification where fumarate irreversibly reacts with cysteine residues. Consequently, this modification, which has been implicated in diseases such as diabetes and cancer, can impair the function of susceptible proteins, and as a result, alter cellular function (Merkley *et al.*, 2014). Accordingly, Piroli *et al.* (2016) have demonstrated for the first time, using *Ndufs4* KO mice that augmented protein succination occurs in regions where pathomorphological changes are also observed. Based on their results, areas that displayed the greatest degree of pathomorphological change were accompanied by a greater degree of increased succination, and included the brainstem, cerebellum and olfactory bulbs. The authors noted that a prominent increase in succination had occurred, in the brainstem in particular, at approximately three weeks of age, after which succination increased progressively until the mice died of respiratory failure at approximately nine weeks. In turn, the respiratory failure was attributed to the vestibular nuclei of the brainstem, which the authors had reported as being one of the areas displaying the greatest pathomorphological changes and increase in protein succination. Moreover, the vestibular nuclei play an important role in the regulation of posture and breathing patterns. Accordingly, in an earlier study, Quintana *et al.* (2012), reported that *Ndufs4* KO mice displayed an increased frequency of breathing irregularities and apnea as they aged. Therefore, the elevated fumarate detected in this study corresponds with existing knowledge on the role of increased succination in the phenotype observed in *Ndufs4* KO mice.

In addition to the inefficient metabolisation of pyruvate (as discussed above), the altered redox status also results in a condition which further contributes to increased levels of pyruvate, lactate and alanine. This condition, known as pseudohypoxia, is a metabolic adaptation which mimics hypoxic conditions, regardless of the O_2 status. Hypoxia-inducible factor 1 (HIF-1) is central to this is adaptation, and may be defined as a ubiquitously expressed transcription factor comprising an alpha subunit (HIF-1α) and a constitutively expressed beta subunit (HIF-1β). The level of HIF-1α is regulated by post-translational modifications, which are based on the cellular O_2

concentration. Under normoxic conditions (i.e. normal cellular O_2 concentration), HIF-1α is hydroxylated by O_2-dependant prolyl hydroxylases (PHDs), thereby enabling its ubiquitination via the von Hippel-Lindau tumour suppressor protein, which allows proteasomal degradation. However, under hypoxic conditions (i.e. insufficient cellular O_2 concentration), the degradation of HIF-1α does not occur, due to the inhibition of PHDs. This enables HIF-1α to dimerise with HIF-1β in the nucleus, which leads to the upregulation of the transcription (and hence, the expression) of genes involved in a multitude of processes. Such processes include the increased expression of enzymes that enhance the glycolytic flux, namely (i) the glucose transporter 1; (ii) glycolytic enzymes; (iii) lactate dehydrogenase A; (iv) as well pyruvate dehydrogenase kinase 1, which decreases the conversion of pyruvate to acetyl-CoA by inhibiting the PDHc (Jochmanová *et al.*, 2013; Mulukutla *et al.*, 2016). Thus, the accumulation of pyruvate and lactate not only occurs due to a shortage of NAD^+, but also as a result of metabolic reprogramming. As stated above, hypoxia may be mimicked via the metabolic adaption called pseudohypoxia. During this adaptation, HIF-1α levels are instead stabilised by a variety of accumulated metabolites, which inhibit the activity of PHDs. Two such metabolites, pyruvate and fumarate, were found to be increased in this study (via untargeted analysis). This metabolic adaption is also supported by a number of studies on *Ndufs4* KO mice, in which the following were detected: (i) an upregulation of HIF-1α messenger RNA (mRNA) levels in the liver (Jin *et al.*, 2014), and HIF-1α protein levels in the brain and skeletal muscle (Lee *et al.*, 2019); (ii) an upregulation of pro-glycolytic genes, which are targeted by HIF-1α, namely 6-phosphofructo-2-kinase/fructose-2,6-biphosphatase 2 (mRNA levels in the liver) (Jin *et al.*, 2014), hexokinase and glucose transporter 1 (protein levels in the brain) (Johnson *et al.*, 2013; Lee *et al.*, 2019), and lactate dehydrogenase A (protein levels in the brain and skeletal muscle) (Lee *et al.*, 2019); and (iii) increased glycolytic intermediates in the brain (Johnson *et al.*, 2013).

To refer back to the TCA cycle, 2-ketoglutarate can also be reduced to 2-hydroxyglutarate via mitochondrial malate dehydrogenase. Considering that the urinary metabolome seems to indicate an altered redox status (i.e. a decreased NAD^+/NADH ratio) in the mitochondrion and that the reduction of 2-ketoglutarate to 2-hydroxyglutarate is NADH-dependant, the decreased level of 2-hydroxyglutarate detected in this study seems rather contradictory, especially since this metabolite has been reported to be elevated in a number of other metabolomic studies that have investigated MDs in humans (Bao *et al.*, 2016; Esterhuizen, 2018; Reinecke *et al.*, 2012; Smuts *et al.*, 2013). The elevated level of 2-hydroxyglutarate revealed in those studies is sensible, since the reduction of 2-ketoglutarate favours high levels of NADH, similar to the conversion of pyruvate to lactate. However, it has been shown that 2-hydroxyglutarate exhibits an inhibitory effect on glycolysis (Oldham *et al.*, 2015). Since glycolysis appears to be upregulated in *Ndufs4* KO mice, as mentioned in Section 4.4.5.1, the accumulation of 2-hydroxyglutarate would be

counterproductive. Thus, not only does the decreased level of 2-hydroxyglutarate agree with an increase in glycolysis, but it also indicates the likelihood that other factors are at play in regulating the formation of 2-hydroxyglutarate, and therefore, warrants further investigation.

4.4.5.2 Protein and lipid catabolism

From this study, an overall decrease of AAs were detected in the urine of the *Ndufs4* KO mice, indicating a possible reduction in the rate of protein catabolism. This finding was supported by a number of additional alterations observed in the urinary metabolome:

Firstly, the levels of glutamine and glutamate were found to be decreased. These two AAs are not only proteinogenic, but also play an important role in carrying amino groups derived from the oxidation of other AAs. There are two ways by which amino groups may be removed from AAs: (i) the predominant manner involves the transfer of the amino group to 2-ketoglutarate to yield glutamate; (ii) the alternative route involves the synthesis of glutamine from glutamate and the amino group (as ammonia) released during the non-oxidative deamination of AAs. Glutamine and glutamate are then transported to the liver where they are metabolised to 2-ketoglutarate and the free ammonia can enter the urea cycle. However, although the KO mice in this study displayed reduced glutamine and glutamate levels, elevated levels of 2-ketoglutarate were observed. This finding was inconsistent with the former, since elevated levels of 2-ketoglutarate can indicate an increase in protein catabolism. Instead, a more plausible explanation is that the elevated 2-ketoglutarate level measured is the result of a congested TCA cycle, which agrees with the observed increase in the levels of fumarate and malate.

Secondly, decreased levels of *N*-acetylglutamate (NAG) were detected. NAG is an allosteric activator of carbamoyl phosphate synthetase (the first enzyme in the urea cycle), and fluctuates in quantity based on the degree of AA oxidation. In other words, in cases of increased AA oxidation (e.g. higher protein intake and an increased gluconeogenic state during the initial stage of fasting), NAG levels will increase in order to upregulate the urea cycle to ensure the detoxification of the increased ammonia level. Thus, the lower level of NAG could be indicative of decreased ureagenesis, an explanation which is further supported by the decreased levels observed for two intermediates of the urea cycle namely, arginine and citrulline.

Thirdly, 1- and 3-methylhistidine, two histidine derivatives, were found to be decreased. The latter derivative is found exclusively in skeletal muscle and the measurement thereof is used as an index of skeletal muscle protein breakdown, since it is not re-utilised after being released (Ballard & Tomas, 1983). Taken together, these results indicate a decrease in the protein catabolism of the *Ndufs4* KO mice, relative to their WT counterparts.

In addition to the observed reduction in protein/AA catabolism, the urinary metabolome of the KO mice also indicates a decrease in the lipid/triacylglycerol catabolism. This is denoted by (i) a

decrease in glycerol, which suggests that there is a reduction in lipolysis, and (ii) by a decrease in the levels of carnitine- (octanoyl- and decanoylcarntine) and glycine- (butyryl-, valeryl- and hexanoylglycine) conjugated fatty acids. Moreover, this is accompanied by an elevated level of free carnitine, which signifies a reduction in free fatty acids and their oxidation via the β-oxidation cycle. In support of these results, Jin *et al.* (2014) detected elevated levels of triacylglycerol and free fatty acids in the serum of *Ndufs4* KO mice, while Johnson *et al.* (2013) reported decreased levels of fatty acids in the brain and liver of these animals. Taken together, these findings could indicate that the uptake of fatty acids is downregulated, resulting in the accumulation thereof in the serum and a decrease of fatty acids in the tissues. This explanation is plausible, considering, as already discussed, that there is an upregulation of glucose transporter 1 in the brain of the *Ndufs4* KO mice, which can be utilised to support glycolysis.

One rather peculiar metabolic perturbation identified, involves propionylcarnitine – the only acylcarnitine that was found to be elevated in the urine of the KO mice. Propionyl-CoA can be derived in various ways, including the catabolism of several essential AAs (isoleucine, methionine, threonine and valine), odd-chain fatty acids, the pyrimidines thymine and uracil, and the side-chains of cholesterol (Sentongo *et al.*, 2009). Considering the reduced AA- and fatty acid catabolism discussed above, as well as the fact that the urinary metabolome of the KO mice suggests a decrease in the catabolism of thymine (decreased 3-amino-isobutyrate) and uracil (decreased uracil, 3-ureidopropionate and 3-alanine), the increased level of propionylcarnitine seems inconsistent. However, another source of propionyl-CoA is the gut microbiota, which produces propionate that can cross the epithelial cell line and undergo esterification with CoA via acyl-CoA synthase in the host. Interestingly, a recent study by Scheiman *et al.* (2019) has shown, using ^{13}C tracing analysis, that lactate is able to cross the epithelial cell line into the intestinal lumen, where it can be metabolised to short chain fatty acids (predominantly propionate) by the gut bacteria, and cross back through the epithelial cell line into the host. Their finding, therefore, provides a possible explanation for the elevated levels of propionylcarnitine, since the *Ndufs4* KO mice had significantly elevated levels of lactate.

Even though propionyl-CoA was not specifically measured in this study, propionylcarnitine has been shown to not only be a successful biomarker in patients with methylmalonic- and propionic acidaemia (Chace *et al.*, 2001), but has also been proven, via untargeted metabolomics, to be the most significant discriminatory feature in these disorders (Wikoff *et al.*, 2007). Thus, one can conclude that propionylcarnitine is an accurate alternative measurement of propionyl-CoA. Propionyl-CoA has been shown to cause mitochondrial dysfunction by affecting a number of enzymes, including the PDHc and 2-ketoglutarate dehydrogenase (Schwab *et al.*, 2006). Consequently, there is a high probability that propionyl-CoA (as represented by propionylcarnitine) contributes to the elevated urinary levels of pyruvate and 2-ketoglutarate (as

detected in this study). Moreover, the increased levels of propionyl-CoA could, in addition to a congested TCA cycle, also have contributed to the elevated levels of fumarate, since propionyl-CoA is metabolised to succinyl-CoA and then succinate, which is finally oxidised to fumarate via CII of the RC. Therefore, this observation underscores the importance of not neglecting the interaction between host and microbial metabolism, which should always be borne in mind when interpreting metabolomic findings.

4.4.5.3 Biosynthetic pathways

In this study, metabolic perturbations were not only observed in the catabolic pathways discussed, but also in some biosynthetic pathways, as was evident from the altered levels of the associated intermediates and products/degraded products, which included: (i) orotate (a substrate required for *de novo* pyrimidine synthesis); (ii) GABA; (iii) glycine, *N,N*-dimethylglycine, *N,N,N*-trimethylglycine, sarcosine, serine, methionine, cystine and cystathionine (metabolites centered around the one-carbon metabolism); (iv) ribose and erythrose (metabolites from the pentose phosphate pathway); (v) glucarate and gluconate (metabolites from the glucuronate pathway – a pathway which can diverge into the ascorbic acid synthesis pathway); as well as (vi) threonate and oxalate (breakdown products of ascorbic acid) – all of which were found to be decreased in the urine of *Ndufs4* KO mice.

Firstly, the reduced levels of orotate (i) and GABA (ii) may be explained by the decreased levels of their respective precursors, glutamine and glutamate. Secondly, apart from the partitioning of glycolysis-derived pyruvate to lactate and alanine, the glycolytic pathway may also divide at various other steps, leading to metabolic pathways, including: the serine synthesis pathway (iii; which leads to one-carbon metabolism); the pentose phosphate pathway (iv); and the glucuronate pathway (v). The decreased flux through the abovementioned pathways (iii-v) may be explained by an upregulated glycolysis. Considering this, it is possible that glucose and the glycolytic intermediates are preferentially oxidised to pyruvate, and that the partitioning of glycolysis into other pathways thus occurs to a lower extent. In addition, feeding difficulties have been reported in *Ndufs4* deficient patients (Ortigoza-Escobar *et al.*, 2016) as well as an *Ndufs4* KO *Drosophila* model (Foriel *et al.*, 2018). Taking this into account, it is further likely that this symptom was present in the *Ndufs4* KO mice, considering the growth retardation and loss in bodyweight displayed by these animals. As a result, a reduction in caloric intake will result in less substrate availability for biosynthetic pathways. Metabolically, glycolysis may thus be used preferentially over the other glucose-utilising pathways, not only to maintain sufficient ATP levels, but also to produce enough gluconeogenic substrates (e.g. lactate and alanine) to maintain glucose homeostasis. This explanation is plausible as the gluconeogenic substrates (AAs and glycerol) were found to be decreased in this study. This notion is further supported by the study of Kruse

et al. (2008), who reported no significant differences in the fasting blood glucose levels of the WT and *Ndufs4* KO mice.

Moreover, *de novo* pyrimidine synthesis (i), one-carbon metabolism (iii) and the pentose phosphate pathway (iv) are important for the synthesis of nucleotides, with the latter two pathways further being required for the reduction of $NADP^+$. Therefore, these three pathways (i, iii and iv) are important for the proliferation of cells (i.e. growth and development). Since a reduced flux was observed in these pathways, cell proliferation might be greatly supressed in the *Ndufs4* KO mice, which can also potentially explain the growth retardation observed. Apart from the important role of NADPH in biosynthetic pathways, it is also key in maintaining ROS homeostasis. A decrease in NADPH could theoretically lead to the accumulation of ROS, resulting in oxidative stress. This theory is corroborated by a number of studies, which have reported augmented ROS in primary skeletal muscle and skin fibroblasts (Valsecchi *et al.*, 2013), as well as an increase in oxidative stress markers in the brain (de Haas *et al.*, 2017; Johnson *et al.*, 2013; Lee *et al.*, 2019) of *Ndufs4* KO mice. Interestingly, unlike humans, mice are also able to synthesise ascorbic acid (vi), which not only aids in ROS homeostasis, but also serves as a cofactor for PHDs. A decrease in ascorbic acid synthesis will therefore additionally contribute to HIF-1α stabilisation and increase ROS production in mice.

CHAPTER 5:
SUMMARY AND CONCLUSIONS

5.1 Introduction

MD remains a challenge within the scientific community, due to the complex genotype-phenotype correlation and our poor understanding of the pathological mechanisms. This explains why there are very limited treatment options available, as well as the absence of evidence supporting their efficacy. Among all MDs known to date, CI deficiencies not only make up the greatest proportion, but also predominantly manifest as LS – the most commonly reported clinical presentation of MDs – for which the *Ndufs4* gene is a mutational hotspot. With a whole-body *Ndufs4* KO mouse model available, which can serve as a suitable representative model for MDs, it is therefore only fitting that this model be at the forefront of MD research. To date, the use of urine as a means to metabolically characterise *Ndufs4* KO mice has been lacking. Since urine is a biofluid, which functions as an excretory medium, it can provide a global view of the altered metabolic status of the *Ndufs4* KO mouse. This study was, therefore, conducted to investigate the metabolic consequences in whole-body *Ndufs4* KO mice, using a urinary metabolomics approach. This aim was achieved through the implementation of two main objectives: (1) the validation of the whole-body *Ndufs4* KO mouse model and (2) the urinary metabolomics analyses of the *Ndufs4* KO and WT mice.

5.2 Summary of the findings and final conclusions

5.2.1 Validation of the whole-body *Ndufs4* KO mouse model

First and foremost, validation of the whole-body *Ndufs4* KO mouse model was required to ensure that any findings derived from the second objective of this study were valid. To this end, validation was performed and achieved on three levels: Firstly, by the genotype assay (PCR) used for animal selection and again at post-mortem for confirmation, which was successful in differentiating between the different genotypes (i.e. *Ndufs4* KO, WT and HET); secondly, by the phenotypic evaluation of the *Ndufs4* KO mice, which displayed symptoms previously reported in this model, including: growth retardation, transient alopecia and hunched back posture; and thirdly, by the evaluation of CI activity in the liver of the mice, where *Ndufs4* KO mice exhibited a significant low level of residual CI activity of only 15%, in comparison to WT mice.

5.2.2 Urinary metabolomic analyses of *Ndufs4* KO and WT mice

Following the successful confirmation of the mouse model, the second objective of this study, which entailed the metabolomic analyses of urine samples using both an untargeted (GC-TOF-MS) and targeted (LC-MS/MS) approach, was implemented. In this study, a pre-acquisition normalisation approach utilising creatinine was followed. Accordingly, the creatinine concentrations of all the urine samples were first determined, which displayed satisfactory intra- and inter-plate precision, followed by the successful metabolomic analyses of the urine samples. Thereafter, the creatinine normalisation approach was evaluated against other methods of normalisation to determine whether creatinine clearance was significantly affected in this disease model. Overall, creatinine as a normalisation factor not only correlated strongly with the other methods of normalisation, but was also found to be very similar between the *Ndufs4* KO and WT urine samples. Furthermore, similar amounts of discriminatory features were derived from each normalisation method (including creatinine), of which the majority were found to be common to all. These results therefore suggested that there was no (or at least no significant) altered creatinine clearance. Next, the data quality was assessed, where both platforms yielded high quality data in terms of precision, biologically relevant information and signal stability. The satisfactory results derived from the abovementioned evaluations thus showed that the metabolomics data was reliable to use for the discovery of discriminatory features/metabolites. Finally, the data was processed and subjected to statistical analyses, which yielded a combined total of 73 discriminatory features/metabolites from both analytical platforms. In turn, these metabolites revealed a global metabolic perturbation caused by the deficiency of the NDUFS4 protein.

Perturbations considered to be a hallmark of MDs due to an altered redox status, were observed, including elevated levels of pyruvate, lactate and alanine as well as the TCA cycle intermediates 2-ketoglutarate, fumarate and malate. Elevated levels of pyruvate and lactate have also been shown to occur as a result of upregulated glycolysis and lactate production via the stabilisation of the transcription factor HIF-1α, which has been implicated in *Ndufs4* KO mice. Even though this study could not provide direct evidence for upregulated glycolysis, since glycolytic intermediates were not detected by the analytical platforms employed, it did, nonetheless, provide evidence that supported the findings of previous studies in two ways: Firstly, this study provided causative evidence by the elevated levels of fumarate, a potent inhibitor of PHDs; and secondly, this study provided consequential evidence by the elevated levels of pyruvate and lactate, which have been shown to be the result of enhanced glycolysis.

Globally, the urine metabolome of the *Ndufs4* KO mouse indicated a downregulation in protein/AA catabolism, as evident by the decreased levels of numerous AAs (e.g. glutamine, glutamate,

leucine, isoleucine, valine and phenylalanine), 3-methylhistine (which is an index of skeletal muscle breakdown) and metabolites associated with the urea cycle (arginine, citrulline and NAG). Similarly, lipid/fatty acid catabolism also seemed to be downregulated, as indicated by lowered levels of glycerol, numerous carnitine- and glycine fatty acid conjugates (octanoyl- and decanoylcarntine; butyryl-, valeryl- and hexanoylglycine) and elevated levels of free carnitine (which indicates decreased fatty acid import into the mitochondrion for β-oxidation). There was also a decrease in the metabolites present in pathways associated with biosynthetic processes and/or ROS scavenging. These included metabolites of the pentose phosphate pathway, one-carbon metabolism and *de novo* pyrimidine synthesis. These pathways, in particular, not only provided supportive evidence for increased oxidative stress, which has been reported in *Ndufs4* KO mice, but could also explain why these mice displayed growth retardation, as these pathways are important for cell proliferation.

When considering the overall findings, two metabolites exhibited unexpected alterations. The first metabolite, 2-hydroxyglutarate, was found to be decreased in *Ndufs4* KO mice, thereby displaying a change in direction, contradictory to the observed altered redox status and what other studies have reported. On the other hand, a decrease in 2-hydroxyglutarate does, however, seem to be in line with the abovementioned findings and other studies that support upregulated glycolysis, since 2-hydroxyglutarate has an inhibitory effect on glycolysis at high concentrations. The second metabolite, propionylcarnitine, was found to be elevated in *Ndufs4* KO mice, regardless of all the propionyl-CoA-producing pathways that were shown to display decreased activity. It is well-known that propionyl-CoA can also be derived from propionibacteria in the intestinal lumen and it has recently been shown that lactate from the host can indeed cross the intestinal epithelial cells into the intestinal lumen, where it can be metabolised by gut bacteria to propionate, which can then cross back into host's bloodstream to ultimately lead to the formation of propionyl-CoA (Scheiman *et al.*, 2019). This provides a possible explanation, since the urinary metabolome displayed significant elevated levels of lactate. From these two metabolites, two important conclusions can thus be drawn: Firstly, that the altered redox status is not the only factor at play; and secondly, that more attention should be given to the gut microbiome-host interactions, which have been shown to have an effect on the phenotype of diseases.

In conclusion, the aim of this study was successfully accomplished and revealed global metabolic perturbations in the *Ndufs4* KO mice, thereby contributing to the scientific community in several ways: Firstly, by being the first study to conduct urinalysis using a multi-platform metabolomics approach in order to provide a global metabolic profile of *Ndufs4* KO mice; secondly, by revealing perturbations in the *Ndufs4* KO mice that validate and support the findings of previous studies; and thirdly, by providing additional insights and raising new questions from the metabolic consequences detected. The findings and contributions of this study reiterate the value of urine

in providing greater insights into diseases, and should therefore encourage researchers to not overlook this biofluid, which serves as a mirror to reflect the overall physiological status.

5.3 Strengths of the study

Researching MDs remains problematic due to the scarcity of patients, which greatly hinders sample availability. Obtaining samples is further hindered due to the fact that these diseases display poor genotype-phenotype correlation and often do not fit into a well-defined syndrome. A major strength of this study, therefore, is the use of a mouse model, which represents the most prevalent clinical presentation reported in MDs, namely LS. Since the mice are genetically homogenous and exposed to the same controlled environmental conditions, heterogeneity is greatly reduced, which simplifies the interpretation of metabolic perturbations. Additionally, due to the fact that mice have short gestation periods and produce large numbers of offspring, this study did not suffer from an insufficient number of samples and thus exhibited a high statistical power.

From a physiological perspective, this study is the first to utilise urine for the multi-platform metabolomic characterisation of *Ndufs4* KO mice. Even though the LS phenotype is considered to be mainly neuropathological, it does not mean that other tissues do not contribute to the overall pathology and symptoms observed in these mice. As already mentioned, this is evident from the study of Jin *et al.* (2014), which demonstrated that a deficiency in NDUFS4 causes systemic inflammation that manifests as transient alopecia. As urine contains a vast number and wide variety of metabolites/waste products derived from all organs/tissues, urinary metabolomics has the potential to reveal metabolic perturbations that might be implicated in the pathophysiology of this disease. Accordingly, this study confirmed the potential of urine to capture metabolic perturbations/differential metabolites that have been implicated in the phenotype of *Ndufs4* KO mice and, therefore, corroborated the findings of previous studies (Section 4.4.5). Additionally, urinary metabolomics also provided new insights into the altered metabolome of *Ndufs4* KO mice: in particular the altered one-carbon metabolism, pentose phosphate pathway and *de novo* pyrimidine synthesis, which might be major contributors in the observed growth retardation and oxidative stress observed in these mice.

Taking into consideration that analytical platforms are biased towards metabolites with specific physical-chemical properties, it would thus be highly beneficial to incorporate multiple platforms to increase the overall metabolome coverage. Unfortunately, the majority of metabolomic studies to date, only employ one analytical platform (Bhinderwala *et al.*, 2018). Therefore, another strength of this study was the incorporation of two analytical platforms, which not only increased

the metabolome coverage, but as seen in Table 4.1, increased the credibility of a number of differential metabolites that were detected in both platforms.

5.4 Limitations of the study

This study was, however, not without limitations. Although genetically homogenous and housed under controlled environmental conditions, the *Ndufs4* KO mice used in the study, nonetheless, still displayed a high degree of variability, as was particularly evident from the PCA projection of the differential metabolites/features (Figure 4.10). Clearly, the age range used in this study (P45-50) was not an optimal indicator of disease progression and severity. Furthermore, taking into consideration that feeding difficulties have been reported in *Ndufs4* deficiency and that the food intake of the mice used in this study was not monitored, this factor could have possibly influenced the results to some degree. With regards to urine collection, the *Ndufs4* KO mice, in general, provided less urine than the WT mice. Even though precautionary measures were taken in order to collect as much urine as possible (i.e. treating the metabolic cages with NaN_3, as described in Section 3.5), it only alleviated the problem to a small degree. Bearing this in mind, and taking into consideration that urine was required (i) to determine the creatinine concentrations, (ii) to prepare QC samples and (iii) to perform the analysis on two analytical platforms, the amount of urine (based on a fixed concentration of creatinine) used for metabolomics analyses had to be reduced, which led to a reduced metabolic coverage in the untargeted analysis (possibly as a result of low abundant metabolites, which hindered metabolite identification by databases due to low quality fragmentation spectra).

5.5 Future prospects

This study established the foundation for many future endeavours. Firstly, if possible, the limitations of this study should be addressed. In order to reduce the variability observed in the metabolome of the *Ndufs4* KO mice as well as the slight overlap between the metabolomes of the *Ndufs4* KO and WT mice (Figure 4.10), it is recommended that phenotype score sheets based on neurobehavioral patterns and physical traits be utilised to ensure a more phenotypically homogenous sample group. Furthermore, feeding habits (the frequency and amount of food intake) should be strictly monitored, to ensure that differential feeding habits do not have a confounding effect on the urinary metabolome.

The overall lower urinary output of *Ndufs4* KO mice is an important issue to look into, especially since this factor restricted the metabolic coverage obtained in the untargeted analysis, as explained in Section 5.4. It is highly recommended that future studies endeavour to obtain a

greater metabolic coverage in order to uncover the possible presence of more metabolic perturbations. A number of steps can be taken to overcome this limitation to some degree: firstly, a study by Stechman *et al.* (2010) demonstrated that mice placed within a new environment (i.e. metabolic cage) require 3-4 days of acclimatisation for variables such as water intake and urinary output to increase and reach stable values. It is, therefore, recommended that future studies allow mice to acclimatise in metabolic cages, which could increase the urinary output of *Ndufs4* KO mice. Secondly, from an analytical standpoint, greater metabolic coverage can be obtained by implementing certain changes, of which some examples include: (i) using other analytical platforms that provide greater sensitivity and/or display less inherent bias towards metabolites with particular physical-chemical properties; (ii) in the case of gas chromatography, using an injection liner that allows for a greater injection volume and/or using lower split ratios; and (iii) although not highly recommended, using a single analytical platform (preferably an analytical platform similar to that stated in the first example), where the volume of urine will not be a limiting factor. Regardless of which approach will be followed, compromises will still have to be made; therefore, it is advised that careful consideration be taken in order to ensure the best possible outcome. For example, researchers from other universities that are interested in expanding on this study, but that are relatively new to metabolomics and have no/limited analytical platforms, could collaborate with other research entities that are metabolomics-driven (e.g. the Centre of Human Metabolomics, where this study was conducted), have many different analytical platforms available and can aid with research inputs in terms of selecting the metabolomic methodologies to be implemented.

One inherent caveat of all untargeted metabolomic studies, and thus not considered/regarded as a limitation in this study, is the presence of unidentifiable features. These can be the result of (i) low abundant metabolites that prevent databases from making correct identifications due to low quality fragmentation spectra; (ii) the use of databases that differ in the number of metabolite entries (Liu *et al.*, 2016); and (iii) metabolites that are yet to be discovered and characterised (Markley *et al.*, 2017). In this study, these unknown differential features were removed, since they could not contribute to biological interpretation. It is, however, recommended that their identities be investigated as they may be metabolites, and not merely analytical artefacts, that can provide further insight into this debilitating disease. In the meantime, while new metabolites are being discovered/characterised and databases' entries are expanding, this caveat can be approached by using additional databases and by analysing more concentrated QC samples that might provide higher quality fragmentation spectra.

From a validation standpoint, a number of steps should be taken to not only corroborate the findings in this study, but to also consolidate the interpretations presented. Firstly, it is advised that the differential features derived from the untargeted analysis (GC-MS), that have ID levels

higher than 1, should be confirmed. This can be achieved using the same approach for unidentified features (i.e. analysing a more concentrated QC sample). Additionally, reference standards (if available) can be analysed by using a matrix-free approach or by spiking them into a QC sample to further aid in verifying feature identities. External biological validation, for example, where a new set of samples is analysed, is also recommended in order to verify that the differential features/metabolites obtained in this study are reproducible. Secondly, validating the metabolic interpretations based on the findings is a critical step, as erroneous interpretation will lead to failure in the development of targeted therapeutic interventions. Here, the affected pathways should be investigated and more targeted approaches (e.g. by developing or using existing targeted methods and incorporating absolute quantification of the metabolites of interest) as well as stable-isotope tracing analyses (e.g. to validate that the elevated levels of propionylcarnitine is the result of the gut microbiome-host interaction) should be included. Additionally, even though a number of studies have provided evidence for upregulated glycolysis, which was further supported by the causative and consequential evidence obtained from this study, it is, nonetheless, recommended that direct evidence be obtained by analysing all glycolytic intermediates in the urine, since this may reveal whether there is a global upregulation in glycolysis. This would provide a better picture relating to the energy metabolism in *Ndufs4* KO mice, since the findings of this study provide evidence for global reduction in protein/AA- and lipid/fatty acid catabolism. This glycolysis-targeted approach should also be performed on tissue samples, since this metabolic reprogramming might not occur in all tissues, due to tissue-specific differences in energy metabolism.

REFERENCES

Abraham, Z., Hawley, E., Hayosh, D., Webster-Wood, V.A. & Akkus, O. 2018. Kinesin and dynein mechanics: measurement methods and research applications. *Journal of Biomechanical Engineering*, 140(2):0208051-02080511.

Alam, M.T., Manjeri, G.R., Rodenburg, R.J., Smeitink, J.A., Notebaart, R.A., Huynen, M., Willems, P.H. & Koopman, W.J. 2015. Skeletal muscle mitochondria of NDUFS4$^{-/-}$ mice display normal maximal pyruvate oxidation and ATP production. *Biochimica et Biophysica Acta (BBA) - Biochemistry*, 1847(6-7):526-533.

Amato, P., Tachibana, M., Sparman, M. & Mitalipov, S. 2014. Three-parent *in vitro* fertilization: gene replacement for the prevention of inherited mitochondrial diseases. *Fertility and Sterility*, 101(1):31-35.

Amoedo, N.D., Punzi, G., Obre, E., Lacombe, D., De Grassi, A., Pierri, C.L. & Rossignol, R. 2016. AGC1/2, the mitochondrial aspartate-glutamate carriers. *Biochimica et Biophysica Acta (BBA) - Molecular Cell Research*, 1863(10):2394-2412.

Aw, W.C., Youngson, N.A. & Ballard, J.W.O. 2016. Can we alter dietary macronutrient compositions and alleviate mitochondrial disease*? Journal of Rare Diseases Research and Treatment*, 3(1):31-37.

Ballard, F.J. & Tomas, F.M. 1983. 3-Methylhistidine as a measure of skeletal muscle protein breakdown in human subjects: the case for its continued use. *Clinical Science*, 65(3):209-215.

Bao, X.R., Ong, S.E., Goldberger, O., Peng, J., Sharma, R., Thompson, D.A., Vafai, S.B., Cox, A.G., Marutani, E., Ichinose, F., Goessling, W., Regev, A., Carr, S.A., Clish, C.B. & Mootha, V.K. 2016. Mitochondrial dysfunction remodels one-carbon metabolism in human cells. *eLife*, 5, e10575.

Barja, G. 2007. Mitochondrial oxygen consumption and reactive oxygen species production are independently modulated: implications for aging studies. *Rejuvenation Research*, 10(2):215-224.

Barrett, M.C. & Dawson, A.P. 1975. Essentiality of ubiquinone for choline oxidation in rat liver mitochondria. *Biochemical Journal*, 148(3):595-597.

Bénit, P., El-Khoury, R., Schiff, M., Sainsard-Chanet, A. & Rustin, P. 2010. Genetic background influences mitochondrial function: modeling mitochondrial disease for therapeutic development. *Trends in Molecular Medicine*, 16(5):210-217.

Bhinderwala, F., Wase, N., DiRusso, C. & Powers, R. 2018. Combining mass spectrometry and NMR improves metabolite detection and annotation. *Journal of Proteome Research*, 17(11):4017-4022.

Bijarnia-Mahay, S. & Kapoor, S. 2019. Testing modalities for inborn errors of metabolism — what a clinician needs to know? *Indian Pediatrics*, 56(9):757-766.

Bouatra, S., Aziat, F., Mandal, R., Guo, A.C., Wilson, M.R., Knox, C., Bjorndahl, T.C., Krishnamurthy, R., Saleem, F., Liu, P., Dame, Z.T., Poelzer, J., Huynh, J., Yallou, F.S., Psychogios, N., Dong, E., Bogumil, R., Roehring, C. & Wishart, D.S. 2013. The human urine metabolome. *PloS one*, 8(9), e73076.

Broadhurst, D., Goodacre, R., Reinke, S.N., Kuligowski, J., Wilson, I.D., Lewis, M.R. & Dunn, W.B. 2018. Guidelines and considerations for the use of system suitability and quality control samples in mass spectrometry assays applied in untargeted clinical metabolomic studies. *Metabolomics*, 14(6), 72.

Brown, M.A. 1997. Tumor suppressor genes and human cancer. *Advances in Genetics*, 36:45-135.

Bugiani, M., Invernizzi, F., Alberio, S., Briem, E., Lamantea, E., Carrara, F., Moroni, I., Farina, L., Spada, M., Donati, M.A., Uziel, G. & Zeviani, M. 2004. Clinical and molecular findings in children with complex I deficiency. *Biochimica et Biophysica Acta (BBA) - Bioenergetics*, 1659(2):136-147.

Buhaescu, I. & Izzedine, H. 2007. Mevalonate pathway: a review of clinical and therapeutical implications. *Clinical Biochemistry*, 40(9):575-584.

Burr, S.P., Pezet, M. & Chinnery, P.F. 2018. Mitochondrial DNA heteroplasmy and purifying selection in the mammalian female germ line. *Development, Growth and Differentiation*, 60(1):21-32.

Calvaruso, M.A., Willems, P., van den Brand, M., Valsecchi, F., Kruse, S., Palmiter, R., Smeitink, J. & Nijtmans, L. 2012. Mitochondrial complex III stabilizes complex I in the absence of NDUFS4 to provide partial activity. *Human Molecular Genetics*, 21(1):115-120.

Calvo, S.E. & Mootha, V.K. 2010. The mitochondrial proteome and human disease. *Annual Review of Genomics and Human Genetics*, 11:25-44.

Cech, N.B. & Enke, C.G. 2001. Practical implications of some recent studies in electrospray ionization fundamentals. *Mass Spectrometry Reviews*, 20(6):362-387.

Chace, D.H., DiPerna, J.C., Kalas, T.A., Johnson, R.W. & Naylor, E.W. 2001. Rapid diagnosis of methylmalonic and propionic acidemias: quantitative tandem mass spectrometric analysis of propionylcarnitine in filter-paper blood specimens obtained from newborns. *Clinical Chemistry*, 47(11):2040-2044.

Chen, L., Cui, Y., Jiang, D., Ma, C.Y., Tse, H.-F., Hwu, W.L. & Lian, Q. 2018. Management of Leigh syndrome: current status and new insights. *Clinical Genetics*, 93(6):1131-1140.

Chinnery, P.F. & Hudson, G. 2013. Mitochondrial genetics. *British Medical Bulletin*, 106(1):135-159.

Chokchaiwong, S., Kuo, Y.T., Hsu, S.P., Hsu, Y.C., Lin, S.H., Zhong, W.B., Lin, Y.F. & Kao, S.H. 2019. ETF-QO mutants uncoupled fatty acid beta-oxidation and mitochondrial bioenergetics leading to lipid pathology. *Cells*, 8, 106.

Craven, L., Alston, C.L., Taylor, R.W. & Turnbull, D.M. 2017. Recent advances in mitochondrial disease. *Annual Review of Genomics and Human Genetics*, 18(1):257-275.

Davison, J., Lemonde, H. & Rahman, S. 2019. Inherited mitochondrial disease. *Paediatrics and Child Health*, 29(3):116-122.

de Haas, R., Das, D., Garanto, A., Renkema, H.G., Greupink, R., van den Broek, P., Pertijs, J., Collin, R.W.J., Willems, P., Beyrath, J., Heerschap, A., Russel, F.G. & Smeitink, J.A. 2017. Therapeutic effects of the mitochondrial ROS-redox modulator KH176 in a mammalian model of Leigh disease. *Scientific Reports*, 7, 11733.

DiMauro, S. & Paradas, C. 2015. Mitochondrial Disorders Due to Mutations in the Mitochondrial Genome. (*In* Rosenberg, R.N. & Pascual, J.M., *eds*. Rosenberg's Molecular and Genetic Basis of Neurological and Psychiatric Disease. 5th ed. Boston: Academic Press. p. 271-281).

Dimond, R. 2013. Patient and family trajectories of mitochondrial disease: diversity, uncertainty and genetic risk. *Life Sciences, Society and Policy*, 9, 2.

Ducker, G.S. & Rabinowitz, J.D. 2017. One-carbon metabolism in health and disease. *Cell Metabolism*, 10(1):27-42.

Dunn, W.B., Wilson, I.D., Nicholls, A.W. & Broadhurst, D. 2012. The importance of experimental design and QC samples in large-scale and MS-driven untargeted metabolomic studies of humans. *Bioanalysis*, 4(18):2249-2264.

Elliott, H.R., Samuels, D.C., Eden, J.A., Relton, C.L. & Chinnery, P.F. 2008. Pathogenic mitochondrial DNA mutations are common in the general population. *American Journal of Human Genetics*, 83(2):254-260.

Esterhuizen, K. 2018. A metabolomics investigation of selected m.3243A>G mutation phenotypes. Potchefstroom: NWU. (Dissertation – M.Sc.).

Esterhuizen, K., van der Westhuizen, F.H. & Louw, R. 2017. Metabolomics of mitochondrial disease. *Mitochondrion*, 35:97-110.

Evans, D.R. & Guy, H.I. 2004. Mammalian pyrimidine biosynthesis: fresh insights into an ancient pathway. *Journal of Biological Chemistry*, 279(32):33035-33038.

Fang, J., Uchiumi, T., Yagi, M., Matsumoto, S., Amamoto, R., Takazaki, S., Yamaza, H., Nonaka, K. & Kang, D. 2013. Dihydro-orotate dehydrogenase is physically associated with the respiratory complex and its loss leads to mitochondrial dysfunction. *Bioscience Reports*, 33(2), e00021.

Fassone, E. & Rahman, S. 2012. Complex I deficiency: clinical features, biochemistry and molecular genetics. *Journal of Medical Genetics*, 49(9):578-590.

FDA. 2001. Guidance for industry: bioanalytical method validation. chrome-extension://oemmndcbldboiebfnladdacbdfmadadm/https://www.fda.gov/files/drugs/published/Bioanalytical-Method-Validation-Guidance-for-Industry.pdf Date of access: 01 Jan. 2020.

Fu, M., Zhang, W., Wu, L., Yang, G., Li, H. & Wang, R. 2012. Hydrogen sulfide (H2S) metabolism in mitochondria and its regulatory role in energy production. *PNAS*, 109(8):2943-2948.

Garrett, R.M., Johnson, J.L., Graf, T.N., Feigenbaum, A. & Rajagopalan, K.V. 1998. Human sulfite oxidase R160Q: identification of the mutation in a sulfite oxidase-deficient patient and expression and characterization of the mutant enzyme. *PNAS*, 95(11):6394-6398.

Gika, H.G., Theodoridis, G.A., Plumb, R.S. & Wilson, I.D. 2014. Current practice of liquid chromatography-mass spectrometry in metabolomics and metabonomics. *Journal of Pharmaceutical and Biomedical Analysis*, 87:12-25.

Giles, R.E., Blanc, H., Cann, H.M. & Wallace, D.C. 1980. Maternal inheritance of human mitochondrial DNA. *PNAS*, 77(11):6715-6719.

Goubern, M., Andriamihaja, M., Nübel, T., Blachier, F. & Bouillaud, F. 2007. Sulfide, the first inorganic substrate for human cells. *FASEB Journal*, 21(8):1699-1706.

Guerrero-Castillo, S., Baertling, F., Kownatzki, D., Wessels, H.J., Arnold, S., Brandt, U. & Nijtmans, L. 2017. The assembly pathway of mitochondrial respiratory chain complex I. *Cell Metabolism*, 25(1):128-139.

Gvozdjáková, A. 2008. Mitochondrial physiology. (*In* Gvozdjáková, A., *ed.* Mitochondrial Medicine: Mitochondrial Metabolism, Diseases, Diagnosis and Therapy. Dordrecht: Springer Netherlands. p. 1-17).

Hammans, S.R., Sweeney, M.G., Brockington, M., Morgan-Hughes, J.A. & Harding, A.E. 1991. Mitochondrial encephalopathies: molecular genetic diagnosis from blood samples. *The Lancet*, 337(8753):1311-1313.

Hancock, C.N., Liu, W., Alvord, W.G. & Phang, J.M. 2016. Co-regulation of mitochondrial respiration by proline dehydrogenase/oxidase and succinate. *Amino Acids*, 48(3):859-872.

Handy, D.E. & Loscalzo, J. 2012. Redox regulation of mitochondrial function. *Antioxidants and Redox Signalling*, 16(11):1323-1367.

Harada, S., Hirayama, A., Chan, Q., Kurihara, A., Fukai, K., Iida, M., Kato, S., Sugiyama, D., Kuwabara, K., Takeuchi, A., Akiyama, M., Okamura, T., Ebbels, T.M., Elliott, P., Tomita, M., Sato, A., Suzuki, C., Sugimoto, M., Soga, T. & Takebayashi, T. 2018. Reliability of plasma polar metabolite concentrations in a large-scale cohort study using capillary electrophoresis-mass spectrometry. *PLoS one*, 13(1), e0191230.

Hargreaves, I.P., Sheena, Y., Land, J.M. & Heales, S.J. 2005. Glutathione deficiency in patients with mitochondrial disease: implications for pathogenesis and treatment. *Journal of Inherited Metabolic Disease*, 28(1):81-88.

Houten, S.M. & Wanders, R.J. 2010. A general introduction to the biochemistry of mitochondrial fatty acid β-oxidation. *Journal of Inherited Metabolic Disease*, 33(5):469-477.

Hunte, C., Zickermann, V. & Brandt, U. 2010. Functional modules and structural basis of conformational coupling in mitochondrial complex I. *Science*, 329(5990):448-451.

Janssen, A.J.M., Trijbels, F.J.M., Sengers, R.C.A., Smeitink, J.A.M., van den Heuvel, L.P., Wintjes, L.T.M., Stoltenborg-Hogenkamp, B.J.M. & Rodenburg, R.J.T. 2007. Spectrophotometric assay for complex I of the respiratory chain in tissue samples and cultured fibroblasts. *Clinical Chemistry*, 53(4):729-734.

Jin, Z., Wei, W., Yang, M., Du, Y. & Wan, Y. 2014. Mitochondrial complex I activity suppresses inflammation and enhances bone resorption by shifting macrophage-osteoclast polarization. *Cell Metabolism*, 20(3):483-498.

Jochmanová, I., Yang, C., Zhuang, Z. & Pacak, K. 2013. Hypoxia-inducible factor signaling in pheochromocytoma: turning the rudder in the right direction. *Journal of the National Cancer Institute*, 105(17):1270-1283.

Johnson, S.C., Yanos, M.E., Kayser, E.-B., Quintana, A., Sangesland, M., Castanza, A., Uhde, L., Hui, J., Wall, V.Z., Gagnidze, A., Oh, K., Wasko, B.M., Ramos, F.J., Palmiter, R.D., Rabinovitch, P.S., Morgan, P.G., Sedensky, M.M. & Kaeberlein, M. 2013. mTOR inhibition alleviates mitochondrial disease in a mouse model of Leigh syndrome. *Science*, 342(6165):1524-1528.

Kalapos, M.P. 2003. On the mammalian acetone metabolism: from chemistry to clinical implications. *Biochim Biophys Acta (BBA) - General Subjects*, 1621(2):122-139.

Kanani, H., Chrysanthopoulos, P.K. & Klapa, M.I. 2008. Standardizing GC-MS metabolomics. *Journal of Chromatography B*, 871(2):191-201.

Kirches, E., Michael, M., Warich-Kirches, M., Schneider, T., Weis, S., Krause, G., Mawrin, C. & Dietzmann, K. 2001. Heterogeneous tissue distribution of a mitochondrial DNA polymorphism in heteroplasmic subjects without mitochondrial disorders. *Journal of Medical Genetics*, 38(5):312-317.

Kmita, K. & Zickermann, V. 2013. Accessory subunits of mitochondrial complex I. *Biochemical Society Transactions*, 41(5):1272-1279.

Koene, S., Rodenburg, R.J., van der Knaap, M.S., Willemsen, M.A.A.P., Sperl, W., Laugel, V., Ostergaard, E., Tarnopolsky, M., Martin, M.A., Nesbitt, V., Fletcher, J., Edvardson, S., Procaccio, V., Slama, A., van den Heuvel, L.P.W.J. & Smeitink, J.A.M. 2012. Natural disease course and genotype-phenotype correlations in Complex I deficiency caused by nuclear gene defects: what we learned from 130 cases. *Journal of Inherited Metabolic Disease*, 35(5):737-747.

Koene, S., Willems, P.H., Roestenberg, P., Koopman, W.J. & Smeitink, J.A. 2011. Mouse models for nuclear DNA-encoded mitochondrial complex I deficiency. *Journal of Inherited Metabolic Disease*, 34(2):293-307.

Koopman, W.J., Distelmaier, F., Smeitink, J.A. & Willems, P.H. 2013. OXPHOS mutations and neurodegeneration. *EMBO Journal*, 32(1):9-29.

Kruse, S.E., Watt, W.C., Marcinek, D.J., Kapur, R.P., Schenkman, K.A. & Palmiter, R.D. 2008. Mice with mitochondrial complex I deficiency develop a fatal encephalomyopathy. *Cell Metabolism*, 7(4):312-320.

Kudo, N., Barr, A.J., Barr, R.L., Desai, S. & Lopaschuk, G.D. 1995. High rates of fatty acid oxidation during reperfusion of ischemic hearts are associated with a decrease in malonyl-CoA levels due to an increase in 5'-AMP-activated protein kinase inhibition of acetyl-CoA carboxylase. *Journal of Biological Chemistry*, 270(29):17513-17520.

Kunji, E.R.S., Aleksandrova, A., King, M.S., Majd, H., Ashton, V.L., Cerson, E., Springett, R., Kibalchenko, M., Tavoulari, S., Crichton, P.G. & Ruprecht, J.J. 2016. The transport mechanism of the mitochondrial ADP/ATP carrier. *Biochimica et Biophysica Acta (BBA) - Molecular Cell Research*, 1863(10):2379-2393.

Kuo, I.Y. & Ehrlich, B.E. 2015. Signaling in muscle contraction. *Cold Spring Harbor Perspectives in Biology*, 7(2):a006023-a006023.

Lake, N.J., Bird, M.J., Isohanni, P. & Paetau, A. 2015. Leigh syndrome: neuropathology and pathogenesis. *Journal of Neuropathology and Experimental Neurology*, 74(6):482-492.

Lake, N.J., Compton, A.G., Rahman, S. & Thorburn, D.R. 2016. Leigh syndrome: one disorder, more than 75 monogenic causes. *Annals of Neurology*, 79(2):190-203.

Le Pogam, P., Le Page, Y., Habauzit, D., Doue, M., Zhadobov, M., Sauleau, R., Le Drean, Y. & Rondeau, D. 2019. Untargeted metabolomics unveil alterations of biomembranes permeability in human HaCaT keratinocytes upon 60 GHz millimeter-wave exposure. *Scientific Reports*, 9, 9343.

Lee, C.F., Caudal, A., Abell, L., Nagana Gowda, G.A. & Tian, R. 2019. Targeting NAD^+ metabolism as interventions for mitochondrial disease. *Scientific Reports*, 9, 3073.

Lee, H.Y., Chung, U., Park, M.J., Yoo, J.-E., Han, G.-R. & Shin, K.-J. 2006. Differential distribution of human mitochondrial DNA in somatic tissues and hairs. *Annals of Human Genetics*, 70(1):59-65.

Lehmann, D. & McFarland, R. 2018. Overview of approaches to mitochondrial disease therapy. *Journal of Inborn Errors of Metabolism and Screening*, DOI.org/10.1177/ 2326409817752960

Leigh, D. 1951. Subacute necrotizing encephalomyelopathy in an infant. *Journal of Neurology, Neurosurgery, and Psychiatry*, 14(3):216-221.

Leong, D.W., Komen, J.C., Hewitt, C.A., Arnaud, E., Mckenzie, M., Phipson, B., Bahlo, M., Laskowski, A., Kinkel, S.A., Davey, G.M., Heath, W.R., Voss, A.K., Zahedi, R.P., Pitt, J.J., Chrast, R., Sickmann, A., Ryan, M.T., Smyth, G.K., Thornburn, D.R. & Scott, H.S. 2012. Proteomic and metabolomic analyses of mitochondrial complex I-deficient mouse model generated by spontaneous B2 short interspersed nuclear element (SINE) insertion into NADH dehydrogenase (ubiquinone) Fe-S protein 4 (Ndufs4) gene. *Journal of Biological Chemistry*, 287(24):20652-20663.

Li, H., Slone, J., Fei, L. & Huang, T. 2019. Mitochondrial DNA variants and common diseases: a mathematical model for the diversity of age-related mtDNA mutations. Cells, 8, 608.

Liang, C., Ahmad, K. & Sue, C.M. 2014. The broadening spectrum of mitochondrial disease: shifts in the diagnostic paradigm. *Biochimica et Biophysica Acta (BBA) - General Subjects*, 1840(4):1360-1367.

Libiad, M., Yadav, P.K., Vitvitsky, V., Martinov, M. & Banerjee, R. 2014. Organization of the human mitochondrial hydrogen sulfide oxidation pathway. *Journal of Biological Chemistry*, 289(45):30901-30910.

Lindeque, J.Z., Levanets, O., Louw, R. & van der Westhuizen, F.H. 2010. The involvement of metallothioneins in mitochondrial function and disease. *Current Protein and Peptide Science*, 11(4):292-309.

Liu, K.H., Walker, D.I., Uppal, K., Tran, V., Rohrbeck, P., Mallon, T.M. & Jones, D.P. 2016. High-resolution metabolomics assessment of military personnel: evaluating analytical strategies for chemical detection. *Journal of Occupational and Environmental Medicine*, 58(8 Suppl 1):S53-61.

Liu, X. & Locasale, J.W. 2017. Metabolomics: a primer. *Trends in Biochemical Sciences*, 42(4):274-284.

Loeffen, J.L.C., Smeitink, J.A.M., Trijbels, J.M.F., Janssen, A.J.M., Triepels, R.H., Sengers, R.C.A. & van den Heuvel, L.P. 2000. Isolated complex I deficiency in children: clinical, biochemical and genetic aspects. *Human Mutation*, 15(2):123-134.

Löffler, M., Grein, K., Knecht, W., Klein, A. & Bergjohann, U. 1998. Dihydroorotate dehydrogenase: profile of a novel target for antiproliferative and immunosuppressive drugs. (*In* Griesmacher, A., Müller, M.M. & Chiba, P., *eds*. Purine and Pyrimidine Metabolism in Man. Boston, MA: Springer US. p. 507-513).

Ma, Y.-Y., Wu, T.-F., Liu, Y.-P., Wang, Q., Song, J.-Q., Li, X.-Y., Shi, X.-Y., Zhang, W.-N., Zhao, M., Hu, L.-Y., Yang, Y.-L. & Zou, L.-P. 2013. Genetic and biochemical findings in Chinese children with Leigh syndrome. *Journal of Clinical Neuroscience*, 20(11):1591-1594.

Madiraju, A.K., Erion, D.M., Rahimi, Y., Zhang, X.-M., Braddock, D.T., Albright, R.A., Prigaro, B.J., Wood, J.L., Bhanot, S., MacDonald, M.J., Jurczak, M.J., Camporez, J.-P., Lee, H.-Y., Cline, G.W., Samuel, V.T., Kibbey, R.G. & Shulman, G.I. 2014. Metformin suppresses gluconeogenesis by inhibiting mitochondrial glycerophosphate dehydrogenase. *Nature*, 510(7506):542-546.

Mailloux, R.J. 2015. Teaching the fundamentals of electron transfer reactions in mitochondria and the production and detection of reactive oxygen species. *Redox Biology*, 4:381-398.

Maldonado, E.N. & Lemasters, J.J. 2014. ATP/ADP ratio, the missed connection between mitochondria and the Warburg effect. *Mitochondrion*, 19 Pt A:78-84.

Mammucari, C., Raffaello, A., Vecellio Reane, D., Gherardi, G., De Mario, A. & Rizzuto, R. 2018. Mitochondrial calcium uptake in organ physiology: from molecular mechanism to animal models. *Pflügers Archiv - European Journal of Physiology*, 470(8):1165-1179.

Marí, M., Colell, A., Morales, A., von Montfort, C., Garcia-Ruiz, C. & Fernández-Checa, J.C. 2010. Redox control of liver function in health and disease. *Antioxidants and Redox Signaling*, 12(11):1295-1331.

Markley, J.L., Bruschweiler, R., Edison, A.S., Eghbalnia, H.R., Powers, R., Raftery, D. & Wishart, D.S. 2017. The future of NMR-based metabolomics. *Current Opinion in Biotechnology*, 43:34-40.

Marquez, J., Lee, S.R., Kim, N. & Han, J. 2016. Post-translational modifications of cardiac mitochondrial proteins in cardiovascular disease: not lost in translation. *Korean Circulation Journal*, 46(1):1-12.

Martin-Blazquez, A., Diaz, C., Gonzalez-Flores, E., Franco-Rivas, D., Jimenez-Luna, C., Melguizo, C., Prados, J., Genilloud, O., Vicente, F., Caba, O. & Perez Del Palacio, J. 2019. Untargeted LC-HRMS-based metabolomics to identify novel biomarkers of metastatic colorectal cancer. *Scientific Reports*, 9, 20198.

Martinez, David L., Tsuchiya, Y. & Gout, I. 2014. Coenzyme A biosynthetic machinery in mammalian cells. *Biochemical Society Transactions*, 42(4):1112-1117.

Mayr, J.A., Haack, T.B., Freisinger, P., Karall, D., Makowski, C., Koch, J., Feichtinger, R.G., Zimmermann, F.A., Rolinski, B., Ahting, U., Meitinger, T., Prokisch, H. & Sperl, W. 2015. Spectrum of combined respiratory chain defects. *Journal of Inherited Metabolic Disease*, 38(4):629-640.

Mayr, J.A., Merkel, O., Kohlwein, S.D., Gebhardt, B.R., Böhles, H., Fötschl, U., Koch, J., Jaksch, M., Lochmüller, H., Horváth, R., Freisinger, P. & Sperl, W. 2007. Mitochondrial phosphate–carrier deficiency: a novel disorder of oxidative phosphorylation. *American Journal of Human Genetics*, 80(3):478-484.

Mazina, M.Y. & Vorobyeva, N.E. 2016. The role of ATP-dependent chromatin remodeling complexes in regulation of genetic processes. *Russian Journal of Genetics*, 52(5):463-472.

Merkley, E.D., Metz, T.O., Smith, R.D., Baynes, J.W. & Frizzell, N. 2014. The succinated proteome. *Mass Spectromerty Reviews*, 33(2):98-109.

Mráček, T., Drahota, Z. & Houštěk, J. 2013. The function and the role of the mitochondrial glycerol-3-phosphate dehydrogenase in mammalian tissues. *Biochimica et Biophysica Acta (BBA) - Bioenergetics*, 1827(3):401-410.

Mulukutla, B.C., Yongky, A., Le, T., Mashek, D.G. & Hu, W.-S. 2016. Regulation of glucose metabolism - a perspective from cell bioprocessing. *Trends in Biotechnology*, 34(8):638-651.

Munnich, A., Rötig, A., Chretien, D., Saudubray, J., Cormier, V. & Rustin, P. 1996. Clinical presentations and laboratory investigations in respiratory chain deficiency. *European Journal of Pediatrics*, 155(4):262-274.

Munro, D., Banh, S., Sotiri, E., Tamanna, N. & Treberg, J.R. 2016. The thioredoxin and glutathione-dependent H2O2 consumption pathways in muscle mitochondria: involvement in H2O2 metabolism and consequence to H2O2 efflux assays. *Free Radical Biology and Medicine*, 96:334-346.

Nicholls, D.G. & Ferguson, S.J. 2002a. Respiratory chains. (*In* Nicholls, D.G. & Ferguson, S.J., *eds.* Bioenergetics. 3rd ed. San Diego, CA: Elsevier Science, Academic Press. p. 89-134).

Nicholls, D.G. & Ferguson, S.J. 2002b. Metabolite and ion transport. (*In* Nicholls, D.G. & Ferguson, S.J., *eds.* Bioenergetics. 3rd ed. San Diego, CA: Elsevier Science, Academic Press. p. 229-230).

Nikkanen, J., Forsstrom, S., Euro, L., Paetau, I., Kohnz, R.A., Wang, L., Chilov, D., Viinamaki, J., Roivainen, A., Marjamaki, P., Liljenback, H., Ahola, S., Buzkova, J., Terzioglu, M., Khan, N.A., Pirnes-Karhu, S., Paetau, A., Lonnqvist, T., Sajantila, A., Isohanni, P., Tyynismaa, H.,

Nomura, D.K., Battersby, B.J., Velagapudi, V., Carroll, C.J. & Suomalainen, A. 2016. Mitochondrial DNA replication defects disturb cellular dNTP pools and remodel one-carbon metabolism. *Cell Metabolism*, 23(4):635-648.

Niyazov, D.M., Kahler, S.G. & Frye, R.E. 2016. Primary mitochondrial disease and secondary mitochondrial dysfunction: importance of distinction for diagnosis and treatment. *Molecular Syndromology*, 7(3):122-137.

Okuno, D., Iino, R. & Noji, H. 2011. Rotation and structure of FoF1-ATP synthase. *Journal of Biochemistry*, 149(6):655-664.

Oldham, W.M., Clish, C.B., Yang, Y. & Loscalzo, J. 2015. Hypoxia-mediated increases in L-2-hydroxyglutarate coordinate the metabolic response to reductive stress. *Cell Metabolism*, 22(2):291-303.

Olpin, S.E. 2013. Pathophysiology of fatty acid oxidation disorders and resultant phenotypic variability. *Journal of Inherited Metabolic Disease*, 36(4):645-658.

Orrenius, S., Gogvadze, V. & Zhivotovsky, B. 2007. Mitochondrial oxidative stress: implications for cell death. *Annual Review of Pharmacology and Toxicology*, 47(1):143-183.

Ortigoza-Escobar, J.D., Oyarzabal, A., Montero, R., Artuch, R., Jou, C., Jiménez, C., Gort, L., Briones, P., Muchart, J., López-Gallardo, E., Emperador, S., Pesini, E.R., Montoya, J., Pérez, B., Rodríguez-Pombo, P. & Pérez-Dueñas, B. 2016. Ndufs4 related Leigh syndrome: a case report and review of the literature. *Mitochondrion*, 28:73-78.

Pasikanti, K.K., Ho, P.C. & Chan, E.C.Y. 2008. Gas chromatography/mass spectrometry in metabolic profiling of biological fluids. *Journal of Chromatography B*, 871(2):202-211.

Pereverzev, M.O., Vygodina, T.V., Konstantinov, A.A. & Skulachev, V.P. 2003. Cytochrome c, an ideal antioxidant. *Biochemical Society Transactions*, 31(6):1312-1315.

Pfeffer, G., Majamaa, K., Turnbull, D.M., Thorburn, D. & Chinnery, P.F. 2012. Treatment for mitochondrial disorders. *Cochrane Database of Systematic Reviews*, 4, CD004426.

Picard, M. & McEwen, B.S. 2018. Psychological stress and mitochondria: a systematic review. *Psychosomatic Medicine*, 80(2):141-153.

Piroli, G.G., Manuel, A.M., Clapper, A.C., Walla, M.D., Baatz, J.E., Palmiter, R.D., Quintana, A. & Frizzell, N. 2016. Succination is increased on select proteins in the brainstem of the NADH dehydrogenase (ubiquinone) Fe-S protein 4 (Ndufs4) knockout mouse, a model of Leigh syndrome. *Molecular and Cellular Proteomics*, 15(2):445-461.

Pirttila, K., Videhult Pierre, P., Haglof, J., Engskog, M., Hedeland, M., Laurell, G., Arvidsson, T. & Pettersson, C. 2019. An LCMS-based untargeted metabolomics protocol for cochlear perilymph: highlighting metabolic effects of hydrogen gas on the inner ear of noise exposed guinea pigs. *Metabolomics*, 15(10):138.

Quintana, A., Zanella, S., Koch, H., Kruse, S.E., Lee, D., Ramirez, J.M. & Palmiter, R.D. 2012. Fatal breathing dysfunction in a mouse model of Leigh syndrome. *Journal of Clinical Investigation*, 122(7):2359-2368.

Rahman, J. & Rahman, S. 2018. Mitochondrial medicine in the omics era. *The Lancet*, 391(10139):2560-2574.

Rahman, S., Blok, R.B., Dahl, H.H.M., Danks, D.M., Kirby, D.M., Chow, C.W., Christodoulou, J. & Thorburn, D.R. 1996. Leigh syndrome: clinical features and biochemical and DNA abnormalities. *Annals of Neurology*, 39(3):343-351.

Reinecke, C.J., Koekemoer, G., van der Westhuizen, F.H., Louw, R., Lindeque, J.Z., Mienie, L.J. & Smuts, I. 2012. Metabolomics of urinary organic acids in respiratory chain deficiencies in children. *Metabolomics*, 8(2):264-283.

Robinson, A.D., Eich, M.L. & Varambally, S. 2020. Dysregulation of de novo nucleotide biosynthetic pathway enzymes in cancer and targeting opportunities. *Cancer Letters*, 470:134-140.

Rodenburg, R.J. 2016. Mitochondrial complex I-linked disease. *Biochimica et Biophysica Acta (BBA) - Bioenergetics*, 1857(7):938-945.

Rogerson, C., Bergamaschi, D. & O'Shaughnessy, R.F.L. 2018. Uncovering mechanisms of nuclear degradation in keratinocytes: a paradigm for nuclear degradation in other tissues. *Nucleus*, 9(1):56-64.

Rutter, J., Winge, D.R. & Schiffman, J.D. 2010. Succinate dehydrogenase - assembly, regulation and role in human disease. *Mitochondrion*, 10(4):393-401.

Ruzzenente, B., Rötig, A. & Metodiev, M.D. 2016. Mouse models for mitochondrial diseases. *Human Molecular Genetics*, 25(R2):R115-R122.

Ryan, D., Robards, K., Prenzler, P.D. & Kendall, M. 2011. Recent and potential developments in the analysis of urine: a review. *Analytica Chimica Acta*, 684(1-2):8-20.

Rydström, J. 2006. Mitochondrial NADPH, transhydrogenase and disease. *Biochimica et Biophysica Acta (BBA) - Bioenergetics*, 1757(5):721-726.

Salway, J.G. 2017. Amino acid metabolism. (*In* Salway, J.G., *ed.* Metabolism at a Glance. 4th ed. Hoboken, NJ: John Wiley and Sons. p. 44-51).

Scaglia, F., Towbin, J.A., Craigen, W.J., Belmont, J.W., Smith, E.O.B., Neish, S.R., Ware, S.M., Hunter, J.V., Fernbach, S.D., Vladutiu, G.D., Wong, L.-J.C. & Vogel, H. 2004. Clinical Spectrum, morbidity, and mortality in 113 pediatric patients with mitochondrial disease. *Pediatrics*, 114(4):925-931.

Scheiman, J., Luber, J.M., Chavkin, T.A., Macdonald, T., Tung, A., Pham, L.-D., Wibowo, M.C., Wurth, R.C., Punthambaker, S., Tierney, B.T., Yang, Z., Hattab, M.W., Avila-Pacheco, J., Clish, C.B., Lessard, S., Church, G.M. & Kostic, A.D. 2019. Meta-omics analysis of elite athletes identifies a performance-enhancing microbe that functions via lactate metabolism. *Nature Medicine*, 25(7):1104-1109.

Schwab, M.A., Sauer, S.W., Okun, J.G., Nijtmans, L.G., Rodenburg, R.J., van den Heuvel, L.P., Dröse, S., Brandt, U., Hoffmann, G.F., Ter Laak, H., Kölker, S. & Smeitink, J.A. 2006. Secondary mitochondrial dysfunction in propionic aciduria: a pathogenic role for endogenous mitochondrial toxins. *Biochemical Journal*, 398(Pt 1):107-112.

Schymanski, E.L., Jeon, J., Gulde, R., Fenner, K., Ruff, M., Singer, H.P. & Hollender, J. 2014. Identifying small molecules via high resolution mass spectrometry: communicating confidence. *Environmental Science and Technology*, 48(4):2097-2098.

Sell, H., Deshaies, Y. & Richard, D. 2004. The brown adipocyte: update on its metabolic role. *International Journal of Biochemistry and Cell Biology*, 36(11):2098-2104.

Sena, L.A. & Chandel, N.S. 2012. Physiological roles of mitochondrial reactive oxygen species. *Molecular Cell*, 48(2):158-167.

Sentongo, T.A., Azzam, R. & Charrow, J. 2009. Vitamin B12 status, methylmalonic acidemia, and bacterial overgrowth in short bowel syndrome. *Journal of Pediatric Gastroenterology and Nutrition*, 48(4):495-497.

Shepherd, D. & Garland, P.B. 1969. The kinetic properties of citrate synthase from rat liver mitochondria. *The Biochemical Journal*, 114(3):597-610.

Simon, M.T., Eftekharian, S.S., Stover, A.E., Osborne, A.F., Braffman, B.H., Chang, R.C., Wang, R.Y., Steenari, M.R., Tang, S., Hwu, P.W.-L., Taft, R.J., Benke, P.J. & Abdenur, J.E. 2019. Novel mutations in the mitochondrial complex I assembly gene NDUFAF5 reveal heterogeneous phenotypes. *Molecular Genetics and Metabolism*, 126(1):53-63.

Smeitink, J.A., van den Heuvel, L.W., Koopman, W.J., Nijtmans, L.G., Ugalde, C. & Willems, P.H. 2004. Cell biological consequences of mitochondrial NADH: ubiquinone oxidoreductase deficiency. *Current Neurovascular Research*, 1(1):29-40.

Smith, P.K., Krohn, R.I., Hermanson, G.T., Mallia, A.K., Gartner, F.H., Provenzano, M.D., Fujimoto, E.K., Goeke, N.M., Olson, B.J. & Klenk, D.C. 1985. Measurement of protein using bicinchoninic acid. *Analytical Biochemistry*, 150(1):76-85.

Smuts, I., van der Westhuizen, F.H., Louw, R., Mienie, L.J., Engelke, U.F.H., Wevers, R.A., Mason, S., Koekemoer, G. & Reinecke, C.J. 2013. Disclosure of a putative biosignature for respiratory chain disorders through a metabolomics approach. *Metabolomics*, 9(2):379-391.

Sofou, K., De Coo, I.F.M., Isohanni, P., Ostergaard, E., Naess, K., De Meirleir, L., Tzoulis, C., Uusimaa, J., De Angst, I.B., Lönnqvist, T., Pihko, H., Mankinen, K., Bindoff, L.A., Tulinius, M. & Darin, N. 2014. A multicenter study on Leigh syndrome: disease course and predictors of survival. *Orphanet Journal of Rare Diseases*, 9, 52.

Spinelli, J.B. & Haigis, M.C. 2018. The multifaceted contributions of mitochondria to cellular metabolism. *Nature Cell Biology*, 20(7):745-754.

Stechman, M.J., Ahmad, B.N., Loh, N.Y., Reed, A.A., Stewart, M., Wells, S., Hough, T., Bentley, L., Cox, R.D., Brown, S.D. & Thakker, R.V. 2010. Establishing normal plasma and 24-hour urinary biochemistry ranges in C3H, BALB/c and C57BL/6J mice following acclimatization in metabolic cages. *Laboratory Animals*, 44(3):218-225.

Suski, J., Lebiedzinska, M., Machado, N.G., Oliveira, P.J., Pinton, P., Duszynski, J. & Wieckowski, M.R. 2011. Mitochondrial tolerance to drugs and toxic agents in ageing and disease. *Current Drug Targets*, 12(6):827-849.

Tahara, E.B., Navarete, F.D.T. & Kowaltowski, A.J. 2009. Tissue-, substrate-, and site-specific characteristics of mitochondrial reactive oxygen species generation. *Free Radical Biology and Medicine*, 46(9):1283-1297.

Tuppen, H.A.L., Blakely, E.L., Turnbull, D.M. & Taylor, R.W. 2010. Mitochondrial DNA mutations and human disease. *Biochimica et Biophysica Acta (BBA) - Bioenergetics*, 1797(2):113-128.

Vafai, S.B. & Mootha, V.K. 2012. Mitochondrial disorders as windows into an ancient organelle. *Nature*, 491(7424):374-383.

Vakifahmetoglu-Norberg, H., Ouchida, A.T. & Norberg, E. 2017. The role of mitochondria in metabolism and cell death. B*iochemical and Biophysical Research Communications*, 482(3):426-431.

Valko, M., Leibfritz, D., Moncol, J., Cronin, M.T., Mazur, M. & Telser, J. 2007. Free radicals and antioxidants in normal physiological functions and human disease. *International Journal of Biochemistry and Cell Biology*, 39(1):44-48.

Valsecchi, F., Grefte, S., Roestenberg, P., Joosten-Wagenaars, J., Smeitink, J.A., Willems, P.H. & Koopman, W.J. 2013. Primary fibroblasts of NDUFS4(-/-) mice display increased ROS levels and aberrant mitochondrial morphology. *Mitochondrion*, 13(5):436-443.

Valsecchi, F., Monge, C., Forkink, M., de Groof, A.J.C., Benard, G., Rossignol, R., Swarts, H.G., van Emst-de Vries, S.E., Rodenburg, R.J., Calvaruso, M.A., Nijtmans, L.G.J., Heeman, B., Roestenberg, P., Wieringa, B., Smeitink, J.A.M., Koopman, W.J.H. & Willems, P.H.G.M. 2012. Metabolic consequences of NDUFS4 gene deletion in immortalized mouse embryonic fibroblasts. *Biochimica et Biophysica Acta (BBA) - Bioenergetics*, 1817(10):1925-1936.

Vasiliou, V., Vasiliou, K. & Nebert, D.W. 2009. Human ATP-binding cassette (ABC) transporter family. *Human Genomics*, 3(3):281-290.

Vinothkumar, K.R., Zhu, J. & Hirst, J. 2014. Architecture of mammalian respiratory complex I. *Nature*, 515(7525):80-84.

Vlastaridis, P., Kyriakidou, P., Chaliotis, A., Van de Peer, Y., Oliver, S.G. & Amoutzias, G.D. 2017. Estimating the total number of phosphoproteins and phosphorylation sites in eukaryotic proteomes. *GigaScience*, 6(2):1-11.

von Kleist-Retzow, J.C., Cormier-Daire, V., de Lonlay, P., Parfait, B., Chretien, D., Rustin, P., Feingold, J., Rötig, A. & Munnich, A. 1998. A high rate (20%-30%) of parental consanguinity in cytochrome-oxidase deficiency. *American Journal of Human Genetics*, 63(2):428-435.

Wallace, D.C. 2018. Mitochondrial genetic medicine. Nature Genetics, 50(12):1642-1649.

Wang, Y. & Hekimi, S. 2016. Understanding ubiquinone. *Trends in Cell Biology*, 26(5):367-378.

Warrack, B.M., Hnatyshyn, S., Ott, K.H., Reily, M.D., Sanders, M., Zhang, H. & Drexler, D.M. 2009. Normalization strategies for metabonomic analysis of urine samples. *Journal of Chromatography B*, 877(5-6):547-552.

Watmough, N.J. & Frerman, F.E. 2010. The electron transfer flavoprotein: ubiquinone oxidoreductases. *Biochimica et Biophysica Acta (BBA) - Bioenergetics*, 1797(12):1910-1916.

Weydert, C.J. & Cullen, J.J. 2010. Measurement of superoxide dismutase, catalase and glutathione peroxidase in cultured cells and tissue. *Nature Protocols*, 5(1):51-66.

Wiedemann, N. & Pfanner, N. 2017. Mitochondrial machineries for protein import and assembly. *Annual Review of Biochemistry*, 86(1):685-714.

Wikoff, W.R., Gangoiti, J.A., Barshop, B.A. & Siuzdak, G. 2007. Metabolomics identifies perturbations in human disorders of propionate metabolism. *Clinical Chemistry*, 53(12):2169-2176.

Xia, M., Zhang, Y., Jin, K., Lu, Z., Zeng, Z. & Xiong, W. 2019. Communication between mitochondria and other organelles: a brand-new perspective on mitochondria in cancer. *Cell and Bioscience*, 9, 27.

Yang, J., Zhao, X., Lu, X., Lin, X. & Xu, G. 2015. A data preprocessing strategy for metabolomics to reduce the mask effect in data analysis. *Frontiers in Molecular Biosciences*, 2, 4.

Zhu, X.-H., Qiao, H., Du, F., Xiong, Q., Liu, X., Zhang, X., Ugurbil, K. & Chen, W. 2012. Quantitative imaging of energy expenditure in human brain. *NeuroImage*, 60(4):2107-2117.

APPENDIX A:

SUPPLIERS OF MATERIALS AND REAGENTS

Table A.1: Materials/reagents used in the study

Material/reagent	Supplier	Catalogue #
10x Bionic™ Buffer	Sigma-Aldrich (MO, USA)	B6185
$^{13}C_4{}^{15}N_2$-Asparagine:H_2O	Cambridge Isotope Laboratories Inc. (Andover, MA, USA)	CNLM-3819-H
$^{13}C_5{}^{15}N_2$-Glutamine	Cambridge Isotope Laboratories Inc. (Andover, MA, USA)	CNLM-1275-H
1-Butanol	Sigma-Aldrich (MO, USA)	281549
1-Methyl-L-histidine	Aldrich	67520
2,2'-dinitro-5,5'-dithiobenzoic acid	Sigma-Aldrich (MO, USA)	D8130
2,6-dichloroindophenol sodium salt hydrate	Sigma-Aldrich (MO, USA)	D1878
2-[4-(2-hydroxyethyl)piperazin-1-yl] ethanesulfonic acid (HEPES)	Sigma-Aldrich (MO, USA)	H3375
$^{2}H_{10}$-Isoleucine	Cambridge Isotope Laboratories Inc. (Andover, MA, USA)	DLM-141-0.1
$^{2}H_3$-Acetyl-L-carnitine hydrochloride	Dr H.J. ten Brink (VU Medical Center, Amsterdam)	N/A
$^{2}H_3$-Octadecanoyl-L-carnitine hydrochloride	Dr H.J. ten Brink (VU Medical Center, Amsterdam)	N/A
$^{2}H_3$-Octanoyl-L-carnitine hydrochloride	Dr H.J. ten Brink (VU Medical Center, Amsterdam)	N/A
$^{2}H_4$-Arginine hydrochloride	Cambridge Isotope Laboratories Inc. (Andover, MA, USA)	DLM-6038
$^{2}H_4$-Citrulline	Cambridge Isotope Laboratories Inc. (Andover, MA, USA)	DLM-6039
$^{2}H_4$-Lysine dihydrochloride	Cambridge Isotope Laboratories Inc. (Andover, MA, USA)	DLM-2640
$^{2}H_8$-Valine	Euriso-top	E161P
3-Alanine	BDH Biochemicals	37009
3-Hydroxy-DL-kynurenine	Sigma	H1771
3-Methyl-L-histidine	Sigma	M9005
3-Phenylbutyrate	Aldrich	116807
4-Aminobutyrate	Sigma	A5835
6x DNA loading dye	Thermo Fisher Scientific™ (MA, USA	SM0242
Acetonitrile	Honeywell Burdick and Jackson®	017-4 or 015-4
Acetyl chloride	Fluka	990
Acetyl-CoA lithium salt	Sigma-Aldrich (MO, USA)	A218
Acetyl-L-carnitine hydrochloride	Dr H.J. ten Brink (VU Medical Center, Amsterdam)	N/A
Agarose	CONDA Pronadisa	8100
Antimycin A	Sigma-Aldrich (MO, USA)	A8674

Bicinchoninic acid (BCA) solution	Sigma-Aldrich (MO, USA)	B9643
BSA	Sigma-Aldrich (MO, USA)	P0914
Butyryl-L-carnitine hydrochloride	Dr H.J. ten Brink (VU Medical Center, Amsterdam)	N/A
Carnitine hydrochloride	Dr H.J. ten Brink (VU Medical Center, Amsterdam)	N/A
Chlorotrimethylsilane	Fluka	92360
Copper(II) sulfate solution	Sigma-Aldrich (MO, USA)	C2284
Creatine Monohydrate	Fluka	27900
Creatinine anhydrous	Sigma-Aldrich (MO, USA)	C4255
Decanoyl-L-carnitine hydrochloride	Dr H.J. ten Brink (VU Medical Center, Amsterdam)	N/A
Decylubiquinone	Sigma-Aldrich (MO, USA)	D7911
Dimethyl sulfoxide	Sigma	D8418
DL-3-Aminoisobutyrate	Fluka	8290
DL-5-Hydroxylysine hydrochloride	Sigma	H0377
DL-Isoleucine	Aldrich	298689
D-Mannitol	Sigma-Aldrich (MO, USA)	M9546
Dodecanoyl-L-carnitine hydrochloride	Dr H.J. ten Brink (VU Medical Center, Amsterdam)	N/A
Ethidium bromide	Sigma-Aldrich (MO, USA)	46065
Ethylene glycol tetraacetic acid (EGTA)	Sigma-Aldrich (MO, USA)	E4378
Ethylenediaminetetraacetic acid tetrasodium salt (EDTA)	Sigma	ED4SS
Formic acid	Sigma-Aldrich	94318
GeneRuler™ 100 bp DNA ladder	Thermo Fisher Scientific™ (MA, USA	SM0241
Glycine	Sigma	G7126
Hexadecanoyl-L-carnitine hydrochloride	Dr H.J. ten Brink (VU Medical Center, Amsterdam)	N/A
Hexanoyl-L-carnitine hydrochloride	Dr H.J. ten Brink (VU Medical Center, Amsterdam)	N/A
Isovaleryl-L-carnitine hydrochloride	Dr H.J. ten Brink (VU Medical Center, Amsterdam)	N/A
L-2-Aminoadipate	Sigma	A7275
L-Alanine	Fluka	5130
L-Arginine	Fluka	11010
L-Asparagine anhydrous	Fluka	11150
L-Aspartate	Fluka	11190
L-Citrulline	Fluka	27510
L-Cystathionine	Fluka	30055
L-Cystine	Fluka	30200
L-Glutamate	Sigma	G-8415
L-Glutamine	Fluka	49419
L-Histidine	Fluka	53320
L-Isothreonine	Sigma	H-6515
L-Kynurenine	Sigma	K8625

L-Leucine	Sigma	L8000
L-Lysine	Fluka	62840
L-Methionine	Fluka	64320
L-Ornithine hydrochloride	Aldrich	O830-5
L-Phenylalanine	Fluka	78020
L-Proline	Sigma	P0380
L-Pyroglutamate	Sigma	F-3634
L-Serine	Fluka	84960
L-Threonine	Fluka	89180
L-Tryptophan	Fluka	93659
L-Tyrosine	Fluka	93830
L-Valine	Sigma-Aldrich (MO, USA)	V0500
Methoxyamine hydrochloride	Aldrich	226904
N,N,N-trimethylglycine anhydrous	Fluka	61962
N,N-dimethylglycine	Sigma	D1156
N,N-dimethyl-L-phenylalanine	Sigma-Aldrich (MO, USA)	273910
N,O-bis(trimethylsilyl)-trifluoroacetamide (BSTFA)	SUPELCO	33027
NADH	Roche Diagnostics	10 107 735 001
Norleucine	Sigma-Aldrich (MO, USA)	74560
Nuclease-free PCR grade H_2O	Qiagen	129114
Octadecanoyl-L-carnitine hydrochloride	Dr H.J. ten Brink (VU Medical Center, Amsterdam)	N/A
Octanoyl-L-carnitine hydrochloride	Dr H.J. ten Brink (VU Medical Center, Amsterdam)	N/A
Oxaloacetate	Sigma-Aldrich (MO, USA)	O4126
Picric acid solution	Fluka	80456
Potassium hydroxide	Sigma-Aldrich (MO, USA)	P5958
Propionyl-L-carnitine hydrochloride	Dr H.J. ten Brink (VU Medical Center, Amsterdam)	N/A
Pyridine	Sigma-Aldrich (MO, USA)	270407
Quick-DNA™ Miniprep Plus Kit	D3050	Inqaba Biotec
Ring-$^2H_5$-phenylalanine	Euriso-top	E151P
Rotenone	Sigma-Aldrich (MO, USA)	R 8 875
Sarcosine	Sigma	S-9881
Sodium azide	Sigma-Aldrich (MO, USA)	S2002
Sodium hydroxide	Sigma-Aldrich (MO, USA)	S8045
Sucrose	Sigma-Aldrich (MO, USA)	S7903
Tetradecanoyl-L-carnitine hydrochloride	Dr H.J. ten Brink (VU Medical Center, Amsterdam)	N/A
trans-4-Hydroxy-L-proline	Sigma-Aldrich (MO, USA)	41875
Triton™X-100	Sigma-Aldrich (MO, USA)	T9284
Tropic acid	Fluka AG, Buchs SG	93540
Tween® 20	Merck	822184 (Art. 822184)
Water	Honeywell Burdick and Jackson®	365-4

Symbols: #, number. Abbreviations: H_2O, water; N/A, not applicable.

APPENDIX B:

EVALUATION OF CREATININE'S VIABILITY AS NORMALISATION APPROACH

B.1 Background

Under normal physiological conditions, urine volume can vary up to 15-fold, stemming from factors such as H_2O intake, diet and the excretion of H_2O via sweating (Ryan *et al.*, 2011). As a result, metabolite concentrations can differ significantly, thereby masking variations that are of biological importance. For this reason, the normalisation of urinary compounds is an absolute critical step in metabolomics (and other clinical applications) to compensate for biologically irrelevant variation (Warrack *et al.*, 2009).

Normalisation can be employed either prior, or subsequent to data acquisition. By performing pre-acquisition normalisation, a more complete data set is obtained (with less missing values). For example, the quantity of many metabolites will be below the analytical detection limit when a diluted urine sample (with a low creatinine concentration) is analysed, leading to missing values in the data. This problem can be circumvented by adjusting the urine samples to similar concentration levels before analysis, which has several advantages for metabolomics data, including obtaining a greater urinary metabolome coverage, which is an especially important aim in untargeted metabolomics; and reducing missing values, which increases the effectivity of downstream data processing procedures (like logarithm transformation).

Clearly, a pre-acquisition normalisation approach is beneficial in untargeted metabolomics, albeit time-consuming. Because of the latter, several analysts prefer normalising data derived from urinary analysis post-analysis, using either the urinary creatinine concentration, urine osmolality or mathematical equations (Warrack *et al.*, 2009). The referenced paper discusses the advantages and pitfalls of each method (which will be briefly addressed below). Therefore, it was decided that the two normalisation strategies be compared.

The use of creatinine as a normalisation factor was employed prior to data acquisition (refer to Section 3.8.1). Creatinine, which is excreted at a relatively constant rate by the kidneys via glomerular filtration, allows for the adjustment of metabolite concentrations to account for differences in urine dilutions. The use of creatinine, however, does raise concerns, especially in studies related to dysfunctional energy metabolism (Esterhuizen, 2018). For this reason, it was deemed important to establish whether the use of creatinine as a surrogate marker was viable in this study by evaluating it against another well-known and effective normalisation approach,

known as mass spectral total useful signal (MSTUS) normalisation (Warrack *et al.*, 2009) – in which all features are normalised against the sum of the signals, common in all samples.

For this comparison, only the data derived from untargeted analyses was used, since this approach yielded a greater number of peaks and thus covered a greater portion of the urine metabolome – an important factor for MSTUS normalisation (Warrack *et al.*, 2009). However, MSTUS may potentially give rise to skewed normalisation factors derived from features that statistically differ significantly between groups (e.g. highly elevated metabolites in one group), consequently leading to inaccurate normalisation. For this reason, a variant of the method [$MSTUS_{(excl.ssf)}$] was evaluated, where all features were also normalised using only the sum of all the statistically insignificant features (i.e. MSTUS minus statistically significant features). Statistically significant features were selected as described in Section 3.8.11. For the final normalisation approach, the data was normalised against the median of all the peaks in a sample. Unlike MSTUS, which can potentially be strongly affected by large abundant metabolites, this method is generally more robust and has also been shown to be an effective normalisation approach in urinary metabolomics (Warrack *et al.*, 2009).

Before these normalisation approaches could be applied, the creatinine normalisation factor first had to be removed from the data. This was achieved by dividing each feature in a sample by the volume of urine used for that sample. Creatinine normalisation was first inspected by comparing the samples' creatinine concentrations against their calculated MSTUS, $MSTUS_{(excl.ssf)}$ and median values (Figure B.1). This was done by conducting a bivariate correlation analysis, using Spearman's correlation to examine the type and strength of relationship between the creatinine concentrations and their calculated MSTUS, $MSTUS_{(excl.ssf)}$ and median values. Since all of the normalisation approaches yielded the same outliers via PCA [one of which fell far outside the 95% confidence region and skewed the correlation of creatinine and the other normalisation approaches in the WT group (data not shown)], the outliers were first removed. This step was deemed crucial, as these outliers could possibly have been the result of technical variance and therefore, could not accurately reflect any relationship when comparing normalisation approaches.

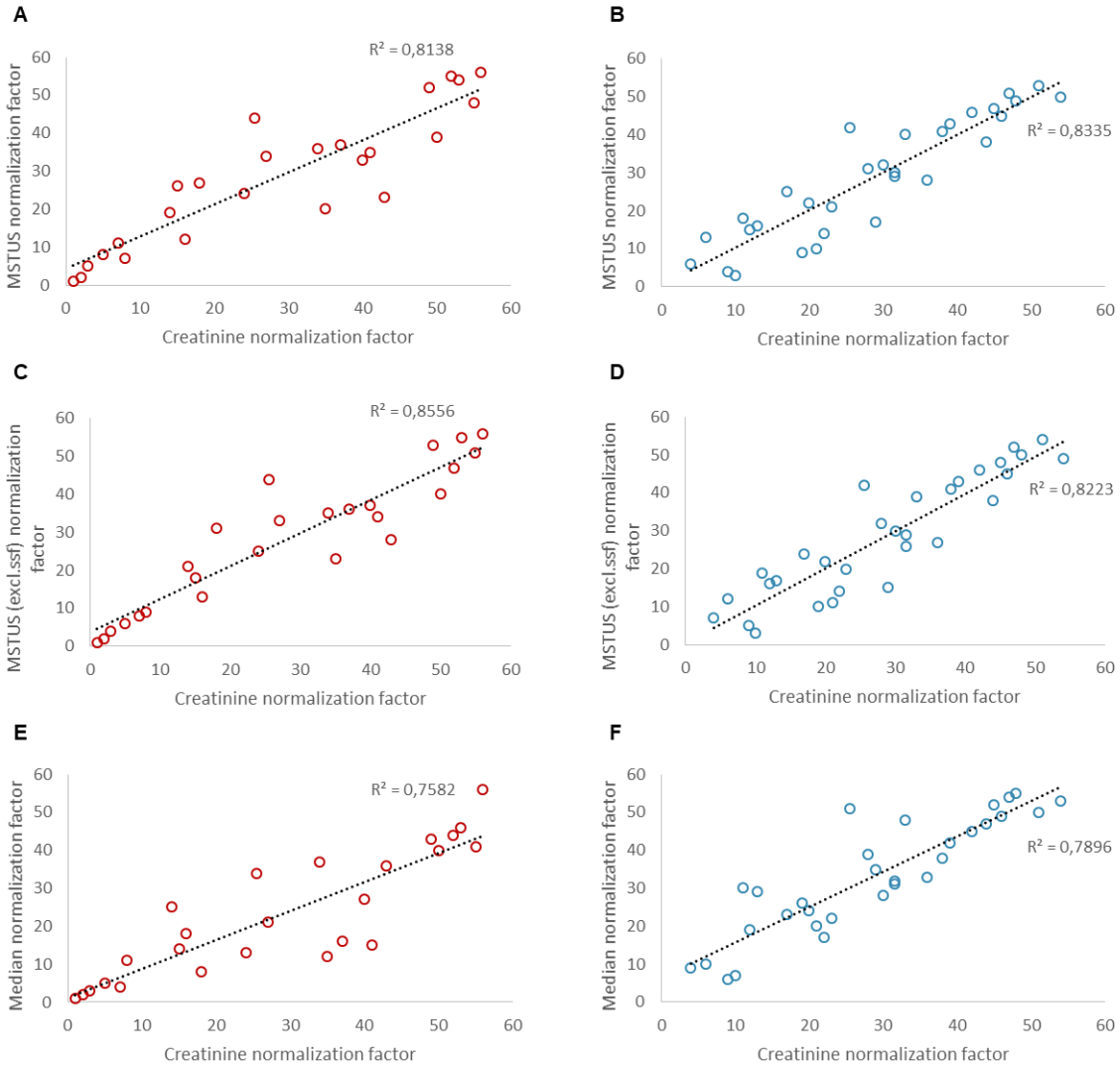

Figure B.1: Correlation between creatinine and three alternative normalisation approaches. Dot blots depicting the comparison of creatinine normalisation with (A-B) MSTUS, (C-D) $MSTUS_{(excl.ssf)}$ and (E-F) median normalisation methods. The normalisation approaches were assessed for both the KO (A, C and E; red) and WT (B, D and F; blue) groups. The regression line (dotted line) and R^2 value are displayed on each graph and outliers have been removed. Abbreviations: KO, knockout; MSTUS, mass spectral total useful signal; R^2, R-squared value (a measure of how well the data fits the regression line); WT, wild-type.

As shown in Figure B.1 A-F, creatinine not only correlated strongly with all of the normalisation factors, but also yielded very similar results in both the WT and KO groups, suggesting that creatinine clearance does not seem to be altered in any significant way in the KO mice. Creatinine displayed the strongest correlation with $MSTUS_{(excl.ssf)}$ (Figure B.1 C and D), and this correlation further differed very little from that observed between creatinine and MSTUS (Figure B.1 A and B). From this, it could thus be concluded that the statistically significant features obtained from MSTUS normalisation had very little (if any) effect on MSTUS as a normalisation factor. Lastly, it

was important to assess the outcome of feature selection among the four normalisation approaches. To this end, a Venn diagram was constructed to illustrate the features common and unique to each normalisation approach. As depicted in Figure B.2, the majority of features remained significant, regardless of normalisation approach.

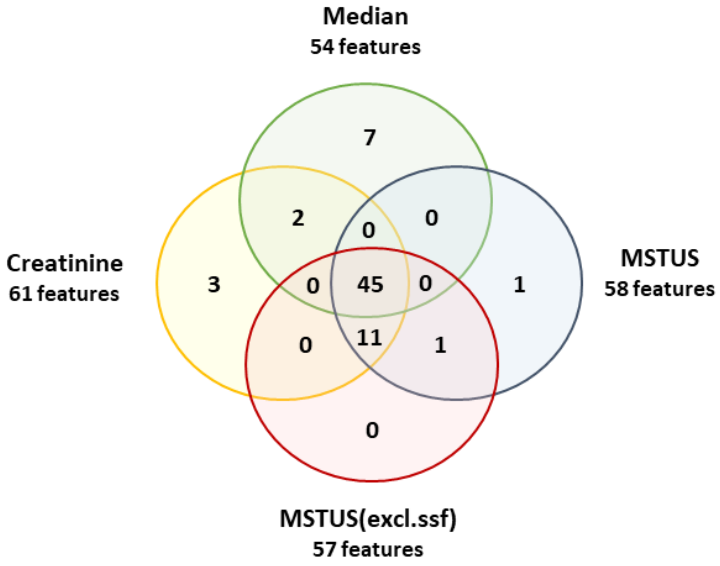

Figure B.2: Venn diagram illustrating the number of common and unique features derived from the four normalisation approaches. The yellow, blue, red and green circles indicate the unique features derived from the creatinine, MSTUS, $MSTUS_{(excl.ssf)}$ and median normalisation approaches, respectively. Abbreviations: MSTUS, mass spectral total useful signal.

Based on these findings, the utilisation of creatinine in this animal model did not seem to be compromised, and was thus acceptable to use as a normalisation factor. As a result of the continued use of creatinine in clinical laboratories today, it was decided to further use creatinine as a normalisation factor in the selection of discriminatory features.

APPENDIX C:

LANGUAGE EDITING CERTIFICATE

EDITING EXCELLENCE

084 365 4320
editingexcellencepotch@gmail.com

This is to certify that the dissertation,

Master of Science Biochemistry

of

Wessel Horak

has been edited by

Valerie Viljoen

Editing Excellence

And includes the following:

Abstract
List of symbols and abbreviations
Chapter 1
Chapter 2
Chapter 3
Chapter 4
Chapter 5
Appendix B

Date:9 March 2020

SATI INDIVIDUAL MEMBER
MEMBER NO. 1003396